Graduate thesis

NTNU
Norwegian University of Science and Technology
Faculty of Engineering
Department of Mechanical and Industrial Engineering

Mathias Audal
Fredrik Gusfre
Jon Paulsen Skjerdingstad

Designing a High Presicion Rotating and Reciprocal Tribometer

To study new green lubricants

Graduate thesis in Bachelor in Mechanical Engineering
Supervisor: Nuria Espallargas
Co-supervisor: Wahyu Wijanarko
January 2022

NTNU
Norwegian University of
Science and Technology

Mathias Audal
Fredrik Gusfre
Jon Paulsen Skjerdingstad

Designing a High Presicion Rotating and Reciprocal Tribometer

To study new green lubricants

Graduate thesis in Bachelor in Mechanical Engineering
Supervisor: Nuria Espallargas
Co-supervisor: Wahyu Wijanarko
January 2022

Norwegian University of Science and Technology
Faculty of Engineering
Department of Mechanical and Industrial Engineering

NTNU
Norwegian University of
Science and Technology

Abstract

This project has focused on the design and development of two high-precision tribometers intended for use in the Tribology Lab at the Department of Mechanical Engineering and Production at NTNU. The objective has been to contribute to the academic environment at the institute and facilitate research on new and more environmentally friendly tribological solutions.

Early on, the group decided to create two tribometers - one for rotational testing and one for linear testing. After thorough exploration of various concepts, careful evaluations were made to select the optimal solution in terms of precision and cost-effectiveness. The project also involved significant financial considerations, as the acquisition of electric motors, sensors, and other laboratory equipment incurred substantial costs.

The guidance provided by advisors from NTNU has been crucial to the project's progress. The group followed an iterative working process, with ongoing feedback contributing to improvements and optimization of the tribometers' design. Discussions within the group have also played a vital role in the development process.

In addition to technical expertise, the group has learned a great deal about collaboration and teamwork through this project. They have gained experience working together towards common goals, sharing responsibilities, and handling any challenges or conflicts that arose. This collaboration has enhanced their communication skills, ability to collaborate effectively and make decisions as a group. This learning about teamwork will be valuable in their future careers as mechanical engineers.

The project concludes that significant progress has been made, and the tribometers meet the requirements for high precision and cost-effectiveness. However, there are still remaining tasks before everything is fully functional. Further testing and fine-tuning must be conducted to ensure accurate and reliable results. There is also a need for continued development of the shared software that will integrate and coordinate testing between the two tribometers.

This project has been a valuable learning experience for the group, as they have gained practical experience working as mechanical engineers. Through the execution of the project, they have been able to apply their theoretical knowledge in a practical setting and strengthen their understanding of mechanical engineering and tribology. Additionally, they have gained valuable insights into collaboration and teamwork, which will be valuable skills in their future careers.

Sammendrag

Dette prosjektet har fokusert på design og utvikling av to tribometere for høy presisjon, som er ment å bli brukt på tribologilaben ved Institutt for maskinteknikk og produksjon på NTNU. Målet har vært å bidra til det akademiske miljøet ved instituttet og tilrettelegge for forskning på nye og mer miljøvennlige smøremidler.

Gruppen tok tidlig beslutningen om å lage to tribometere - ett for roterende testing og ett for lineær testing. Etter grundige utforskninger av ulike konsepter, ble det gjort nøye vurderinger for å velge den optimale løsningen med hensyn til presisjon og kostnadseffektivitet. Prosjektet involverte også betydelige økonomiske vurderinger, da anskaffelse av elektriske motorer, sensorer og annet laboratorieutstyr var kostnadskrevende. I tillegg var begrenset tid utfordrende i forbindelse med prosjektarbeidet.

Veiledernes bidrag fra NTNU har vært avgjørende i prosjektets fremgang. Gruppen har fulgt en iterativ arbeidsprosess, der kontinuerlige tilbakemeldinger har bidratt til forbedringer og optimalisering av tribometerenes design. Diskusjoner innad i gruppen har også spilt en viktig rolle i utviklingen.

I tillegg til teknisk kompetanse har gruppen også lært mye om samarbeid og teamarbeid gjennom dette prosjektet. De har opparbeidet seg erfaring med å jobbe sammen mot felles mål, dele ansvar og håndtere eventuelle utfordringer og konflikter som har oppstått. Samarbeidet har forbedret deres kommunikasjonsferdigheter, evne til å samarbeide effektivt og ta beslutninger som en gruppe. Denne læringen om teamarbeid vil være verdifull i deres fremtidige karrierer som maskiningeniører.

Konklusjonen av prosjektet er at mye fremgang har blitt gjort, og tribometerne oppfyller kravene til høy presisjon og kostnadseffektivitet. Likevel er det fortsatt arbeid som gjenstår før alt er fullstendig funksjonelt. Videre testing og finjusteringer må gjennomføres for å sikre nøyaktige og pålitelige resultater. Det er også behov for videreutvikling av den felles programvaren som skal integrere og koordinere testingen mellom de to tribometerene.

Dette prosjektet har vært en verdifull læringsprosess for gruppen, da de har fått praktisk erfaring med å jobbe som maskiningeniører. Gjennom utførelsen av prosjektet har de kunnet anvende sin teoretiske kunnskap i en praktisk setting, og styrke sin forståelse for maskinteknikk og tribologi. Samtidig har de fått verdifull innsikt i samarbeid og teamarbeid, noe som vil være en verdifull ferdighet i deres fremtidige karriere.

Preface

This bachelor's thesis is written as a completion of our bachelor's degree in Mechanical Engineering at the Department of Mechanical and Industrial Engineering at NTNU. The thesis is written by Mathias Audal, Fredrik Gusfre, and Jon Paulsen Skjerdingsstad, all of us specializing in machine construction. We all have different backgrounds and personalities, and it was a valuable experience to work together on this bachelor's thesis. The thesis consists of a written report and a final oral presentation corresponding to 20-grade points in our degree.

The thesis is about designing and developing a reciprocal and rotating tribometer for the tribology lab at NTNU, primarily to study new green lubricants. Throughout the project, our knowledge of mechatronics, mechanics, and machine construction has been of great value. We have learned a lot while working on the project and helped each other achieve our goals. There have been multiple challenges throughout the project, affecting both the result and the progress of the project. On the other hand, the challenges have enabled us to develop our problem-solving skills significantly and have made us better understand possible challenges during engineering projects. These challenges will help us in future academic and professional projects, and we are thankful for the invaluable experiences.

Throughout the project, we have received excellent help and supervision from several persons, and we would like to thank the following persons:

Nuria Espallargas, Adviser and project owner.

Wahyu Wijanarko, Adviser and project owner.

Anna Olsen, course coordinator.

Håvard Nitter Vestad, responsible for the mechatronics lab.

Other helpful persons at the tribology and mechatronics lab.

Contents

Abstract i

Preface iii

Contents vi

List of Figures vii

List of Tables x

Notations and Abbreviations xi

1 Introduction 1
- 1.1 Background . . . 1
- 1.2 Project description . . . 2
- 1.3 Motivation . . . 2
- 1.4 Objectives . . . 3
  - 1.4.1 Project goals . . . 3
  - 1.4.2 Effect goals . . . 3
- 1.5 Structure of the report . . . 3

2 Theory 5
- 2.1 Tribology . . . 5
  - 2.1.1 Friction . . . 6
  - 2.1.2 Wear . . . 7
  - 2.1.3 Lubrication . . . 8
  - 2.1.4 Tribosystems . . . 8
  - 2.1.5 Tribometers . . . 9
- 2.2 Materials . . . 11
  - 2.2.1 Steel . . . 12
  - 2.2.2 Aluminum . . . 13
  - 2.2.3 Plastics . . . 13
- 2.3 Motorized positioning stages . . . 14
  - 2.3.1 Motor types . . . 14
  - 2.3.2 Manufacturers . . . 15
- 2.4 Force transducers . . . 19
  - 2.4.1 Piezoelectric load cell . . . 20
  - 2.4.2 Strain gauges . . . 20
- 2.5 Electrical . . . 20
  - 2.5.1 Prototyping boards . . . 20
  - 2.5.2 Soldering . . . 21
- 2.6 Software . . . 21
  - 2.6.1 Languages . . . 21
  - 2.6.2 Libraries . . . 22
  - 2.6.3 Matlab . . . 22
  - 2.6.4 Arduino . . . 22

3 Methodology **23**
3.1 Design methodology . . . 23
3.1.1 Design process . . . 23
3.1.2 Computer-aided design and simulation . . . 25
3.1.3 Prototyping . . . 25
3.2 Risk management . . . 26
3.3 Troubleshooting . . . 26

4 Project Constraints **28**
4.1 Previous tribometer . . . 28
4.1.1 Optical board . . . 29
4.1.2 Sensor . . . 29
4.1.3 Pin . . . 30
4.1.4 Sample holders . . . 30
4.1.5 Potentiostat . . . 31
4.2 Sample . . . 31
4.3 Load capacity . . . 31
4.4 Velocities . . . 32
4.5 Wear track . . . 32
4.6 Software . . . 32

5 Design and Development **33**
5.1 Design criteria . . . 33
5.2 Reciprocal tribometer . . . 34
5.2.1 Load cell . . . 34
5.2.2 Motorized positioning stage . . . 36
5.2.3 Sample holders . . . 38
5.2.4 Possible solutions . . . 40
5.3 Rotational tribometer . . . 44
5.3.1 Load cell . . . 44
5.3.2 Motorized positioning stage . . . 47
5.3.3 Linear translation stage . . . 49
5.3.4 Tribocorrosion . . . 51
5.3.5 Possible solutions . . . 54
5.4 Electronics . . . 56
5.4.1 Safety circuit . . . 57
5.4.2 Power supply . . . 58
5.5 Software . . . 58
5.5.1 Design Criteria . . . 58
5.5.2 Visual layout . . . 59
5.5.3 Calibration . . . 60
5.5.4 Data gathering . . . 60
5.5.5 Arduino . . . 61
5.6 Additional notes . . . 61

6 Final Product **62**
6.1 Reciprocal tribometer . . . 62
6.1.1 Arm . . . 63
6.1.2 Axle base . . . 64
6.1.3 Tribocorrosion cell . . . 65
6.1.4 Mounting and connections . . . 65
6.1.5 Materials . . . 69
6.1.6 Calculations . . . 70

6.1.7 Simulations . . . 74
6.2 Rotational tribometer . . . 77
6.2.1 Main Frame . . . 78
6.2.2 Pin arm design . . . 79
6.2.3 Load cell . . . 79
6.2.4 Load cell and pin arm linkage . . . 80
6.2.5 Center of gravity . . . 82
6.2.6 Main joint . . . 83
6.2.7 Tribocorrosion . . . 85
6.2.8 Materials . . . 86
6.2.9 Calculations . . . 88
6.2.10 Simulations . . . 90
6.2.11 Maximum loads and load charts . . . 91
6.3 Software . . . 93
6.4 Safety circuit . . . 95
6.5 Additional notes . . . 96

7 Challenges and Troubleshooting 97
7.1 Challenges . . . 97
7.1.1 Communication . . . 97
7.1.2 Lead times and deliveries . . . 98
7.1.3 Failure of components . . . 98
7.1.4 Time frame of the project . . . 98
7.1.5 Software . . . 99
7.1.6 Electronics . . . 99
7.2 Troubleshooting . . . 99

8 Further Development 101

9 Conclusion 102

References 104

List of Figures

2.1.1 Contact interaction between two surfaces. . . . 6
2.1.2 Basic sliding friction and wear mechanisms. . . . 7
2.1.3 Mechanisms of adhesive wear. . . . 7
2.1.4 Illustration of the principles of viscosity. . . . 8
2.1.5 Illustration of a simplified tribosystem. . . . 8
2.1.6 Working principle of a rotating pin-on-disk tribometer. . . . 9
2.1.7 Tribocorrosion sample holder and working principle. . . . 10
2.2.1 General engineering tensile stress to tensile strain curve. . . . 11
2.3.1 Aerotech ANT95L-050. . . . 15
2.3.2 Aerotech ANT95L-050. . . . 16
2.3.3 PI M-403. . . . 17
2.3.4 PI A-63X. . . . 17
2.3.5 MM Engineering MPT3012-AK-S. . . . 18
2.3.6 MM Engineering MDT360110-QN-MO-S. . . . 19

3.1.1 Engineering design process. . . . 23

4.1.1 Schematic view of old tribometer. . . . 28
4.1.2 Techmfg 78-225-12R optical board illustration. . . . 29
4.1.3 Kistler 9327A drawing. . . . 29
4.1.4 Pin. . . . 30
4.1.5 Drawing of existing dry and lubrication sample holders (designed by one of the scientists at the tribology laboratory). . . . 31

5.2.1 Reciprocal tribometer. . . . 34
5.2.2 Mounting of the Kistler 9327A . . . 35
5.2.3 The Kistler 5018A Amplifier . . . 36
5.2.4 Model of the MM-Engineering MPT3012-AK-S with motor, top view, side section view, isometric view . . . 37
5.2.5 Model of the mounting plate for the MTP3012-AK-S. . . . 38
5.2.6 Drawing of existing dry and lubrication sample holders. . . . 38
5.2.7 Mounting of tribocorrosion sample holdere. . . . 39
5.2.8 Mounting of tribocorrosion sample holder. . . . 40
5.2.9 Centre of mass, reciprocal tribometer. . . . 41
5.2.10 Solution 1 for the arm in the reciprocal tribometer. . . . 41
5.2.11 Solution 2 for the arm in the reciprocal tribometer. . . . 42
5.2.12 Solution 3. . . . 43
5.3.1 Influence on reaction force caused by the distance between pin and load cell linkage. 44
5.3.2 Tedea-Huntleigh Model 1006. . . . 47
5.3.3 Illustration of Load Cell Amp and Arduino for the rotational tribometer. . . . 47
5.3.4 Technical data for MDT360110-QN from MM Engineering. . . . 48
5.3.5 Load chart for MDT360110-QN from MM Engineering. . . . 49
5.3.6 Linear translation stage and support. . . . 50
5.3.7 Dimensions and force diagram of PT2512 short positioning table from MM Engineering. . . . 50
5.3.8 Alternative to linear translation stage, rotating tribometer. . . . 51
5.3.9 Solution of rotational tribometer design, with Kistler load cell. . . . 54
5.3.10 Solution of rotational tribometer design, with Kistler force cap load cell. . . . 55

5.3.11 Solution of rotational tribometer design, with Tedea-Huntleigh strain gauge. Fixed connection. . . . 56
5.4.1 Safety circuit depicted in manual . . . 57
5.4.2 Safety circuit single line diagram. . . . 57
5.5.1 Example GUI. . . . 60
5.5.2 Developed GUI. . . . 60
5.6.1 Drawing of risers. . . . 61

6.1.1 Final design of reciprocal tribometer with tribocorrosion sample holder. . . . 62
6.1.2 Final design of reciprocal tribometer with dry sample holder. . . . 62
6.1.3 Final design of the arm. . . . 63
6.1.4 Assembly of the axle base, the motorized positioning stage and the motor stage. 64
6.1.5 Mounting of the tribocorrosion sample holder. . . . 65
6.1.6 Mounting holes for the sensor base and the sensor top. . . . 66
6.1.7 Top view of sample stage. . . . 66
6.1.8 Mounting of the tribocorrosion sample cell to Kistler 9327A. . . . 67
6.1.9 Mounting of the tribocorrosion sample holder. . . . 68
6.1.10 Connection between arm and axle base. . . . 68
6.1.11 Connection between arm and axle base. . . . 69
6.1.12 Additional fasteners for conterweight. . . . 69
6.1.13 Illustration of arm marking the length l and h. . . . 70
6.1.14 Simplified illustration of arm marking the length l and h. . . . 71
6.1.15 FBD of the arm when there is no acceleration. . . . 71
6.1.16 FBD of the arm when it is accelerated backwards. . . . 72
6.1.17 FBD of the arm when it is accelerated forwards. . . . 72
6.1.18 Static simulation of arm solution 3. . . . 74
6.1.19 Static simulation of the arm. . . . 75
6.1.20 Static simulation of the pin. . . . 76
6.2.1 Final design of rotational tribometer, without tribocorrosion sample. . . . 77
6.2.2 Final design of rotational tribometer, with tribocorrosion sample. . . . 77
6.2.3 Name of main components, rotational tribometer. . . . 78
6.2.4 Main frame, rotational tribometer. . . . 78
6.2.5 Pin arm hinge support, rotational tribometer. . . . 79
6.2.6 Speedring M6x1 ball joint used in the rotational tribometer. . . . 80
6.2.7 Ball joint connection, rotational tribometer. . . . 80
6.2.8 Initial adapter design for connection between load cell and pin arm. . . . 81
6.2.9 Alternative design for the adapter for connection between load cell and pin arm, as suggested by advicor. . . . 81
6.2.10 Rearmost center of gravity, single counterweight. . . . 82
6.2.11 Rearmost center of gravity, double counterweight. . . . 83
6.2.12 Foremost center of gravity, single counterweight. . . . 83
6.2.13 Exploded view of main joint, with DP4 flange bushing and locknut. . . . 84
6.2.14 PSC-X12 SERIES slip ring dimensions. . . . 85
6.2.15 Tribocorrosion sample holder, rotational tribometer. . . . 86
6.2.16 Motor assembly with slip ring feature, rotational tribometer. . . . 86
6.2.17 Three-dimensional FBD on pin, pin-arm, and load cell. . . . 88
6.2.18 Influence on reaction force caused by the distance between pin and load cell linkage. 88
6.2.19 Von Mises and displacement simulation of pin-arm, linkage and strain gauge. $F_f = 30\ N$, $COF = 1$, and $T_f = 1.35\ Nm$. . . . 90
6.2.20 Von Mises and displacement simulation of pin-arm, linkage and strain gauge. $F_f = 50\ N$, $COF = 1$, and $T_f = 2.25\ Nm$. . . . 90

6.2.21 Max allowable friction force with Tedea-Huntleigh Model 1006, 3 kg. Values are in Newton [N]. 91
6.2.22 Max allowable friction force with Tedea-Huntleigh Model 1006, 5 kg. Values are in Newton [N]. 91
6.2.23 Load chart for rotational tribometer with 3 kg load cell. 92
6.2.24 Load chart for rotational tribometer with 5 kg load cell. 92
6.2.25 Tedea-Huntleigh Model 1006 rated capacity and safety factors. 93
6.3.1 Program running, plotting data (Note: uncalibrated). 94
6.3.2 Result file with recorded data. 94
6.4.1 Safety circuit for rotational table motor. 95
6.5.1 Block diagram of system. 96

List of Tables

2.2.1 Properties of hot-rolled metal products based on EN10025. 12
2.3.1 Some chosen mechanical properties for Aerotech ANT95L-050. Information attained from the Aerotech ANT95L data sheet. 16
2.3.2 Some chosen mechanical properties for Aerotech ADRS100. Information attained from the Aerotech ADRS data sheet. 16
2.3.3 Selected mechanical properties for PI M-403. Information attained from the PI M-403 data sheet. 17
2.3.4 Some chosen mechanical properties for PI A-63X. Information attained from the PI A-63X data sheet. 18
2.3.5 Some chosen mechanical properties for MM Engeneering MPT3012-AK-S. Information attained from the MM Engeneering MPT3012-AK-S data sheet. 19
2.3.6 Some chosen mechanical properties for MM Engeneering MDT360110-QN-MO-S. Information attained from the MM Engeneering MDT360110-QN-MO-S data sheet. 19

4.1.1 Some chosen mechanical properties for Kistler 9327A. 30

5.3.1 Kistler load cell comparison. 45

Notations and Abbreviations

Notations

Symbols:	Description:
σ	Stress
ν	Poisson's ratio
μ	Coefficient of friction
F_R	Reaction force
F_N	Normal force
F_f	Friction force
r	Radius
τ	Torque

Abbreviations

- **CAD** Computer Aided Design
- **COF** Coefficient of Friction
- **FBD** Free Body Diagram
- **NTNU** Norwegian University of Science and Technology
- **PCA** Principal Component Analysis
- **GUI** Graphical User Interface
- **PCB** Printed Circuit Board
- **IC** Integrated Circuit
- **ADC** Analog to Digital Converter
- **A/Amps** Ampere
- **V** Volts
- **NOK** Norwegian Krone

Introduction

1.1 Background

Tribology is the study of friction, wear, and lubrication of materials in relative motion. The field is highly interdisciplinary and utilizes skills from mechanical engineering, materials science, chemistry, physics, and more (STLE, no date). The field of tribology is relevant to a lot of aspects of mechanical engineering, and the importance of understanding friction and wear cannot be understated. Many mechanical systems have moving parts, and friction and wear will always be present. The effect of friction and wear on the environment is significant, and it is estimated that 23% of the world's energy consumption originates from tribological contact (Holmberg and Erdemir, 2017). Tribology is therefore, highly relevant to environmental issues, and developing better and more environmentally friendly tribological solutions is essential.

A tribometer is often used in the study of tribology and in the development of new tribological solutions. A tribometer is a scientific instrument that measures the tribological aspects of a tribosystem, such as the friction force, the coefficient of friction, and wear between two or more surfaces in relative motion. As explained, a tribometer consists of a point contact, a loading force above that point contact, a sample, a drive causing relative motion between the sample and point contact, and a force sensor. The point contact or the sample is driven in either a rotating or reciprocating motion under a set load, and the frictional force between the point contact and sample is measured by the force sensor (Beronque, 2018). There are several types of tribometers arranged by the specific contact arrangements they simulate. Some examples of common tribometer types are "pin-on-disk," "pin-on-slab," and "ring-on-ring" tribometers. There are a few commercial tribometers on the market today, but the price tag of such a tribometer usually ranges well above 500.000,- NOK.

In this project, the project group has worked with the tribology laboratory at the Department of Mechanical and Industrial Engineering at NTNU to develop a tribometer consisting of two modules, one for reciprocating motion and one for rotating motion. The two modules needed the capability of tribocorrosion testing in addition to regular tribological testing, considering that none of the existing tribometers in the lab have this capability.

1.2 Project description

The project is about designing and building a high-precision tribometer to study new lubrication formulas. The tribometer will have the ability of both rotating and reciprocal testing and will consist of two electric motors; one for rotational motion and a second for reciprocal movement. In addition to having the ability of both rotational and reciprocal testing, the tribometer will have the ability of tribocorrosion testing. To control the normal load on the sample, the tribometer will be able to test with variable loads. This will be done using free weights. The use of free weights will provide a user-friendly method of configuring the normal force before each test. To be able to interpret the test results, the tribometer will include software to provide the test results. The test results will be provided in the form of digital graphs through Matlab as the main software.

The project's primary stakeholders are the tribology laboratory at NTNU, the researchers, and the postdocs at the laboratory. The advisors and project owners are researchers and postdocs at the laboratory and are the primary stakeholders in the project. Additionally, the project group itself is a stakeholder in the project.

1.3 Motivation

As future mechanical engineers, the science of tribology is highly relevant. As mentioned, friction and wear will always be present in mechanical systems. The possibility of gaining valuable knowledge within the field is a significant motivational factor. The project will allow us to implement our knowledge in a real engineering problem, learn more, and develop our understanding of mechanical engineering, materials science, and tribology. The project is highly interdisciplinary, and almost all our skills learned in class will come to use. This will prepare us for future careers as mechanical engineers or researchers in the field. Some of us are interested in pursuing an academic career, and the possibility of working with skilled professors and being a part of a thriving research environment is also a significant motivational factor. As mentioned earlier, tribological contact is estimated to contribute to 23% of global energy consumption (Holmberg and Erdemir, 2017). Therefore, research and development on new tribological solutions are crucial from an environmental perspective, as new and better solutions can contribute to reducing this energy consumption. This is also a significant motivational factor.

1.4 Objectives

1.4.1 Project goals

- Design and build a functional "pin-on-disk" tribometer with the ability of both reciprocal and rotational testing as well as the possibility of variable normal loads using free weights.
- Design of different sample holders for different types of tribological testing, such as lubricated and tribocorrosion testing.
- Software with the capability of providing test results in a user-friendly way, and the ability to save test results to CSV or xls files.

1.4.2 Effect goals

- Contributing to the tribology laboratory at NTNU, and providing better test equipment for tribology research and development.
- Contribute to the project group's understanding of tribology, mechanical engineering, and machine design, and prepare us for future engineering projects.
- Strengthen the project group's understanding of project work, and the importance of good collaboration, communication, and teamwork.

1.5 Structure of the report

The report will first give the reader a brief introduction to the relevant theoretical concepts regarding tribology and tribometer design. Theoretical information regarding evaluated components will also be presented, as well as the theory relevant to the components used in the final design. All relevant theoretical aspects of the design and development process will be presented to the reader, to give a foundation of understanding the design choices made by the project group.

After that, the project frames and information regarding the existing equipment will be presented. Information regarding the project frames will give the reader a wider understanding of the limits and constraints relevant to the design of the tribometers. Additionally, information about existing equipment implemented in the new tribometers designed by the project group will be presented.

When all relevant theoretical information and descriptions regarding the project frames have been presented, the design and development phase will be proposed. In the design and development chapter, relevant information regarding the design choices and options evaluated will be explained in detail. Different design solutions, components, and explanations of the design choices made by the project group will be proposed.

Thereafter, the final designs will be proposed to the reader. This chapter will give the reader a detailed explanation of the final design choices made by the project group. This chapter presents material choices, calculations, simulation results, and final design solutions in detail.

Challenges and suggestions for further development will thereafter be presented. This chapter will describe the difficulties and challenges that occurred during the project, and how the project group solved these challenges. Additionally, suggestions for further development will be presented in detail. Due to the limited time frame of the project, certain elements and ideas were not implemented in the final designs. These ideas will be presented, to give room for further development and improvement of the design provided by the project group.

At the end of the report, a conclusion on the project will be proposed. A brief discussion regarding both the achievement of the project goals and the process from initiation to end will be presented.

Theory

2.1 Tribology

Tribology is the study of friction, wear, and lubrication between contacting surfaces in relative motion. "The term tribology is based on the Greek word for rubbing and, although the term itself was not coined until 1964, there are images of tribology in action from as long ago as ancient Egypt, when early tribologists used oil to help facilitate the sliding of large statues" (STLE, no date). The oils were used for minimizing friction between the two contacting surfaces in motion to reduce the energy lost to tribological contact when moving statues or building blocks. In today's society, it is estimated that 23% of the world's energy consumption originates from tribological contact (Holmberg and Erdemir, 2017). The development of new tribological solutions is critical in order to reduce this unwanted energy loss. This is especially important in industries like manufacturing, transport, and energy production, where unwanted energy loss needs to be at a minimum.

Tribology is a diverse and highly interdisciplinary field and includes aspects from chemical engineering, materials science, physics, mathematics, mechanical engineering, and more (Lennard, 2014a). Examples of tribological systems are bearings, joints, gears, and engines. Tribological research and development are crucial in order to achieve greater efficiency, reliability, duration, and wear resistance.

Friction is one of the most significant tribological aspects. To fully understand tribology, one has to understand friction and the mechanisms involved. Friction can cause energy loss, heat generation, and wear on contacting surfaces, and greatly reduce the efficiency and lifespan of machines and other tribological systems. Wear is also a significant part of the science of tribology, and encompasses the destruction and material loss caused by tribological contact. Wear can contribute to surface damage and mechanical failure, and it is critical to understand the mechanisms involved in order to reduce the wear caused by tribological contact. Lubrication is also a significant aspect of tribology and encompasses the introduction of fluids between contacting surfaces in relative motion. Lubrication can contribute to less friction and wear, and also introduce characteristics such as corrosion resistance. The combination of friction, wear, and lubrication forms the basis of tribology.

2.1.1 Friction

Friction is a significant aspect of tribology and describes the opposing forces acting on contacting surfaces in relative motion. In general, there are two forms of friction; static friction and dynamic friction. Static friction describes the friction between two stationary surfaces before relative motion occurs, while dynamic friction describes the friction between surfaces in relative motion. Friction can further be divided into rolling friction and sliding friction. The field of friction is diverse and extensive, and only the general principles and theories of sliding friction between metals will be described in this chapter to give the reader a basis for understanding tribology and tribological testing with a pin-on-disk tribometer.

Friction arises from the contact forces between two bodies and is independent of the apparent area of contact (Persson, 2000). The sources of friction originate from adhesion, deformation of the surfaces in contact, van der Waals forces, chemical bonding, capillary forces, and so on (Tribonet, 2016). In general, the friction force is only dependent on the normal force between the surfaces in contact and the friction properties of the contacting materials described by a coefficient of friction (COF). The general formula of friction is described in terms of the normal force acting perpendicular to the surfaces in contact multiplied with the COF of the materials, $F_f = \mu \cdot F_N$. The COF is different for each material combination and what kind of friction is involved (static or dynamic). Friction is not a material property, but rather a system property defined by the different materials, lubrication, and environments involved. The most prevalent causes of sliding friction between metals are adhesion and plowing. As described by Bowden and Tabor (1974), "Friction is the force required to shear intermetallic junctions plus the force required to plow the surface of the softer metal by asperities on the harder surface".

Adhesion describes the bonding of two metals caused by high pressure between the surfaces in contact. Friction forces arise due to the shear forces needed to break these intermetallic junctions. The bonding occurs at the asperities of the surfaces, as described by Lennard (2014b), and illustrated in Figure 2.1.1 (Lennard, 2014b).

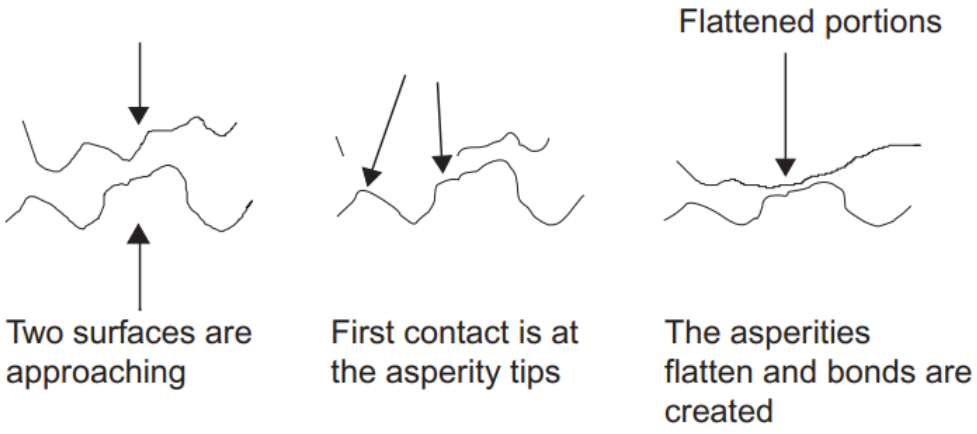

Figure 2.1.1: Contact interaction between two surfaces (Lennard, 2014b).

As mentioned above, the friction force is independent of the apparent area of contact. As illustrated in Figure 2.1.1, true contact happens at the asperities of the contacting surfaces. Due to the small area of contact, and the normal forces between them, bonds are created at the asperities. The higher the normal force between the contacting surfaces, the more asperities will bond and more force are required to shear off the bonded asperities between the metals. This contributes to friction and is referred to as adhesion (Lennard, 2014b).

Ploughing is the phenomena where the harder material will plough the softer material at the asperities of the harder surface, and create grooves in the softer metal. This is together with

adhesion the most significant cause of friction between two surfaces in contact during sliding motion. As described by Holmberg, Ronkainen, et al. (2007), ploughing "is resistance originating from elastic and possibly plastic deformation when a harder counter surface moves through a softer or more elastic surface". The mechanisms of adhesion and ploughing are illustrated in Figure 2.1.2.

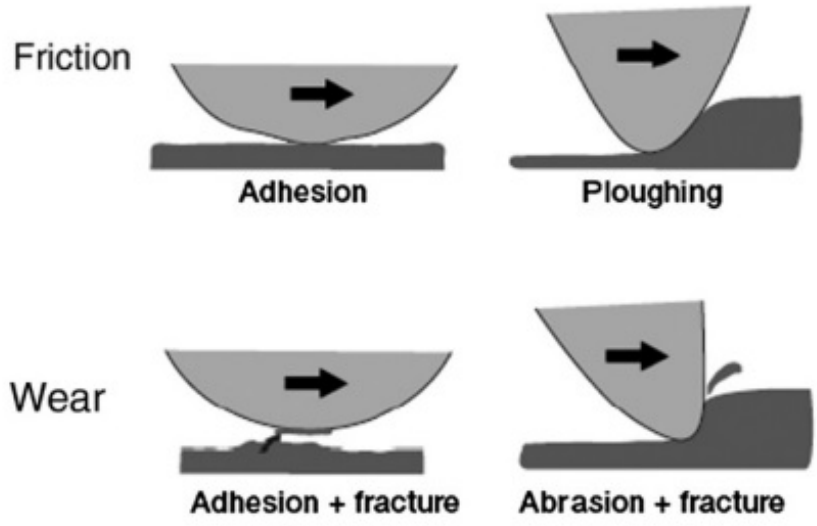

Figure 2.1.2: Basic sliding friction and wear mechanisms (Holmberg, Ronkainen, et al., 2007, p.1036).

2.1.2 Wear

Wear is the loss of material usually caused by contacting surfaces in relative motion. Wear can increase friction and contribute to unwanted energy loss, and ultimately lead to component failure if not managed properly. In general, the two most common types of wear are adhesive and abrasive wear. The difference between these two types is how the material is lost, and if the material is lost or transferred between the contacting surfaces (STLE, No Date).

Adhesive wear describes the phenomena where bonded asperities are transferred off the softer material and adhere to the harder material. According to Kovaříková et al. (2009), "If the strength of the adhesive bonds is greater than that of the softer friction partner, material eventually detaches from the deformed surface of the softer friction partner and is transferred to the harder one". The mechanisms of adhesive wear are illustrated in Figure 2.1.3 and Figure 2.1.2.

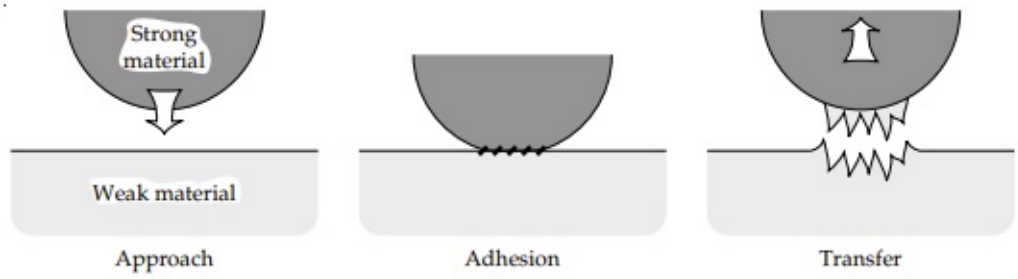

Figure 2.1.3: Mechanisms of adhesive wear (Stachowiak and Batchelor, 2014, p.578).

Abrasive wear occurs due to ploughing of the contacting surfaces. As mentioned above, ploughing occurs when the harder material ploughs the softer material and creates a groove in the softer

material. The differences between frictional ploughing and wear is if material is lost in the process. Abrasive wear describes the phenomena where the material is lost and removed from the softer material due to ploughing. This happens when the two contacting materials have equal or greater hardness, and fracture due to repeated ploughing occurs and material is lost (Kovaříková et al., 2009).

2.1.3 Lubrication

The topic of lubrication is diverse and extensive, and only the basic principles are included in this chapter to give the reader a basis of understanding tribosystems and tribological testing.

Lubrication is the introduction of fluid between two or more contacting surfaces. Lubrication is usually introduced to reduce friction and wear of the components involved and can consist of different chemicals and oils depending on the requirements and the environment of the tribosystem. There are several types of lubrication, usually divided into the following categories: Hydrodynamic lubrication, aerodynamic lubrication, elasto-hydrodynamic lubrication, and boundary lubrication (Bowden and Tabor, 1974). Lubricants usually consist of different elements such as mineral oils and synthetic fluids, greases, oil-soluble additives, and/or solids such as graphite or glass (Bartz, 1978).

Viscosity is the measure of the flow-rate of the lubricant and describes the fluids resistance to flow. High viscosity corresponds to a low flow-rate, and low viscosity corresponds to a high flow-rate. The value of the viscosity of a fluid is determined by the shear stresses and the gradient of the velocity of the flow, more commonly explained as the ratio of the shearing stresses in the fluid divided by the shear rate of the fluid (The Engineering Toolbox, n.d.). The principles of viscosity in general parallel flow are illustrated in Figure 2.1.4.

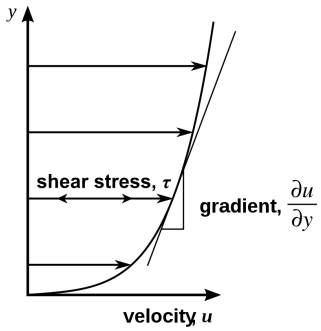

Figure 2.1.4: Illustration of the principles of viscosity (Wikipedia, 2023c).

2.1.4 Tribosystems

A tribosystem is generally a combination of all the topics described above; contacting surfaces, friction, wear, and lubrication. Typically, a tribosystem is a system in which tribological elements interact with each other. It usually consists of two or more surfaces in contact, the environment surrounding them, and an interfacial element such as lubrication between the surfaces (Massola et al., 2016). A simplification of a typical tribosystem is illustrated in Figure 2.1.5. Examples of common tribosystems are gears, engines, bearings, and joints. Tribology is the study of tribosystems, and tribological testing is usually executed as a tribosystem itself.

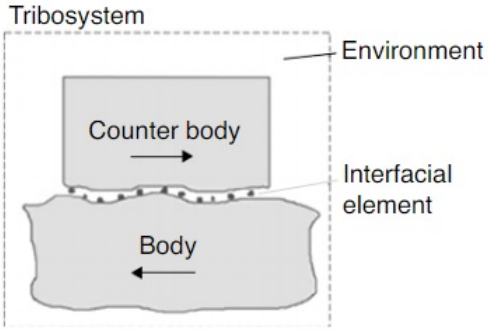

Figure 2.1.5: Illustration of a simplified tribosystem (Massola et al., 2016, p.2).

2.1.5 Tribometers

When studying and doing research on the tribological properties of a tribosystem such as friction, wear, and lubrication between contacting surfaces in relative motion, a tribometer is often used. A tribometer is a scientific device that is used for studying tribological properties of tribosystems, such as the coefficient of friction, wear, and the effect of different lubricants. All these factors are studied between contacting surfaces in relative motion (Corrosionpedia, 2017).

There are several types of tribometers, separated by the different tribosystems they imitate. Common tribometer types include pin-on-disk, ball-on-disk, four-ball, or pin-on-slab tribometers, each simulating different tribosystems. The pin-on-disk tribometer is the primary focus of this project.

A pin-on-disk tribometer measures tribological properties of materials such as friction force, coefficient of friction, wear volume, and the properties of lubricants between a point-contact and a sample in relative motion. The way these types of tribometers work is by applying force between the point contact at the end of the pin and a sample in relative motion. This can be done either by moving the pin and having a stationary sample, or moving the sample and having the pin stationary. The most common way is having the pin stationary and moving the sample in either a reciprocal or rotating motion. By applying normal force between the pin and the sample, frictional forces will arise due to the relative motion and normal force. The friction force between the pin and the sample can then be recorded by a load cell. The load cell is usually placed close to the pin and works as a support as the friction force presses against the pin. This way, the friction force can be calculated based on the normal force and the horizontal distance between the load cell, and the contact point between the pin and the sample.

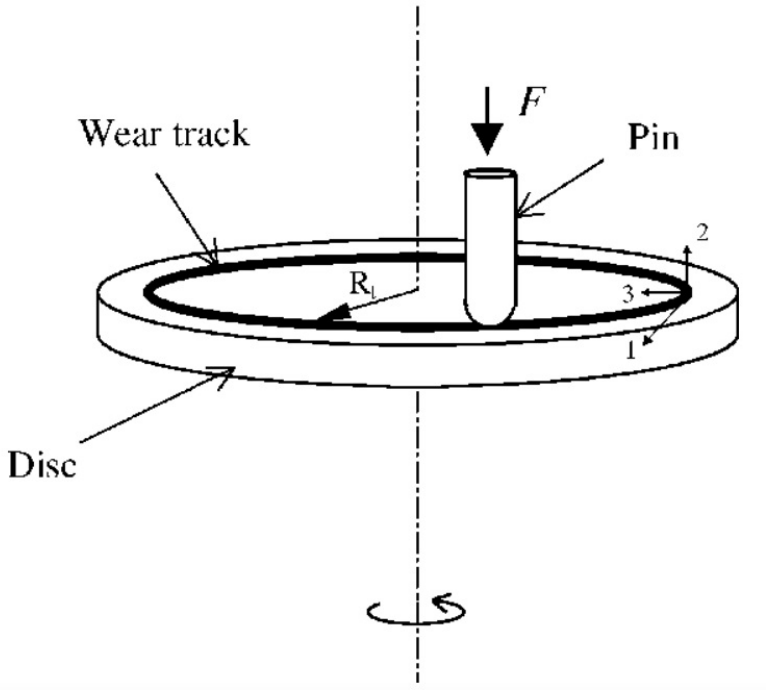

Figure 2.1.6: Working principle of a rotating pin-on-disk tribometer (Yan et al., 2002, p.450).

As illustrated in Figure 2.1.6, a force is applied directly on top of the pin so that normal forces are introduced from the sample on the pin. The relative motion between the pin and sample leads to frictional forces on the pin, which further can be recorded by a load cell. The forces recorded by the load cell can then be used to calculate the COF of the tribosystem currently being tested. This is done by using the formula of friction force, as illustrated in Equation 2.1.

$$F_f = \mu \cdot F_N$$
$$\rightarrow \mu = \frac{F_f}{F_N} \tag{2.1}$$

The value of the COF recorded depends upon what materials are used in the sample and point contact on the pin, and if there is any form of lubrication during testing.

Tribometers can also have the ability of tribocorrosion testing. This is a form of tribological testing where corrosion is present on the sample and contributes to friction and wear. This is done by leading electricity through the sample and an electrolyte, with the help of a working electrode and a reference electrode. To conduct tribocorrosion testing using a tribometer, a special sample holder is needed. The tribocorrosion sample holder work as a sealed container with an electrolyte, capable of leading electricity through the sample and into the electrolyte. The working electrode is placed underneath the sample and is connected to a power supply (commonly a potentiostat). The reference electrode is placed in contact with the electrolyte in the sample holder, to enable electricity flow through the sample and electrolyte. An illustration of a typical tribocorrosion sample holder and working principle are illustrated in Figure 2.1.7.

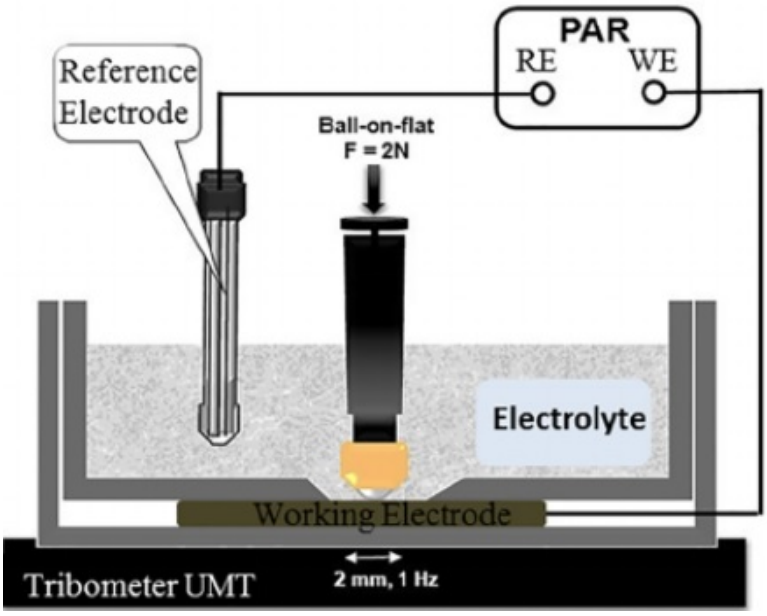

Figure 2.1.7: Tribocorrosion sample holder and working principle (Ramos, 2017, p.3).

2.2 Materials

When designing a machine or construction, the selection of materials with the right characteristics is important. Every material has its own characteristics, and different materials are suitable for different applications. One can classify engineering materials as either metals or non-metals. The metal category includes materials such as iron, steel, copper, titanium, and so on. The non-metal category consists of materials such as plastics, ceramics, rubber, wood, and so on. Metals are widely used in machine construction because of their rigidity, broad and diverse characteristics.

The metal category can further be divided into ferrous and non-ferrous metals. Ferrous metals are metals that contain iron, such as steel and cast iron, and non-ferrous metals are metals without iron. Steel is the most common ferrous metal. Examples of common non-ferrous metals are titanium, copper or aluminum.

The strength and elasticity of materials are described by Young's modulus of the material. Young's modulus is defined as the ratio of tensile stress (σ) to tensile strain (ε) and is usually presented in the form of graphs (Birmingham, no date). The graph below illustrates the standard engineering tensile stress to tensile strain curve and describes the different phases of elastic to plastic deformation before a fracture occurs. The graph will be different depending on what material it represents.

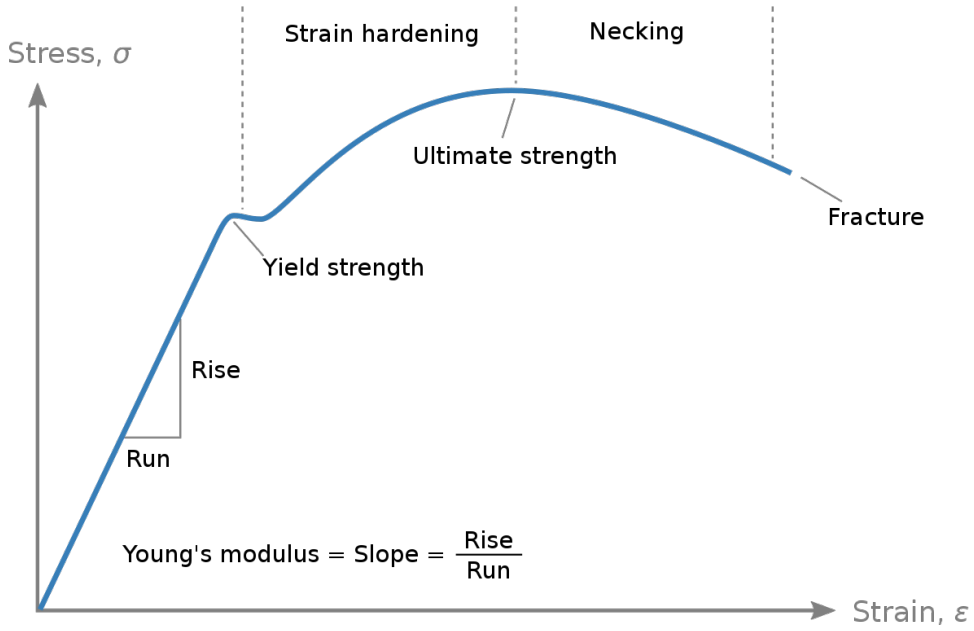

Figure 2.2.1: General engineering tensile stress to tensile strain curve (Wikipedia, 2023b).

The linear phase illustrated in the graph is called the elastic area and describes the elastic properties of the material. In this area, the material will return to its original shape after the load is removed. The point illustrated in the graph as "Yield strength" describes the maximum stress before the material will start its plastic deformation, where permanent deformation will occur. The ultimate strength of the material describes the maximum stress the material can handle before fracture occurs. Strain hardening describes the changes in material properties during plastic deformation. During strain hardening the material will often achieve greater strength, but become more brittle as the stresses increase. Necking is the reduction in the cross-sectional area as the fracture is approaching. The Young's modulus of the material is described as the ratio of tensile stress to tensile strain, and describes the stiffness of the material.

The yield strength of the material is a significant parameter when deciding on what materials to use. It is important to select a strong enough material so that the yield strength is not exceeded. In some applications, engineers want the material to exceed the yield strength, but usually, the aim is to avoid this. If the yield strength is exceeded, the material will deform permanently.

Poisson's ratio (ν) is another important parameter to take into account when deciding what material to use. Poisson's ratio describes the deformation of the material perpendicular to the direction of applied loads.

Some other material characteristics that needs to be taken into account depending on the application of the material are corrosion characteristics, electrical conductivity, and thermal conductivity.

2.2.1 Steel

The reason why steel is the most common ferrous material is because of its relatively low price, high versatility, and the ability of altering it's characteristics using different alloying elements. Basic steel is iron with a carbon percentage ranging by weight between 0.02% to 2.22%, and is often referred to as carbon steel. Carbon steels can further be alloyed with other alloying elements such as manganese, chromium, nickel, aluminum, and/or molybdenum (Groover, 2010, p.111). Every alloy has its own characteristics, and are suitable for different applications and environments. Steel can be divided into four main categories: plain carbon steels, low alloy steels, stainless steels, and tool steels (Groover, 2019).

Plain carbon steels and stainless steels are commonly used for machine design and construction. The amount of carbon determines the characteristics of the metal, and more carbon usually corresponds to greater strength and hardness and decreased ductility. Plain carbon steels are divided into the following three categories: low-carbon steels (less than 0.2% carbon), medium-carbon steels (between 0.2% and 0.5% carbon), and high-carbon steels (greater than 0.5% carbon) (Groover, 2019, p.94). The table below illustrates the properties of common low-carbon steel grades based on EN-10025 (standard of hot-rolled products of structural steels).

Steel Grades - EN10025				
Grade	**Carbon Percentage [%]**	**Yield Strenght [N/mm^2]**	**Tensile Strenght [N/mm^2]**	**Young's Modulus [N/mm^2]**
S235JR	0.17 - 0.20	225	340 - 470	206 000
S235JRG2	0.17 - 0.19	215 - 225	340 - 370	206 000
S275J0	0.18	235 - 265	410 - 560	206 000
S355J0	0.20	315 - 345	490 - 630	206 000

Table 2.2.1: Properties of hot-rolled metal products based on EN10025 (Johannessen, 2002, p.68).

2.2.2 Aluminum

Aluminum is another common construction material, and has different properties than steel. Aluminum is a non-ferrous material with generally lower yield strength and higher ductility than steel. Aluminum are lighter than steel and is often used in constructions where light weight is important. It is not as strong as steels, and is therefore only applicable for light to moderate loads depending on the yield strength. Aluminum has high thermal and electrical conductivity, as well as great corrosion resistance. It is usually alloyed with other elements, and/or heat-treated, to enhance its properties (Groover, 2019, p.99).

2.2.3 Plastics

Another common material used in tribometer design are plastics. Plastics are made out of polymers, which is a series of long-chained molecules. There are many different types of plastics, but in general they are divided into two categories called thermosetting polymers and thermoplastic polymers (Groover, 2019).

Thermosetting polymers are generally more rigid and brittle, and have greater hardness than thermoplastics. Thermosetting polymers are not suitable for reheating and reforming, and will degrade when reheated. This is unlike thermoplastics which are capable of reheating and reforming. Thermoplastics does also generally have lower hardness and greater ductility and elasticity than most thermosetting polymers (Groover, 2019).

Polyether ether ketone (PEEK) is a thermoplastic polymer commonly used in a wide range of engineering applications, including tribometer design. PEEK has outstanding chemical resistance, excellent mechanical strength-to-weight ratio across a wide temperature range, and high rigidity. These characteristics makes PEEK an excellent material choice in applications where high chemical resistance, temperature fluctuations, high strength and low weight are important. The yield strength of PEEK is in the range of 65 MPa to 120 MPa (Greene, T., 2023).

Polylactic acid (PLA) is another thermoplastic polymer commonly used in 3D printers used for prototyping. PLA is derived from organic material, such as corn starch or sugar cane. This makes the production of PLA more environmentally friendly than the petrochemical production of certain other plastics. PLA is also a biodegradable material. The yield strength of PLA is estimated to be at around 60 MPa (TWI Global, no date).

2.3 Motorized positioning stages

When providing mechanical energy to a system such as a tribometer, an electrical motor is a common and useful way of introducing that energy in the optimal direction and orientation. There are motors designed and made to fit or meet almost every prerequisite. For a tribometer, there can be requirements for speed, accuracy, position control, strength, and reliability. All of these factors depend on the size, intention, and scale of the tribometer, and are among the limiting factors for the machine after construction. When building a tribometer the motor needs to be connected to a stage (hereafter referred to as the positioning stage). The motor stage will transfer motion caused by the motor to the part intended to move. The motor stage is often a plate with threaded holes so that the movable part can easily be mounted. The motor also needs to be connected to a microcontroller and a motor driver, to enable connection and control of the motor through software. Often the microcontroller and the motor driver come as one unit referred to as a motor controller. These three components connected (motor controller, motor and motor stage) will further be referred to as a "motorized positioning stage".

Contradictory to the market of commercial tribometers, the market of motorized positioning stages are considerable. There are many different manufacturers, each with different approaches to how they design the connection between motor, motor stage and motor controller. Some manufacturers will build all these components in one unit, while some will keep them separated. The most common alternative is that the manufacturer will sell the motor and motor stage as one unit and the motor controller as an additional component.

2.3.1 Motor types

When selecting a motorized positioning stage it is important to have knowledge about some of the different types of electric motors that can be used in a motorized positioning stage. Some common and widely used electrical motor types are direct current (DC) motors, servo motors, and stepper motors. Each motor type has certain advantages and disadvantages such as power output, precision, working principle, and price. In some of the motorized positioning stages on the market today, the manufacturer will often give the buyer a choice on what motor type to include.

2.3.1.1 DC motor

DC motors are very common electrical motors, that transform electrical energy into mechanical energy using direct current as the primary energy source. Direct current will flow through copper wires, referred to as coils, wrapped around a metal base called the armature so that an electromagnetic field is generated when the DC motor is turned on. Permanent, stationary magnets, called stators, are placed on the outside of the rotating armature. To enable continuous rotation, the direction of the electromagnetic field generated by the coils and the armature needs to switch continuously. This is done by changing the direction of the current flowing through the coils and armature. There are two types of DC motors, with or without a commutator and brushes (brushless DC-motor). The difference between these is how the direction of the current is switched continuously.

DC motors are commonly used in a wide range of applications, such as electric vehicles, robotics, and industrial machinery, due to their simple deisgn and reliable performance. DC motors come in different sizes, shapes, and power ratings, making them versatile for many different applications. The DC motor is often easy to use and simple to install.

2.3.1.2 Servo motor

The servo motor is quite similar to the DC motor, but in addition to the driving parts of the motor, it has a sensor that monitors the positioning of the motor axle. The control of the motor is achieved by evaluating the angular position of the shaft through the sensor. The servo motor can be a bit more complicated than the regular DC motor, but the reward is that it is easier to control and determine the position of the motor. Servo motors are commonly used in today's market for motorized positioning stages, and high precision and control can be achieved by using a servo motor.

2.3.1.3 Stepper motor

The stepper motor is another type of electrical motor using direct current as the primary energy source. Stepper motors are commonly used in applications where high precision and control are necessary. Stepper motors consist of a stationary stator with individual phases on each step. The rotation occurs by changing what phase is energized on the stator, surrounding the rotating magnet called the rotor. The rotation occurs in steps, thereafter the name "stepper motor". A stepper motor usually has four inputs and two circuits, and typically 200 steps for a full rotation of 360 degrees (Omega, no date). Stepper motors have very good precision and control characteristics, without the need of a complicated controller. This makes stepper motors very useful in applications such as robotics, positioning systems and automation.

2.3.2 Manufacturers

To provide further information about motorized positioning stages it can be useful to look at some specific examples of manufacturers and motorized positioning stages available on the market today. Considering that the project group has worked with two types of tribometers, reciprocal and rotational, this section of the report will examine motorized positioning stages for both reciprocal and rotating motion.

2.3.2.1 Aerotech

Aerotech is an American company that has produced motion control systems since 1970. The company produces their motorized positioning stages with the motor and the motor stage as one unit but keeps the motor controller separated. Some Aerotech motion control systems have the possibility of having multiple motors connected to one single controller. Aerotech is a company that produces motion control systems aimed at industries such as aerospace, electronics, optics & photonics, medical and science & research (Aerotech, 2020b). Both of the motors in the positioning stages evaluated by this manufacturer are brushless servo motors. One of the main reasons that the project group considered Aerotech as the supplier for the motorized positioning stages for the tribometers, is that one of the previous tribometers in the laboratory had a reciprocal motor produced by this company.

For reciprocating motion the ANT95L-050 illustrated in Figure 2.3.1 is a suitable alternative for the reciprocating tribometer. The ANTL95L-050 motorized positioning stage is easy to use and can achieve very high accuracy and precise motion control. The motor stage includes a 75x90 mm surface with 13 threaded M4 mounting holes, which makes mounting the movable part of the tribometer to the motorized positioning stage relatively easy.

Figure 2.3.1: Aerotech ANT95L-050 (Aerotech, 2020b).

As illustrated in Table 2.3.1, the ANT95L-050 has a

travel range of 50 mm and a maximum speed of 500 mm/s. This makes the motorized positioning stage well suited for tribological testing, as the normal wear track length is between 10 mm to 20 mm. The normal velocity of reciprocating movement in tribological testing is between 20 mm/s to 40 mm/s. The ANT95L has a maximum vertical load capacity of 7 kg (68,67 N), and can provide a maximum driving force of 9.5 N.

For the rotating motorized positioning stage, the ADRS100 illustated in Figure 2.3.2 is a suitable alternative. Like the ANT95L, the ADRS100 is designed for easy use and have very precise motion control. The motor stage of the ADRS100 has a diameter of 95 mm, fitted with 4 M4 threaded mounting holes. It also has a through hole in the center, useful for different sample holder alternatives for tribocorrosion testing. The through hole in the center only has a diameter of 6 mm, and possible design solutions are limited by this. The motor has a maximum axial load of 7 kg (68,67 N), and is capable of providing a maximum torque of 0.48 Nm.

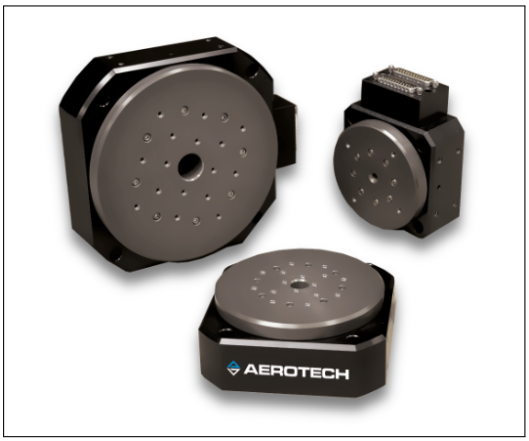

Figure 2.3.2: Aerotech ANT95L-050 (Aerotech, 2020b).

Travel range	50mm
Accuracy-Base Performance	±2.5 µm
Flatness	±1.0 µm
Maximum Force (Continuous)	9.5N
Load Capacity - Horizontal	7kg
Load Capacity - side	5kg
Material	Anodized Aluminum
Maximum Acceleration (No Load)	4g
Maximum Speed	500 mm/s

Table 2.3.1: Some chosen mechanical properties for Aerotech ANT95L-050. Information attained from the Aerotech ANT95L data sheet (Aerotech, 2020b).

Accuracy-Uncalibrated	388 µrad
Axial Error Motion	5 µm
Radial Error Motion	5 µm
Maximum Torque (continuous)	2.36Nm
Load Capacity Axial	20kg
Load Capacity Radial	10kg
Material	Anodized Aluminum
Maximum Speed	600 rpm

Table 2.3.2: Some chosen mechanical properties for Aerotech ADRS100. Information attained from the Aerotech ADRS data sheet (Aerotech, 2020a).

2.3.2.2 Physik Instrumente

Physike Instrumente (PI) is a German manufacturer of motorized positioning stages established in 1970. Most of the motorized positioning stages produced by PI include both a motor and a motor stage included in one unit. The motor controller can also be included depending on the type of motorized positioning stage selected. PI produces positioning stages with both stepper, DC, and servo motors.

For the reciprocating tribometer, a motorized positioning stage of model M-403 illustrated in Figure 2.3.3 is a suitable alternative. The M-403 is a motorized positioning stage with both a motor and a motor stage included as one unit. The motor included is either a DC motor or a stepper motor, depending on the requests from the buyer. The dimensions of the motor stage is 87x80mm with four M4 threaded mounting holes.

Figure 2.3.3: PI M-403 (*M-403 Datasheet* 2022).

As illustrated in Table 2.3.3, the M-403 motor has a maximum vertical load capacity of 200 N and can provide a horizontal driving force of 50 N. This limits the construction on top of the motorized positioning stage to 20.4 kg, ($\frac{200N}{9.81}$). The drawback with the M-403 is that it is relatively slow with a maximum velocity of 10 mm/s.

For the rotational tribometer, a suitable motorized positioning stage is the A-63X illustrated in Figure 2.3.4. The A-63X includes a servo motor and a motor stage as one unit. The motor stage is relatively big, as the smallest version of the A-63X has a motor stage with a diameter of 151 mm with M4 threaded mounting holes. As illustrated in Table 2.3.4, the motorized positioning stage is capable of providing a maximum torque of 4.7 Nm and a maximum driving force of 190 N. If this motor were to be used in a tribometer it would be capable of handling high loads and measuring large frictional forces.

Figure 2.3.4: PI A-63X (*A-63X Datasheet* n.d.).

Travel range	25mm
Maximum Force (Continuous)	50N
Permissible push force vertical	200N
Permissible push force side	100N
Material	Anodized Aluminum
Maximum Speed	10 mm/s

Table 2.3.3: Some chosen mechanical properties for PI M-403. Information attained from the PI M-403 data sheet (*M-403 Datasheet* 2022).

Accuracy-Calibrated	8 µrad
Maximum Torque	4.7Nm
Permissible push force Axial	190N
Permissible push force Radial	40N
Material	Hardcoat Aluminum, Stainless steel
Maximum Speed	500 rpm

Table 2.3.4: Some chosen mechanical properties for PI A-63X. Information attained from the PI A-63X data sheet (*A-63X Datasheet* n.d.).

2.3.2.3 MM Engineering

MM Engineering is a small company from Germany established in 1996. MM Engineering makes only the positioning stage itself and connects this to a motor and motor controller from a company called GUNDA Automation.

Their system utilizes a stepper motor connected to a motor controller, providing the flexibility to disconnect and replace either the positioning stage or the motor and motor controller individually in case of any malfunctions. This modular design enhances the overall maintenance and repairability of the system. Furthermore, the chosen stepper motors offer a cost-efficient solution, priced at approximately 10,000 NOK, making them more affordable compared to other manufacturers in the current market.

For the reciprocating motion, it would be possible to use the MM Engineering MPT3012-AK-S, illustrated in 2.3.5. The motor stage is a 75x75mm surface with four M4 threaded mounting holes, each placed in one corner. MPT3012-AK-S has a maximum driving force of 60 N and a maximum permissible vertical load of 60 N. The motorized positioning stage has a maximum velocity of 20 mm/s. This is not as fast as many of the other manufacturers on the market and can be a limitation considering that normal velocities during tribological testing range between 20 mm/s to 40 mm/s.

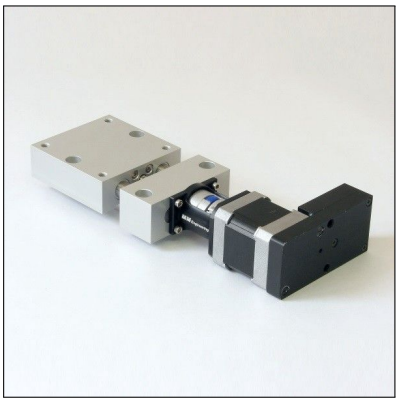

Figure 2.3.5: MM Engineering MPT3012-AK-S (*Motor positioning tables* 2021).

For the rotating stage, an MDT360110-QN-MO-S could be a suitable alternative, illustrated in Figure 2.3.6. The MDT360110-QN-MO-S has four M6 threaded mounting holes, and two additional M4 threaded mounting holes, making mounting symmetrical assemblies on top of the stage easy and user-friendly. As illustrated in Table 2.3.6, the MDT360110-QN-MO-S has a maximum torque of 1.75 Nm and a maximum permissible vertical load of 190 N. The maximum output speed of the MDT360110-QN-MO-S is 300 rpm.

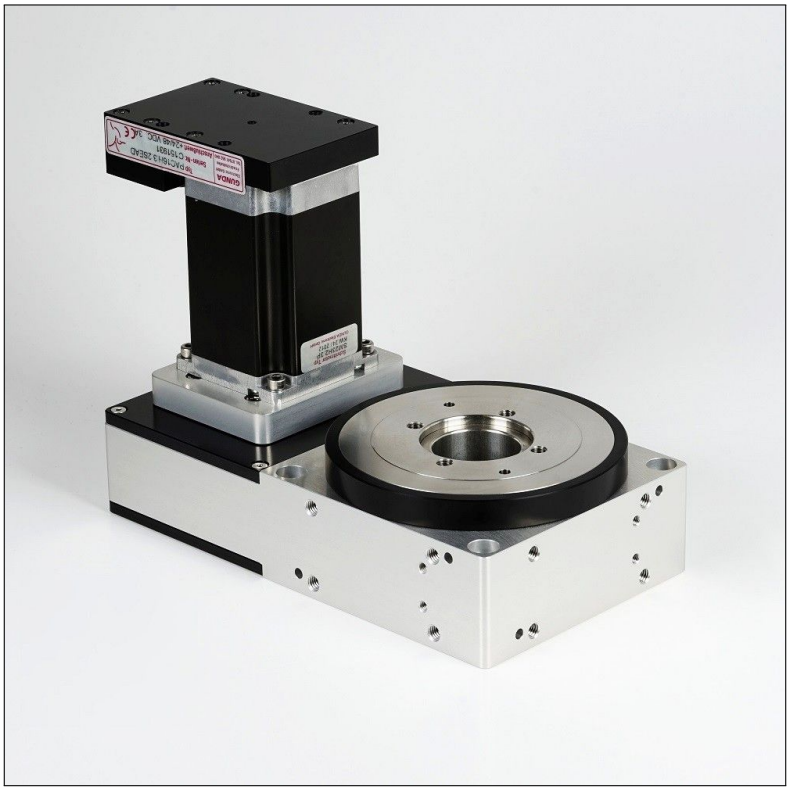

Figure 2.3.6: MM Engineering MDT360110-QN-MO-S (*Motor rotary tables* 2021).

Travel range	30mm
Maximum Force	60N
Permissible force vertical	60N
Permissible force side	100N
Material	Anodized Aluminum, stainless steel, Plastic
Maximum Speed	20 mm/s

Table 2.3.5: Some chosen mechanical properties for MM Engeneering MPT3012-AK-S. Information attained from the MM Engineering MPT3012-AK-S data sheet (*Motor positioning tables* 2021).

Maximum Torque	1.75Nm
Permissible force Axial	190N
Permissible push force Radial	40N
Material	Hardcoat Aluminum, Stainless steel
Maximum Speed	300 rpm

Table 2.3.6: Some chosen mechanical properties for MM Engeneering MDT360110-QN-MO-S. Information attained from the MM Engineering MDT360110-QN-MO-S data sheet (*Motor rotary tables* 2021).

2.4 Force transducers

In order to record the friction forces during tribological testing, a load cell or some other type of sensor is commonly used. There are several types of sensors and load cells suitable for this purpose, but the most common and relevant are piezoelectric load cells and strain gauges. Both piezoelectric load cells and strain gauges convert forces into electrical signals that can be

measured and recorded. The electrical signals increase as the force increase. The common name for such sensors are force transducers (Wikipedia, 2023a).

2.4.1 Piezoelectric load cell

Piezoelectric load cells are usually small and compact sensors capable of measuring dynamic or quasistatic forces, such as compressive and tensile forces. Piezoelectric load cells consist of a crystal element (commonly quartz) that emits voltage proportional to the load applied. This voltage can further be integrated into a circuit (normally through a charge amplifier) and used to track and record the forces applied to the piezoelectric load cell (Cadence PCB Solutions, 2020). Piezoelectric load cells are commonly used to measure dynamic forces, such as acceleration, vibrations, and/or rapidly changing forces. Additionally, piezoelectric sensors are usually small and compact in size and can achieve precise measurement results over a wide range.

2.4.2 Strain gauges

Strain gauges are sensors that measure the strain or deformation of the object it is installed on. The resistance in the electrical circuit of the strain gauge varies proportionally to the strain or deformation applied to the object. This variation in resistance can further be included in an electrical circuit so that the strain or deformation can be recorded. This information can be used to calculate the force needed to achieve the strain of the object. The way this works is that when a strain gauge is installed on the object, and deformation or strain is present, the strain gauge will stretch or compress. This causes the resistance in the circuit of the strain gauge to vary accordingly. Strain gauges are highly sensitive and accurate and are capable of measuring small changes in strain and deformation, and therefore also suitable for measuring small forces. Strain gauges are commonly combined with a Wheatstone bridge circuit to measure small forces or strains with high sensitivity. A Wheatstone bridge is a small electrical circuit with four resistors, including the strain gauge. This circuit converts a change in resistance into a corresponding change in output voltage (Sirohi, 2017; Mohammed et al., 2014).

2.5 Electrical

When working with electrical connections, and motors, electrical knowledge is important. An electrical circuit can consist of many different elements, such as wires, capacitors, transistors, diodes, and so on. These components are combined to create electronic circuits that perform specific functions, such as amplifying signals, storing information, or generating power. It is also important to have knowledge about the main elements of electricity, such as voltage, current, and resistance. Voltage (V) describes the difference in potential energy between two points in a circuit. More voltage corresponds to more electric potential between the two points in the circuit. Voltage is what makes the electric current flow between two points in a circuit (Hioki, no date). Current (I) describes the amount of electricity flowing through each wire. The more current, the more electrons are flowing through the wire. Usually, this means that for a higher current, a wider cable is needed to make room for the electrons. Resistance (Ω) describes the resistance of current flow in a circuit, wire, or electrical component. More resistance usually corresponds to less current flow through the resistor (Mazur, 2001).

2.5.1 Prototyping boards

Prototyping boards in short are used to prototype electrical circuits and test circuit designs, layouts, and components before committing to make a PCB or creating some permanent version of the circuit. There are multiple types of prototyping boards where some are solderable and some are solderless.

Breadboards are a type of prototyping board used to quickly build, test and evaluate low-power circuits. It usually consists of a plastic board with a grid of holes arranged in rows and columns, including metal clips or springs inside the holes to allow electronic components such as resistors, capacitors, and integrated circuits to be inserted and connected together without the need for soldering.

2.5.2 Soldering

As opposed to breadboards, a more permanent solution of connecting electrical components can be done using soldering. Soldering is a process used to join two or more metal objects together by heating them to a temperature where a filler metal (solder) melts and flows into the joint, forming a semi-permanent bond when it cools and solidifies. The soldering process typically involves the use of a soldering iron or other heating tools, along with a flux material that helps to clean the metal surfaces and improve the flow of the solder. Soldering is commonly used in electronics to join components together and create a semi-permanent electrical connection between them.

2.6 Software

Programming is the creation of digital instructions for both digital and physical components to achieve specific tasks. The choice of a programming language depends on factors such as intended use, available assets and functionalities, integration capabilities, code structure, optimization needs, and graphical interface requirements. It allows for the development of software and interfaces by leveraging a variety of languages, libraries, and tools.

2.6.1 Languages

Programming languages are used to create software applications for various purposes, including data analysis, web development, and game development. The choice of programming language depends on the requirements of the project, available resources, and personal preferences. Some popular programming languages include:

- Python - A high-level programming language known for its simplicity, readability, and versatility. It is commonly used for data analysis, machine learning, web development, and scientific computing.
- Java - An object-oriented programming language used to create desktop applications, web applications, and mobile applications. It is known for its portability, security features, and large community support.
- C/C++ - Low-level programming languages used for system programming, embedded systems, and developing software for microcontrollers. They are known for their efficiency, speed, and ability to directly access hardware.
- JavaScript - A programming language used for web development and creating interactive user interfaces. It is known for its flexibility, versatility, and ability to manipulate web page elements.
- MATLAB - A high-level programming language that is widely used in engineering, science, and mathematics.

2.6.2 Libraries

In the context of programming, a library is a collection of precompiled code modules or functions that provide specific functionality or resources that can be utilized by other software applications. It is designed to simplify programming tasks by providing ready-to-use components, algorithms, or tools that developers can leverage in their projects.

A library typically includes a set of functions, classes, or data structures that encapsulate specific functionalities or provide access to external resources, such as databases, hardware devices, or network protocols. Libraries can be written in various programming languages and can range from small utility libraries to large and comprehensive frameworks (Rouse, 2016).

Libraries are reusable and modular, allowing developers to save time and effort by incorporating existing code rather than writing everything from scratch. They promote code reusability, modularity, and maintainability by encapsulating complex functionalities into well-defined and easily accessible components.

2.6.3 Matlab

MATLAB is a widely used high-level programming language specifically designed for engineering, science, and mathematical applications (MathWorks, no date). Its user-friendly nature and intuitive interface make it accessible to both novice and experienced programmers. MATLAB's key strengths lie in its comprehensive support for numerical analysis, linear algebra, and data visualization, as well as its extensive library of specialized toolboxes for domains like signal processing, control systems, and optimization. This language is particularly advantageous for data analysis tasks, offering robust capabilities for importing, cleaning, manipulating, and visualizing data. Moreover, MATLAB excels in algorithm development, simulations, and model implementation, boasting a vast collection of built-in functions and support for object-oriented programming. With its ability to interface with external hardware, such as Arduino boards, MATLAB is widely used for prototyping, developing control systems, and creating embedded applications. Overall, MATLAB's versatility, powerful features, and broad application scope make it an indispensable tool in the fields of science and engineering.

2.6.4 Arduino

Arduino is a popular open-source electronics platform that can be programmed to read and process sensor data. With the help of sensors and modules such as accelerometers, gyroscopes, temperature sensors, and distance sensors, Arduino can read physical phenomena and convert them into electrical signals. These signals are then processed by the microcontroller on the Arduino board, which runs a program created by the user. The program can be written in the Arduino Integrated Development Environment (IDE), which is a free software application that simplifies the process of writing code for Arduino boards (Arduino, 2018).

Once the program is uploaded to the board, the Arduino can read the sensor data and communicate it to a computer through a serial connection. The computer can then process and analyze the data using programming languages such as MATLAB, Python, or C++. This makes it possible to create a wide range of applications, from simple data logging to complex real-time control systems.

Methodology

3.1 Design methodology

The design and development process during this project is based on the book *The Mechanical Design Process* (2010) by David G. Ullman. The book describes the fundamentals of mechanical design and the different steps and pathways to follow during the design and development of mechanical products. The information given in the book was used as a basis for the design and development process during the project, and to give the project group a guide for planning the design and development process.

3.1.1 Design process

The design process was based on the process described as "the engineering design process", as illustrated in Figure 3.1.1, in addition to the *The Mechanical Design Process* (2010) by David G. Ullman. The design and development module of the project was based on an iterative approach, where suggested solutions were tested, evaluated, and improved.

The "engineering design process" describes the common practice of how engineering projects often are planned and executed. This method was used by the project group when planning and executing the project and made it easier to plan, organize and structure the work. The "engineering design process" is a useful approach when planning and executing engineering projects, as it gives a clear method and guidelines on how to approach and execute a project. The "engineering design process" and its basic principles are illustrated in Figure 3.1.1. The method is especially useful when planning and designing a machine, as it is based on an iterative approach where brainstorming, prototyping, testing, and iterative improvements are common practices.

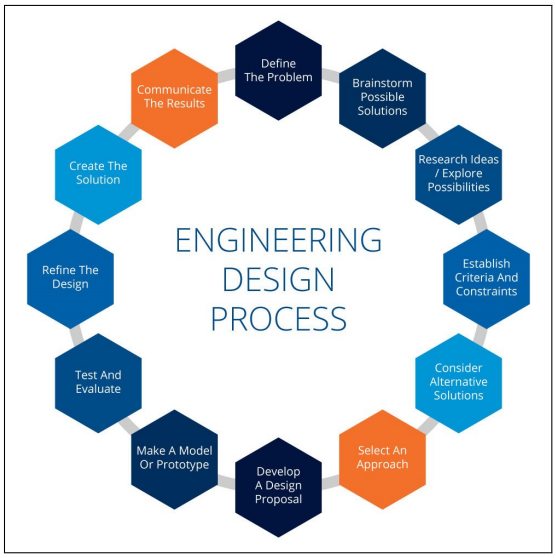

Figure 3.1.1: Engineering design process (Teach Engineering, No Date).

The methods used by the project group to plan, execute and evaluate the design and development of the tribometers are explained in detail in this chapter.

- **Define the problem.** In the initiation phase of the project, the project group first started by defining the problem. This was done together with advisors and project owners, to make sure that everyone in the project group had a clear understanding of the problem. A clear problem definition is important in order to make a good plan on how to solve the problem. The problem, in this case, was that the tribology laboratory did not have a rotating tribometer capable of conducting normal and tribocorrosion testing. The reciprocal motor had broken down, and the tribology laboratory needed a new reciprocal tribometer. The problem definition was established in a document (the project rationale) and made available to all project members. This way, each project member had access to the problem definition at all times. Additionally, the project goals were included in the document, and all other relevant information regarding the problem, reasons for the needs, and future goals and

expectations.

- **Research and attain knowledge and information.** The next step in the design and development process was to research already existing literature regarding tribology and tribometers. Additionally, a literature database was created to gather all relevant literature in one common place. This was done to establish a foundation of knowledge within the field of tribology and tribometer design, and to make sure that all project members had access to relevant literature. The quality of the literature selected was also evaluated continually. ScienceDirect and Researchgate were primary sources of literature, but other databases were used as well. Certain books were acquired from the library at NTNU, to gather additional information relevant to the project. Additionally, the project group did several observations of already existing tribometers. This was done to attain as much information as possible on previous tribometer designs, and their working principles. Conversations and meetings with advisors and professionals in the field of tribology were done, in order to establish a solid understanding of tribology and the working principles of a tribometer. The project group also applied to the course "Tribology and Surface Technology" at NTNU, to gather even more useful knowledge relevant to the project.
- **Establish design criteria and requirements.** The next step was to gather as much information as possible about the requirements and specifications of the new tribometer, such as expected load cases, operating conditions, test methods, potential users, equipment needed, budget, and so on. Already existing tools, parts, and calibration methods were taken into consideration, to make sure all relevant information was included. Additionally, information regarding existing parts available to use was established in this phase. In this phase, the project group was made familiar with the equipment at the tribology laboratory at NTNU, and where the new tribometers would be stationed. The information gathered in this stage of the design process was stored in a common document, to make sure that all project members had access to the design criteria and information at all times.
- **Brainstorm ideas and possible solutions.** Thereafter, sketching and brainstorming ideas on how to include all requirements and specifications in the best way possible was done. This was done during several meetings within the project group, with guidance and supervision from advisors and researchers in the field. A list of suitable concepts and design solutions was developed, where the weaknesses and strengths of each idea were discussed. This was a very collaborative phase of the project, as multiple meetings and consultations were executed. The most suitable designs, with the best solutions, were selected as the main basis for developing the tribometers. Additionally, iterative improvements on design ideas and sketches were done in this stage of the design process as new and better ideas were proposed. Suitable parts and components needed were also discussed during this phase, and consultations with several manufacturers and suppliers were established.
- **CAD-Modelling, simulations, and iterative improvement.** Thereafter, CAD modeling and simulations were conducted to ensure that the proposed design solutions could handle the expected load cases. Additionally, design improvements and the development of new concepts were done. This was an iterative process, where new and better design solutions were implemented when needed. The selection of materials was also done during CAD modeling and simulation, with consideration to all requirements such as corrosion resistance and requirements of rigidity and stiffness.
- **Prototype and test.** The next stage of the design process was the prototyping of parts. This was done using 3D printers with PLA filament. The first prototypes were printed with 15% infill, to accelerate the prototyping stage and save time. Prototyping with 100% infill was done during the final stages of the prototyping stage, to ensure that all parts and components fitted together before planning the production and manufacturing stage. Not all parts or components were printed with 100% infill, due to limited time, capacity, and

access to 3D printers.

- **Redesign and improve.** When the first stages of prototyping were complete, and all parts and components were assembled. The strength and weaknesses of the prototypes were evaluated. Poor design solutions and non-optimal parts are easier to evaluate with a physical prototype. The prototyping phase was a very iterative process, where multiple improvements and implementation of new and better ideas were conducted. Collaboration within the project group was also very present in this phase of the project, where frequent feedback and evaluation were encouraged.

3.1.2 Computer-aided design and simulation

The process of CAD involves using specialized software and tools to generate, modify, and analyze designs in a virtual environment. The project group had the following methodic approach to the computer-aided design process.

- **Conceptualization and sketching.** Initially, hand-drawn sketches and design ideas were created to explore various concepts. The project group reviewed and agreed upon the most promising ideas within the team before proceeding to the CAD modeling phase.
- **Solidworks modeling.** The selected design ideas were then modeled using Solidworks. The group accurately translated the hand-drawn sketches into 3D models and established suitable dimensions for the components to ensure proper assembly and meet the given requirements.
- **Assembly and mating.** Once the individual components were modeled, an assembly was created within Solidworks. This step involved ensuring the correct mating of the parts and making necessary adjustments or modifications to achieve proper fit and functionality.
- **Material selection.** After the assembly was completed, the project group considered various factors such as strength requirements, rigidity, corrosion resistance, and machinability to select suitable materials for each component. These material selections were then implemented into the CAD model.
- **Static analysis.** To evaluate the structural integrity and performance of the design, static analysis was conducted. The project group defined appropriate boundary conditions and load cases based on the intended application. Meshing, which involves dividing the model into smaller elements, was applied to accurately simulate the behavior of the components.
- **Simulation evaluation.** The results obtained from the static analysis, including stresses and displacements, were thoroughly examined to ensure they met acceptable criteria. If any discrepancies were identified, the designs were improved by making necessary modifications, and new simulations were performed to validate the changes.
- **Iterative improvements and development.** Throughout the CAD modeling and simulation procedure, the project group followed an iterative approach. They continuously refined and developed the parts and components based on the insights gained from the simulations. This iterative process enabled them to achieve increased design accuracy, improved efficiency, faster iterations, and the ability to explore and test designs before eventual physical production.

3.1.3 Prototyping

To prototype the various mechanisms and components, the project group made extensive use of the 3D printing capabilities available in the faculty's mechatronics laboratory. The CAD

software played a crucial role in this process, as it allowed for the creation of digital models that could be translated into physical prototypes.

The CAD software provided numerous benefits for the prototyping process. Firstly, it enabled the project group to visualize their designs in a virtual environment, allowing them to assess the functionality and aesthetics of the prototypes before printing. This helped in identifying any potential design flaws or areas for improvement.

Additionally, the CAD software allowed for easy modification and iteration of the designs. If a prototype did not meet the desired requirements or needed adjustments, the digital model could be quickly modified, and a new prototype could be printed. This iterative approach facilitated the exploration of multiple design solutions and the ability to refine the prototypes based on test results and feedback.

The 3D printing technology in the mechatronics laboratory was instrumental in bringing the CAD designs to life. It enabled the project group to physically realize the prototypes using various materials and printing techniques. This hands-on approach allowed for a more tangible evaluation of the design's functionality, fit, and overall performance.

By leveraging the benefits of CAD software and 3D printing, the project group could efficiently prototype different mechanisms and components, accelerating the development process and enabling them to choose the most suitable design solutions for the project.

3.2 Risk management

In order to mitigate the potential risks associated with component failure or other unforeseen modes of failure, the project group implemented a risk management approach within the constraints of time and budget.

Where feasible, the project group tried where possible to strategically order multiple copies of essential chips or components, examples of such purchases are the HX711 chip and power cable for the Arduino. This redundancy in critical components aimed to provide a backup in case of failure, ensuring that the project could continue without significant disruption.

However, it was recognized that certain components, such as the motor and rotational table, were too expensive to have redundant replacements. The cost implications, along with considerations such as insurance coverage, were taken into account when making decisions about component redundancy. In these cases, the project group relied on the assistance and advice of experts in the field, leveraging their expertise to minimize risks and optimize the use of available resources.

By incorporating risk management practices, such as component redundancy where possible, the project group aimed to reduce the impact of potential failures and enhance the overall resilience of the project.

3.3 Troubleshooting

To streamline the troubleshooting process and minimize time spent on identifying and resolving issues, a systematic approach inspired by scientific methodology was adopted. The key principle was to modify only one variable at a time, allowing for a focused investigation to identify the potential source of the problem.

By following this approach, the project group aimed to systematically exclude their own efforts as the cause of the issue before exploring other factors. This method helped to eliminate common

pitfalls often referred to as "PICNIC" (Problem In Chair, Not In Computer) problems, where the source of the issue is a human error rather than a technical malfunction.

Once the project group had ruled out any errors or oversights on their part, attention was shifted to other elements, such as the components used, wiring connections, or external factors that could affect the system's performance. This systematic troubleshooting methodology facilitated a more efficient and targeted problem-solving process, ultimately leading to more effective resolutions and reduced downtime.

Project Constraints

This chapter will present the limitations and constraints associated with the design and development of the new tribometer. Many of these constraints are somehow connected to the tribology laboratory at the Institute of Industrial and Mechanical Engineering at NTNU. In this laboratory, different tribometers used for research are located and this is where the tribometers developed by the project group will be placed.

Building a new laboratory device requires extensive knowledge of how the device can be utilized and implemented with the rest of the laboratory. While working at the tribology laboratory, it becomes to a realization that the people working there are surrounded by loose parts such as samples, pins, sample holders, etc. It is therefore preferred that as many tribometers as possible use the same type of loose parts, such as samples, sample holders, and pins. This makes the work in the laboratory more effective, user-friendly, and modular.

4.1 Previous tribometer

One of the main reasons why the project group got to work on the project was that the motor in a tribometer in the laboratory broke down. This tribometer was a reciprocating tribometer with the possibility to perform tribocorrosion experiments. The previous tribometer is illustrated in Figure 4.1.1. One of the major aspects of the task was to cover the need this tribometer had, as well as develop a better design solution. To make the construction more cost-efficient, it was desired that some of the old tribometer's components be used in the new one, such as the optical table, potentiostat, and sensor.

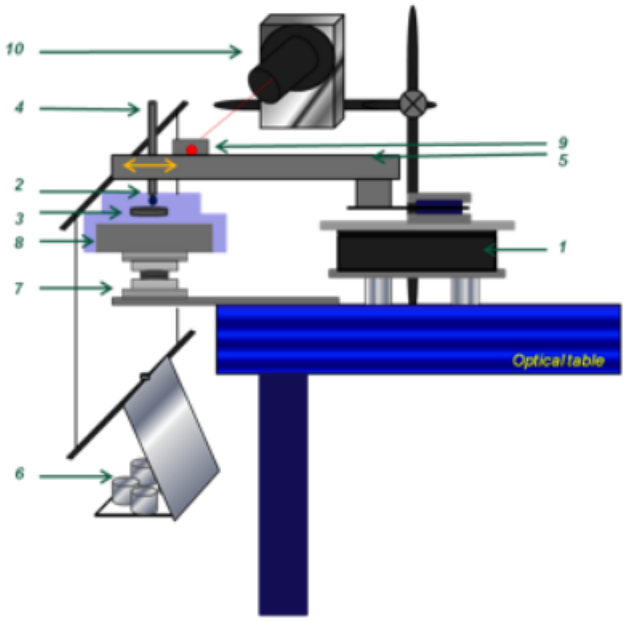

Figure 4.1.1: Schematic view of old tribometer (Laurent and C., 2013).

4.1.1 Optical board

The tribometers developed by the project group needed to fit the optical board used by the previous tribometer. The equipment is mounted on the optical board to limit disturbances to the measurements caused by vibrations or other factors. The optical board is a rigid vibration control platform designed to have minimal deflection. The top surface of the optical table has the following dimensions: 750x750mm, with 25 mm centers - M6 threaded holes in a grid pattern. Every part designed by the project group to be mounted and fixed on the optical board is fitted with close M6 clearance holes centered 25, 50, 75, 100... mm apart, as illustrated in Figure 4.1.2. The optical board is placed on top of a heavy steel table with a rigid shelf below, giving extra space for placing motor controllers, potentiostat, amplifiers, and other components. Because the tribometers are going to be placed on the same optical board, To avoid interference between the rotary and reciprocal tribometers' results, it was decided not to operate them simultaneously.

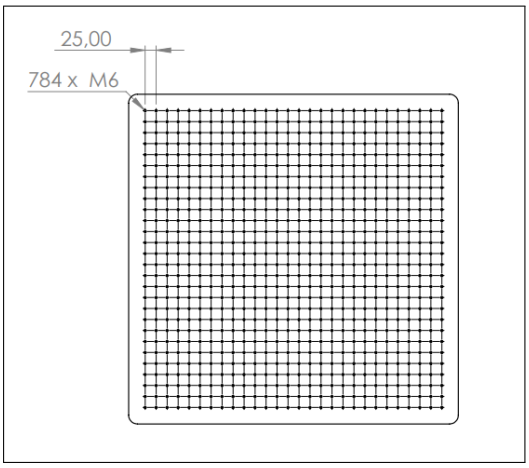

Figure 4.1.2: Techmfg 78-225-12R optical board illustration.

4.1.2 Sensor

From the earlier tribometer, the group had access to a force sensor that would be used in the project. The sensor is a triaxial piezoelectric sensor from Kistler with model number 9327A. The Kistler 9327A is mounted under preload between two plates and can measure compressive and tensile forces (*Kistler-9327A-datasheet* n.d.). For this sensor, the project group also had access to two Kistler 5018A charge amplifiers.

As illustrated in Table 4.1.1, the 9327A can measure a force in the y-direction from $-2700N$ to $2700N$ with a sensitivity of $-7,912pC/N$, which is the direction where the friction force will occur when the tribometer is running. In the z-direction, the sensor can measure up to $-5000N$ with a sensitivity of -3.755pC/N. Each signal is amplified by a Kistler 5018A charge amplifier. The mounting of the sensor is done with eight M6 screws, as illustrated in Figure 4.1.3. Considering that the mounting holes in the sensor are threaded and do not have an equal center distance as the optical table, the sensor needs to be built on top of a plate (referred to as the sensor stage).

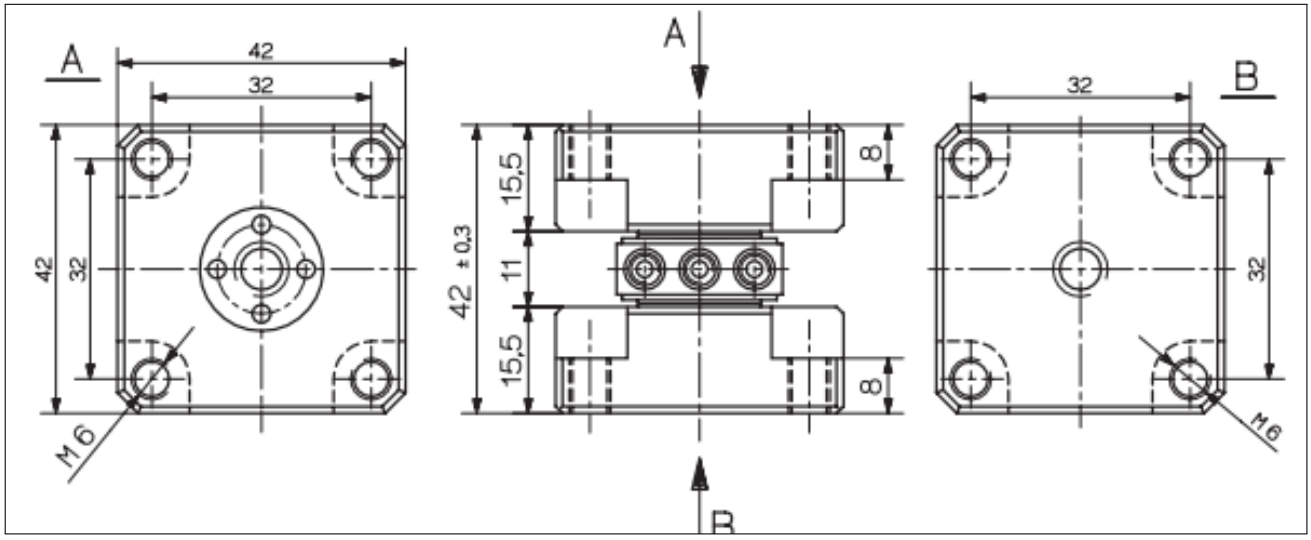

Figure 4.1.3: Kistler 9327A drawing (*Kistler-9327A-datasheet* n.d.).

Range F_x, F_y	$-2.7kN$-$2.7kN$
Range F_z	$-5kN$-$5kN$
Sensitivity F_x, F_y	$-7,912pC/N$
Sensitivity F_z	$-3,755pC/N$
Max. moments	$\pm$14Nm
Weight	$0.39kg$

Table 4.1.1: Some chosen mechanical properties for Kistler 9327A (*Kistler-9327A-datasheet* n.d.).

The sensor stage was built as a plate with four holes in a rectangle with dimensions 75x50 mm so that it would fit the optical table. The mounting holes for the sensor are counterbore holes so that the mounting screws have a head clearance, to allow for correct assembly with the optical table.

4.1.3 Pin

The pins used in the old tribometer are the same pins that are used in one of the other tribometers at the laboratory. The project group wanted to build new tribometers with the ability to use the same pins. The pins are cylindrical with a height of 100 mm and a diameter of 10 mm. The material used for the pins is Polyether Ether Ketone (PEEK).

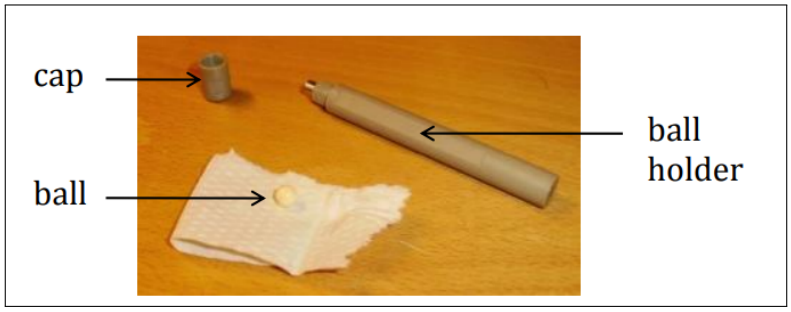

Figure 4.1.4: Pin (Laurent and C., 2013).

4.1.4 Sample holders

In the laboratory, there are several types of sample holders available for dry and lubricated testing. One of the requirements for these is that they need to be able to hold 20 mL of liquid. A preferred sample holder designed by one of the scientists in the laboratory is a stainless steel ring with an indent for the sample and an o-ring to secure the lubricant from leaking out during testing. It is therefore requested that the project group design the tribometers with the capability of using these, or very similar rings during testing.

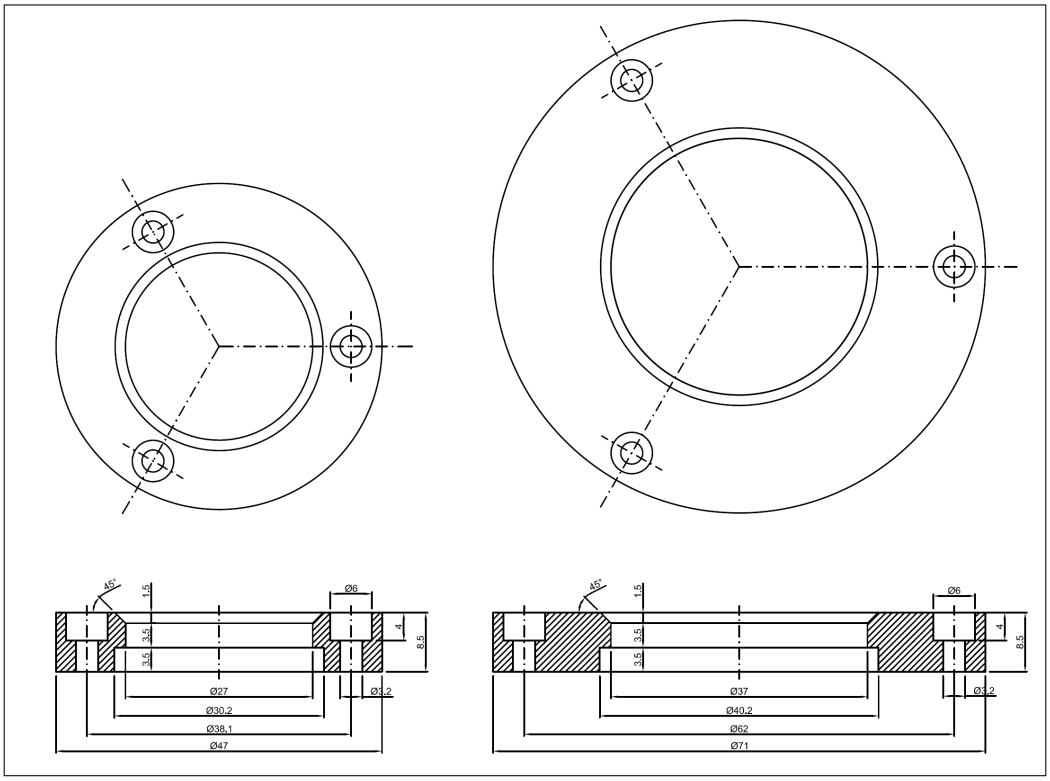

Figure 4.1.5: Drawing of existing dry and lubrication sample holders (designed by one of the scientists at the tribology laboratory).

4.1.5 Potentiostat

One of the primary functions of the previous tribometer was to conduct tribocorrosion testing, which involved connecting the test samples to a potentiostat. The existing potentiostat remains functional, and the project framework includes the provision for the tribometer samples to be compatible with it. Typically, this is achieved by developing a specialized sample holder dedicated to tribocorrosion testing. The sample holder must be constructed using an insulating material capable of containing 50 mL of liquid. Regarding reciprocating motion, the laboratory already possesses some tribocorrosion sample holders that are intended for use. However, these sample holders are not suitable for rotational motion. Therefore, a more intricate solution is required, necessitating the design efforts of the project group.

4.2 Sample

After consulting with advisors it was determined that the sample dimensions would be a disc with a diameter of 30 mm and 40 mm. The thickness and material of the sample vary between 4 mm to 7 mm depending on the test. Therefore, the project group had to design sample holders capable of using samples with the dimensions mentioned above.

4.3 Load capacity

The tribometers must be capable of conducting tribological experiments with normal loads ranging from 10 N to 50 N. These loads will be applied directly above the contact point of the pin, using existing free weights in the laboratory. To ensure the tribometers' ability to withstand this force, a safety factor of 1.2 was incorporated into the calculations, resulting in a maximum dimensioning load of 60 N (50 N $\cdot$ 1.2). Moreover, to enable the measurement of all friction

forces that may occur during experiments, the tribometers will be designed to measure friction coefficients within the range of 0 to 1.

4.4 Velocities

In order to meet the experiment specifications, it is necessary for the tribometers to have the capability to set the velocity within the software. For the reciprocating tribometer, it is required that the experiment's velocity can be adjusted up to 25 mm/s. This velocity will result in a 1 Hz oscillation for the tribometer when conducting experiments with a 10 mm wear track. On the other hand, the rotational tribometer must be able to achieve a velocity of 300 rpm. These requirements will influence the selection of motorized positioning stages that are well-suited for the tribometers. It should be noted that the velocity will be set prior to initiating the experiment, and there is no requirement for the tribometers to adjust the velocity once an experiment is ongoing.

4.5 Wear track

Another essential requirement for the tribometers is the ability to adjust the length of the wear tracks. In the case of the reciprocating tribometer, it is necessary to have the capability to set the wear track length within the range of 0 to 20 mm. Similarly, for the rotational tribometer, the requirement is to adjust the wear track length from 0 to 15 mm. It is important to note that the wear track length will be established prior to the commencement of the experiment, and there is no requirement for the tribometers to be able to modify the wear track length once the experiment is in progress.

4.6 Software

To ensure a user-friendly presentation of the test results, the tribometers are connected to software that offers real-time test results and the ability to save data in a retrievable file format, such as CSV or Excel. The software is installed on a stationary computer located within the laboratory, establishing a direct connection to the tribometers. This setup enables seamless data acquisition, analysis, and storage of the test results, enhancing convenience and accessibility for the users. The software's features facilitate efficient data management and allow for easy retrieval and utilization of the test data for further analysis and reporting.

Design and Development

5.1 Design criteria

When developing different solutions and prototypes, the group set four criteria to evaluate the effectiveness of the design. The criteria are listed below.

- **High rigidity and stability.** The tribometers must be highly rigid and stable to secure trustworthy test results. The tribometers are not designed to limit weight or to use the least amount of material but rather focus on rigidity and stability. The loads on the tribometer are small, and the construction is "over-dimensioned".
- **Modular and user-friendly design.** The tribometers need to be modular and user friendly, to provide possibilities of moving and easy mounting. Therefore, the tribometers are designed with a focus on easy assembly and disassembly. they are highly modular and easily configurable. Most of the main fasteners are M6 or M4 socket head screws, as these types are easily accessible at the laboratory, and to standardize the assembly.
- **Stable load onto sample**. The load on the tribometers is going to be applied with dead weights. Too much movement in the system might influence the weight transfer of these weights, and it is, therefore, important to evaluate how well the force generated by the dead weights gets applied to the sample.
- **Simplicity** The parts in the constructions are going to be machined, and it is therefore important to evaluate which constructions that are going to be possible to produce.

Certain requirements for the tribometers were also established at the beginning of the project, as listed below.

- **Load capacity of 50 N.** The load capacity of the tribometers needed to be 50 N, with a maximum COF of 1. This was the initial request by the project owners but was reduced to 20 N for the rotational tribometer.
- **Possibility of testing both with and without tribocorrosion.**
- **Adjustable wear track for the rotational tribometer.** The rotational tribometer needed to have the ability to adjust the wear track from 0 mm to 15 mm.
- **Adjustable COG.** The tribometers needed to have the ability to adjust the COG, to ensure that the weight of the tribometer and its components do not influence the normal force applied to the sample.
- **Software to provide test results.** The tribometers needed to have included software to provide test results in a user-friendly way, both live and as a file post-testing.

5.2 Reciprocal tribometer

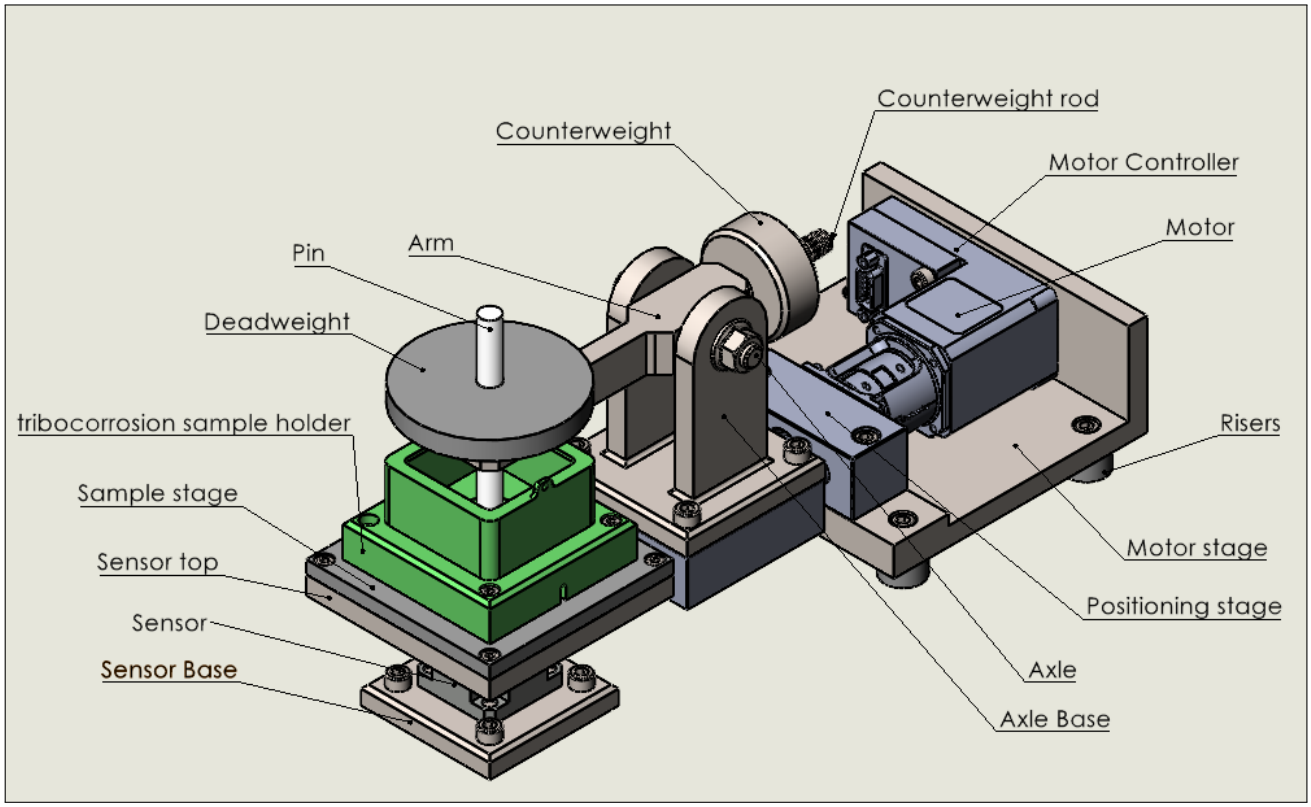

Figure 5.2.1: Reciprocal tribometer.

When designing the reciprocal tribometer it was quickly decided that the sample was going to be placed on top of the sensor as in the previous tribometer. This was because it would be the easiest solution to utilize the characteristics of the Kistler 9327A sensor in the project. After consulting with the advisors it was quickly established that it was desired to build a tribometer with similar functions as the one they had earlier, and therefore, a natural first step was to map out the different components and the different parts in the laboratory that could be used in the new tribometer. Integrating the machine into the laboratory setup and optimizing material usage were key considerations. Placing the sample on top of the sensor necessitated positioning the arm and dead weights on the motorized stage, which would move back and forth. As a result, the force exerted by the system of dead weights and the arm would impact both the sample and the motor's acceleration. To ensure proper functioning of the tribometer, it was crucial to achieve a well-balanced configuration with a relatively low mass.

5.2.1 Load cell

When designing a reciprocating tribometer it is possible to mount the load cell both to the arm or to the sample. The advantage of assembling the sensor to the arm is that the arm and the deadweights are going to be stationary, which will give the sample a more stable load than mounting the sample to the sensor. When researching the landscape of other reciprocal tribometers, the project group discovered that the most common introduction of the movement was through the sample and not the arm. The project group had access to the Kistler 9327A sensor and the required amplifier. This sensor would be well-suited because of its high precision and is ideal with static samples. However, considering the movable arm in the setup, it was anticipated that using this sensor in the reciprocal tribometer would yield more accurate measurements compared to using a cheaper strain gauge mounted on the arm. Hence, it was concluded that the optimal utilization of the sensor would be in the reciprocal tribometer con-

figuration. Additionally, the project group wanted to make one tribometer with a movable arm and one tribometer with a stationary arm, and making a rotational tribometer with a movable arm would be much more difficult than a reciprocating one. This means that the arm needs to be connected to the motorized positioning stage. This is the same solution used in the old tribometer, and the sensor is well-suited for a solution like this.

Since the dimensions of the sensor and the optical table are not the same, the sensor needed to be built onto a stage (sensor stage). The sensor stage was constructed as a rectangular plate measuring 75x50 mm, specifically designed to fit the dimensions of the optical table. Four CBORE holes were incorporated into the plate to accommodate the sensor. This design choice ensures that the screw heads do not protrude from the underside of the plate, providing flexibility for designing other components in the assembly. Additionally, a second plate with similar CBORE holes, but with size and shape influenced by the sample holders, would be placed on top of the sensor. (figure: 5.2.2)

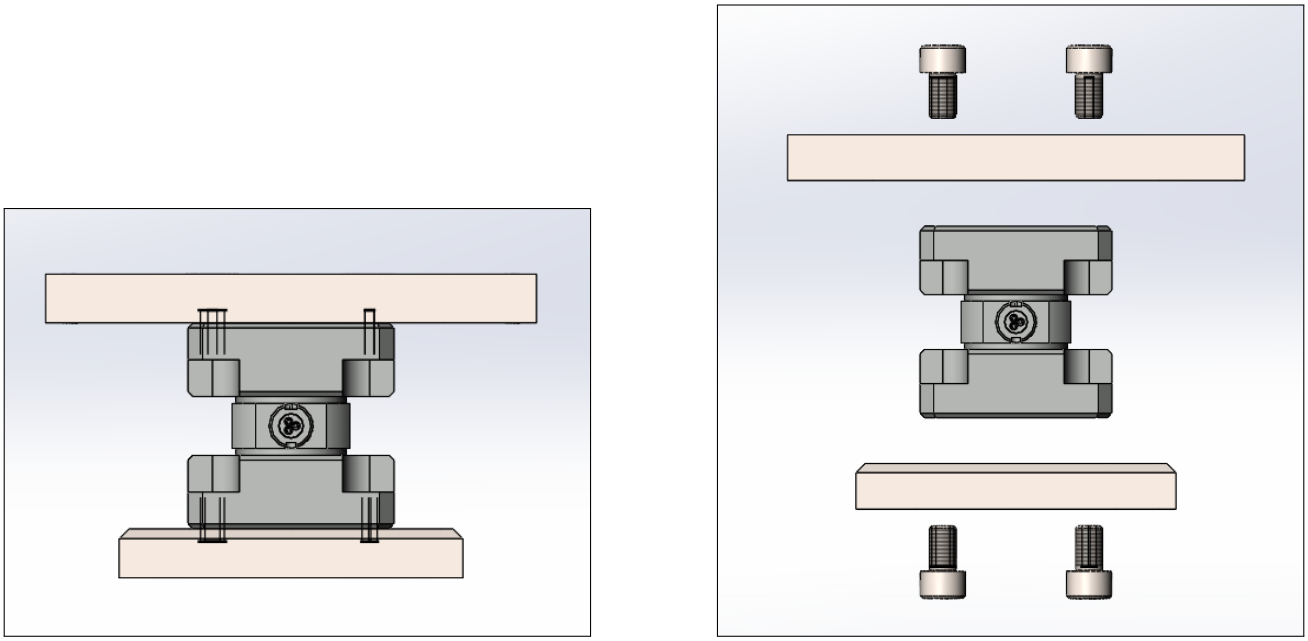

(a) Kistler 9327A with mounted plates.

(b) Exploded view Kistler 9327A with mounted plates.

Figure 5.2.2: Mounting of the Kistler 9327A

Given the load requirements in Chapter 4.3 added with a safety factor of 1.2, the maximum vertical load the sensor needs to withstand is 60N added with the weight of the sample and sample cell. The maximum load capacity of the sensor is 5000N (table 4.1.1), and since the project group can assume that the weight of the sample and the sample stage will be much less than 4940N, the load capacity is more than high enough for the tribometer. The maximum friction force that is going to be measured in the tribometer will be decided by the maximum added normal force of added load multiplied by the maximum coefficient of friction of 1. This gives us:

$$F_f = F_N \cdot \mu$$
$$F_f = 60N \cdot 1$$
$$F_f = 60N$$

Since the movement on top of the sensor is reciprocating, this means that the sensor needs to be able to measure a force between -60N to 60N. As indicated in Table 4.1.1, the applied force falls within the measurement range of the sensor, which spans from -2700N to 2700N.

The Kistler 9327A is a triaxial sensor meaning it has the capacity of measuring on both x, y, and z-axis. Anyways in the tribometer, the project group is only going to use the y-axis to measure the friction force, and will therefore only need one amplifier. The amplifier that will be used is a Kistler 5018A which is already present at the laboratory (illustrated in Figure 5.2.3). This charge amplifier was designed primarily for application in modern internal combustion engines with piezoelectric pressure sensors. However, it is also suitable for various other applications in research, development, and laboratory settings (*Kistler 5018A Manual* 2017).

Figure 5.2.3: The Kistler 5018A Amplifier, (*Kistler 5018A Manual* 2017).

5.2.2 Motorized positioning stage

Initially, the plan for the reciprocal tribometer was to utilize the Aerotech ANT95L motorized positioning stage. This choice was driven by the fact that the laboratory already had the required motor controller and power supply. However, after conducting research, it became apparent that the Aerotech ANT95L was prohibitively expensive. Consequently, the decision was made to seek an alternative motorized positioning stage that combined both the motor and positioning stage into a single unit. Unfortunately, during market exploration, it was discovered that these integrated motorized positioning stages often are very expensive, exceeding 50.000,- NOK. Due to this, a more affordable option from MM-Engineering was selected as a suitable alternative.

The motorized positioning stage chosen for the reciprocating tribometer was the MM Engineering MPT3012-AK-S. The background for this decision is that the MPT3012-AK-S can contribute to fulfilling the requirements for the tribometer, as well as it is one of the cheaper motorized positioning stages that were considered by the project group. The project group also wanted to buy the reciprocating and rotational motor from the same manufacturer as this makes it easier to implement the motors to the same software setup and the electrical circuit. An additional advantage of this motor is its modular design, with separate components for the positioning stage and the motor. This modular setup offers the flexibility to replace or repair individual parts in the event of damage or malfunction. The motor and motor controller are integrated as a single unit, but with basic knowledge of mechatronics, it is relatively straightforward to separate them for maintenance or replacement purposes.

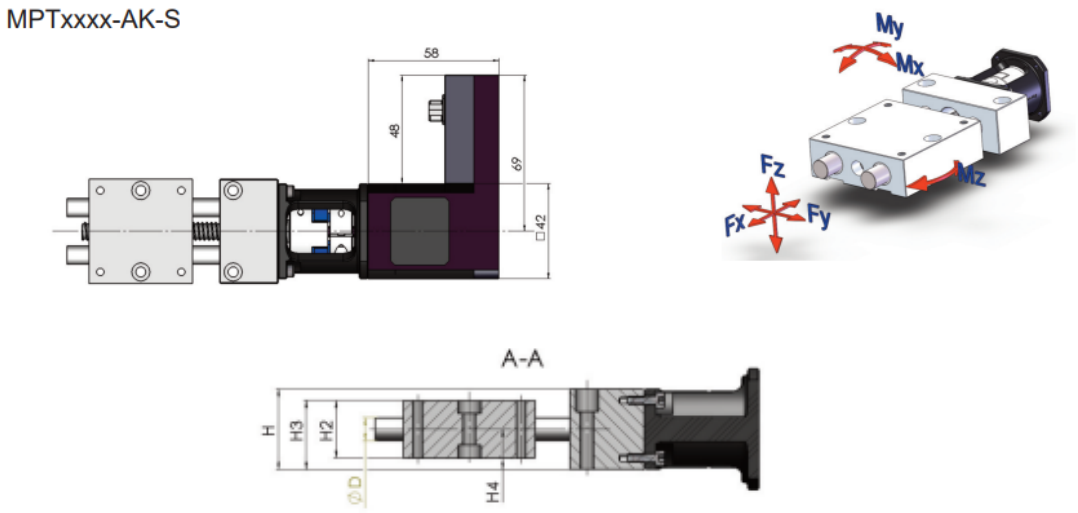

Figure 5.2.4: Model of the MM-Engineering MPT3012-AK-S with motor, top view, side section view, isometric view, (*Motor positioning tables* 2021).

The MPT3012-AK-S can withstand a load on the z-axis of 60 N. This means that the construction of the arm cannot have a weight greater than this. Due to the reciprocating motion of the tribometer, acceleration will be experienced at each endpoint of the movement. Because of Newton's second law, Equation 5.1, this acceleration will be affected by the mass of the arm, the friction force that is measured, and the mass of the dead weights. In the reciprocal tribometer, it is desired that this acceleration is as small as possible, and since the project group cannot affect the friction force and the mass of the dead weights it is desired that the construction of the arm has a relatively low mass.

$$\Sigma F = m \cdot a \tag{5.1}$$

Since the MPT3012-AK-S has an asymmetrical shape and is built with the positioning stage held up by two rods that are only supported in one end (illustrated in Figure 5.2.4), it was important to build a stable mounting plate for the unit. The MPT3012-AK-S has two mounting holes (Ø6) that are not threaded in the base of the positioning stage and two mounting holes (Ø5.2) that go through the motor controller. Since it is a small difference in the height of the motor controller and the positioning stage seen in figure: 5.2.4, the mounting plate needs to be built with a different height where the unit is going to be mounted in the base of the positioning stage. The mounting holes that go through the motor controller are also vertical giving the plate the "wall" at the base of the controller. The positioning stage was made with an easy square design so that it would be as easy to produce as possible.

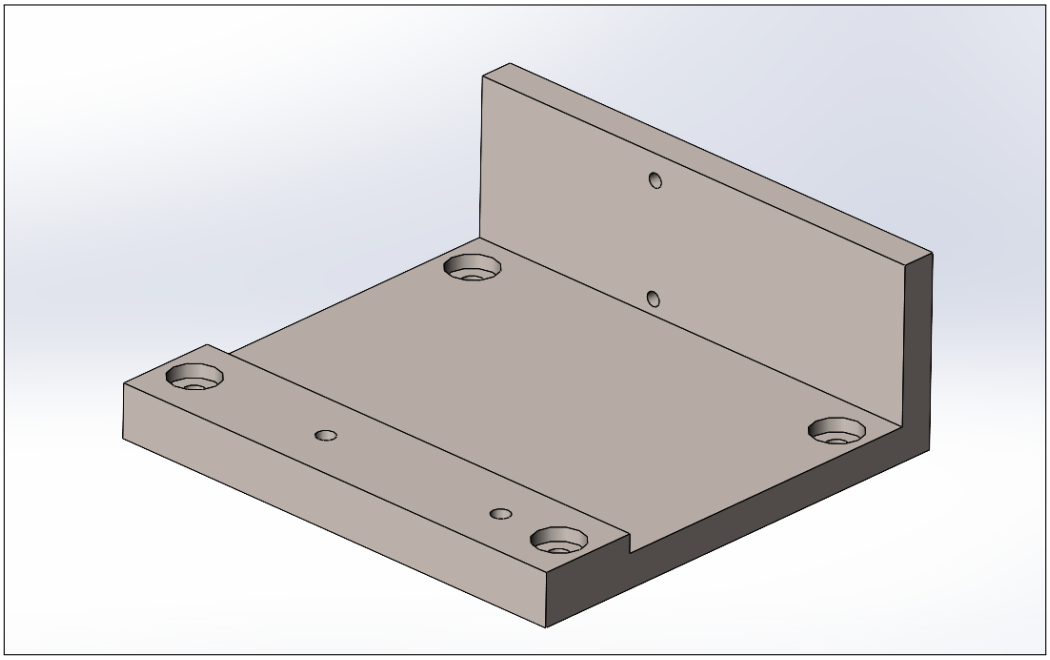

Figure 5.2.5: Model of the mounting plate for the MTP3012-AK-S.

5.2.3 Sample holders

In the reciprocating tribometer, the objective was to have a single sample stage that can accommodate both dry and tribocorrosion testing. The aim was to minimize the time required for sample mounting. Furthermore, there are existing sample holders in the laboratory that are utilized for other tribometers, and it would be desirable to incorporate them into the reciprocal design (figure: 5.2.6).

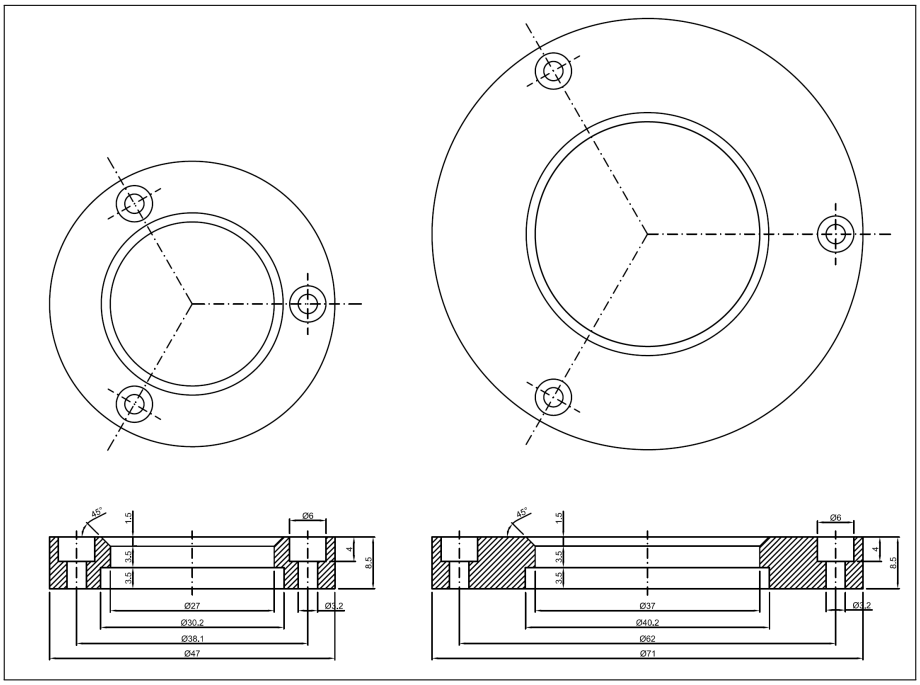

Figure 5.2.6: Drawing of existing dry and lubrication sample holders.

The initial requirement for the project was to accommodate samples with a diameter of 30 mm. However, in the laboratory, it is common to work with samples of 40 mm diameter. Fortunately, adapting the reciprocal tribometer to handle the larger samples is a straightforward task. As a

result, it was decided that the sample stage to be designed to accommodate both 30 mm and 40 mm diameter samples.

In order to facilitate tribocorrosion testing and allow easy interchangeability with the sample holder used for dry and lubrication testing, a redesigned sample holder was required. The following criteria were established for the new sample holder:

- Sealed and waterproof sample holder with the ability to hold 50 mL (electrolyte).
- Ease of assembly and mounting.
- The ability to transfer electricity from the potentiostat through the sample.
- Safe design.

To meet these criteria, it was decided to design the sample holder using Polyether Ether Ketone (PEEK), a non-conductive material suitable for 3D printing. This choice provides more design flexibility due to the manufacturing process. PEEK is already extensively used for creating load cells in laboratory settings.

It is worth noting that the sample holder for tribocorrosion testing will be connected to the potentiostat, which is responsible for the electrochemical control of the tested material. This connection will be established using a three-electrode setup, where the sample acts as the working electrode, while the reference and counter electrodes are immersed in the electrolyte. The counter electrode will consist of a 99.99% pure platinum wire measuring approximately 500µm in diameter and 90cm in length. Therefore, it is important to design the tribocorrosion sample holder with sufficient width to prevent collision between the electrodes immersed in the electrolyte and the pin.

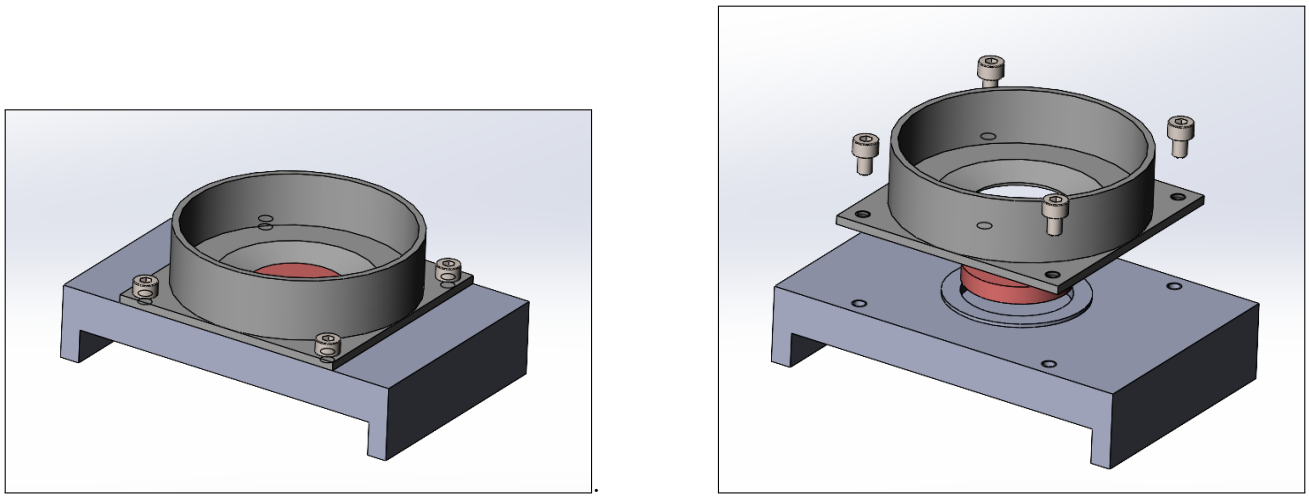

(a) The tribocorrosion holder. **(b)** Exploded view of tribocorrosion holder.

Figure 5.2.7: Mounting of tribocorrosion sample holdere.

In Figure 5.2.7, a design for a tribocorrosion holder is presented, taking inspiration from the previous tribometer's holder. It was crucial for the project to measure and reconstruct this model since none of the group members had prior experience with tribocorrosion testing. By doing so, the project group gained a better understanding of the required dimensions for a tribocorrosion sample holder.

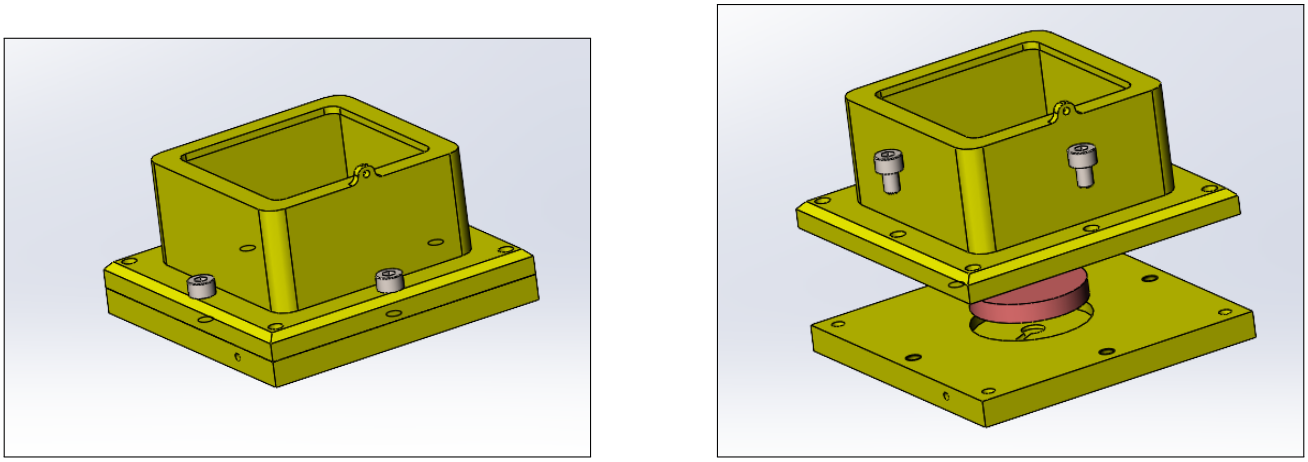

(a) The tribocorrosion holder.

(b) Exploded view of tribocorrosion holder.

Figure 5.2.8: Mounting of tribocorrosion sample holder.

In Figure 5.2.8, a suggested design for a tribocorrosion holder is depicted. This new holder demonstrates enhanced efficiency compared to the previous one, particularly concerning the choice of material. Additionally, it features a specifically designed hole at the top edge to accommodate the platinum electrode. Furthermore, this sample holder adopts a square shape for the electrolyte instead of a cylindrical one. The intention behind this design choice is to provide users with an intuitive way to differentiate between the sample holders intended for use with the reciprocal tribometer and those meant for the rotational one.

However, it is important to note a disadvantage of this sample holder: it requires multiple screws for assembly. Consequently, there is a risk of confusion regarding which screws are responsible for holding the sample holder together and which ones are meant for disconnecting it from the load cell. This confusion could potentially result in inadvertently opening the sample holder while it is positioned atop the sensor and filled with liquid. Such an occurrence would be undesirable.

5.2.4 Possible solutions

In this section, various solutions for the arm will be presented. These solutions share several common characteristics. They all consist of an arm connected to a motor via an axle, and they all incorporate a threaded counterweight positioned at the opposite end of the pin. This configuration enables the arm to adjust the center of gravity so that it aligns precisely on top of the axle. This adjustment is crucial to ensure that the weight of the pin and arm does not interfere with the experimental results. As depicted in Figure 5.2.9, it is evident that the placement of the counterweight affects the positioning of the center of mass. Specifically, the farther the counterweight is from the axle, the more the center of mass is shifted toward the rear.

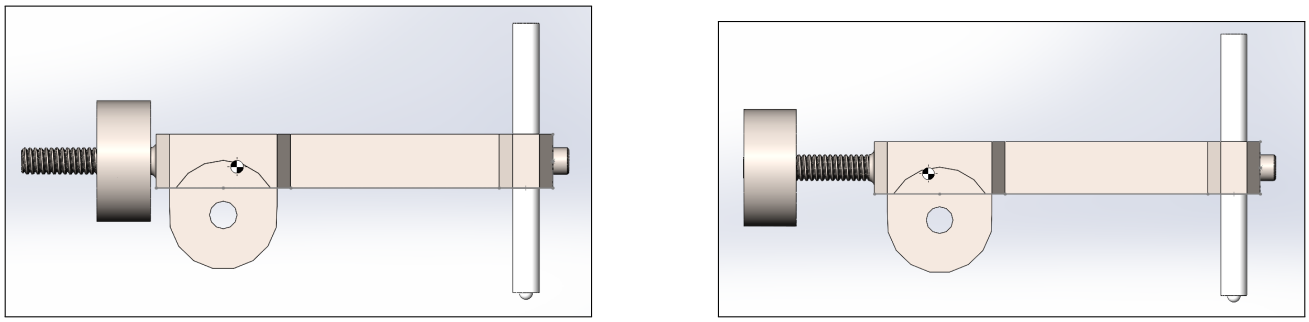

(a) Foremost centre of mass. **(b)** Rearmost center of mass.

Figure 5.2.9: Centre of mass, reciprocal tribometer.

5.2.4.1 Solution 1

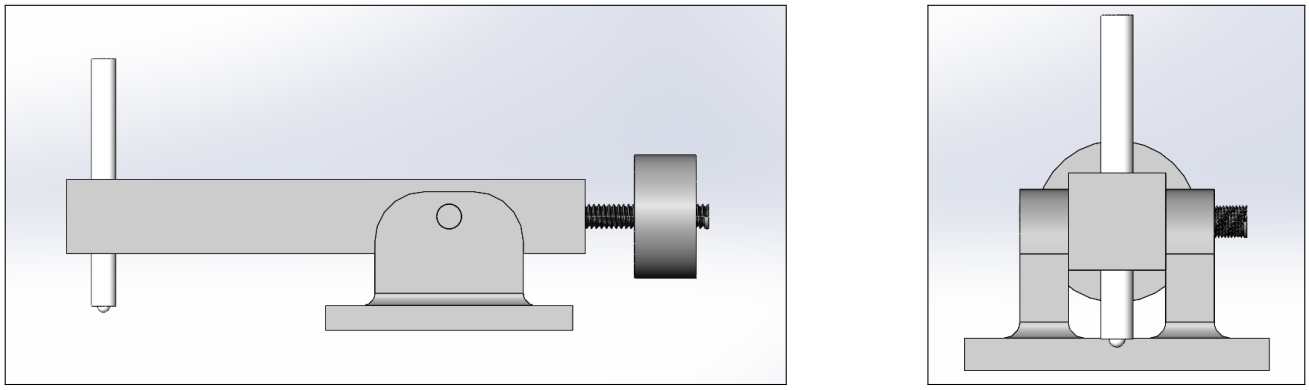

Figure 5.2.10: Solution 1 for the arm in the reciprocal tribometer.

The initial solution for the reciprocal tribometer focused on simplicity and ease of production. In this solution, the arm was designed as a beam with a square cross-section measuring 30x30mm. The pin was attached to the front end of the beam. The construction included a rod and a threaded counterweight, allowing for adjustment of the arm and pin's center of gravity. Setting the center of gravity directly above the axle is crucial during testing to prevent the weight of the arm from affecting the experiment. The intention was to use aluminum for this solution, meaning bearings would be necessary between the arm and the axle holder to mitigate potential friction issues associated with aluminum.

However, there were several challenges with this solution. Firstly, the construction's mass was significant, which could affect the motor's acceleration capability. Additionally, the long arm length required larger dimensions for the counterweight.

Another noteworthy aspect is that this solution had the axle positioned at the middle of the arm along the z-axis. While this allowed for proper adjustment of the counterweight, it prevented the arm from staying tilted back when changing samples or performing other actions. On the positive side, this positioning reduced the momentum created (as discussed in Chapter 6.1.6) compared to placing the axle further down.

5.2.4.2 Solution 2

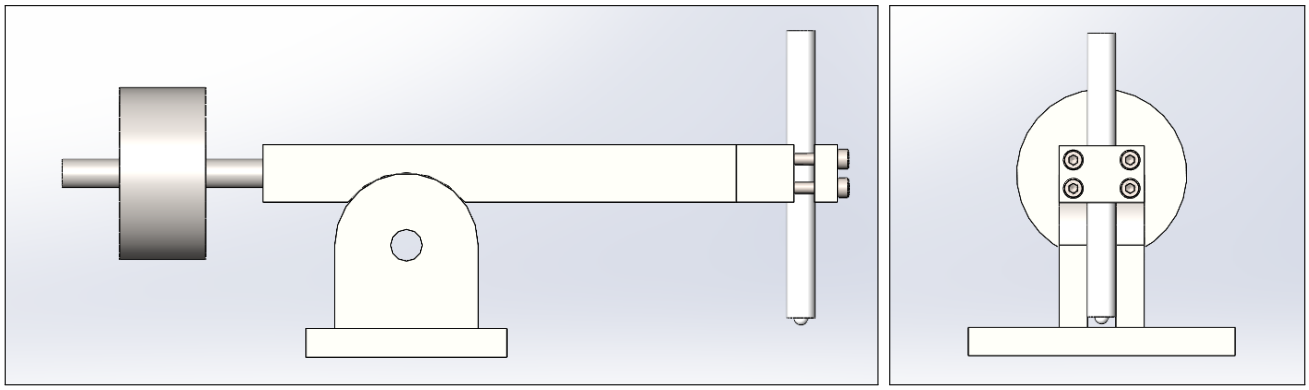

Figure 5.2.11: Solution 2 for the arm in the reciprocal tribometer.

The second solution shares several characteristics with the first one but is significantly slimmed down. Notably, the arm is designed with two indents on each side, ensuring that the axle holder aligns with the arm's width. This design choice provides increased stability to the sides of the tribometer. However, it introduces the disadvantage of increased friction between the arm and the axle holder. It is desirable for the arm to tip with minimal friction so that the majority of the load from the deadweights is transferred to the sample.

With this prototype, the group also experimented with the connection between the arm and the pin. In this particular solution, the pin is clamped using four screws, ensuring even pressure distribution on the pin's surface. This method is advantageous compared to the alternative approach shown in solution 3, where a screw is inserted into the side of the pin. The use of solution 2 reduces wear on the pin, which is made of PEEK and is susceptible to damage from contact with metal components.

However, it was noted that this solution would require more time for setting up the experiment. As a result, the project group made the decision to proceed with the project without implementing this particular solution.

5.2.4.3 Solution 3

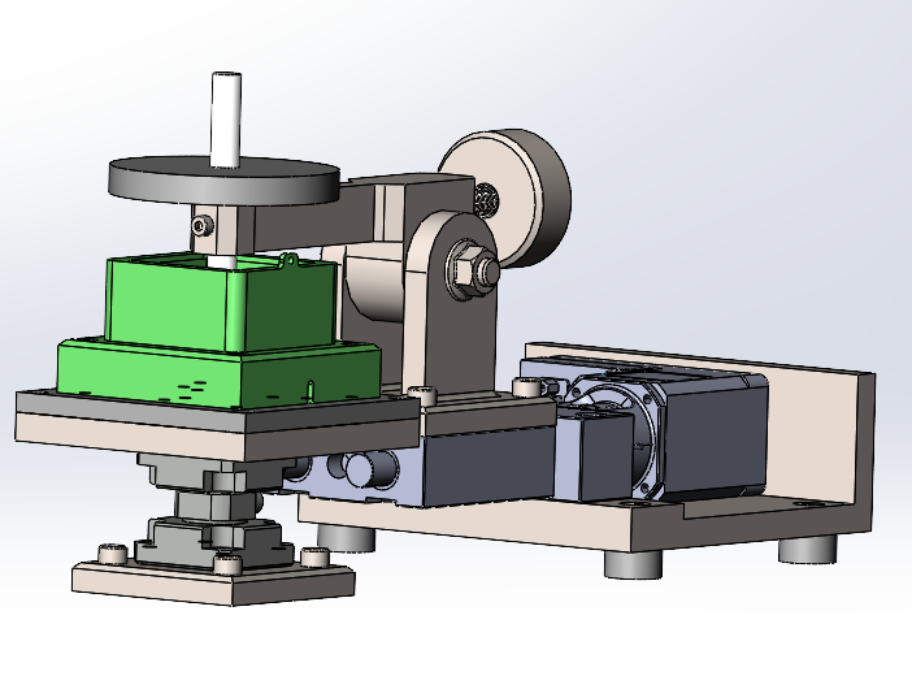

Figure 5.2.12: Solution 3.

In Figure 5.2.12, a solution is shown where the arm is mounted together with the motor and load cell. In this particular solution, the arm is slightly shorter compared to solutions 2 and 3. The advantage of having a shorter arm is that if the tip of the arm is subjected to sideways force, the impact on the axle will be reduced compared to a longer arm. However, the drawback is that the momentum generated by the acceleration and the deadweights will have a greater impact on the normal force (as discussed in Chapter 6.1.6), affecting the friction force and measurement of the friction coefficient. Nonetheless, a shorter arm provides overall stability to the tribometer, making this solution one of the better options considered.

The reason why this solution was not ultimately chosen as the final design was due to the placement of the axle. Although placing the axle off-center would have made the tribometer more user-friendly when changing samples, the project group decided that having the axle positioned directly in the middle of the arm was more desirable. This decision was based on considerations related to balancing the tribometer and managing the momentum generated during operation.

5.3 Rotational tribometer

5.3.1 Load cell

In order to record the frictional forces during tribological testing, a load cell is needed in the rotational tribometer. One of the initial requests from the project owners was that the load cell would be compatible with the Kistler 5018A charge amplifier already present at the lab. In addition to this, the load cell required a load capacity capable of tracking small forces to the maximum dimensioning frictional force. The maximum dimensioning frictional force was calculated using a COF of 1, based on common dynamic COFs of steels sliding against other metals in dry conditions, and an initial maximum normal load of 50 N. The force on the load cell depends on where the load cell linkage is placed along the pin arm. If the load cell linkage is placed directly beside the pin, the maximum reaction force of the load cell will be 50 N with a COF of 1. The force on the load cell will increase if the load cell linkage is placed behind the pin, because of the arm between the pin and the load cell linkage. The longer the arm between the pin and load cell linkage, the greater the reaction force on the load cell. This is illustrated in Figure 6.2.18, and in Equations 5.2.

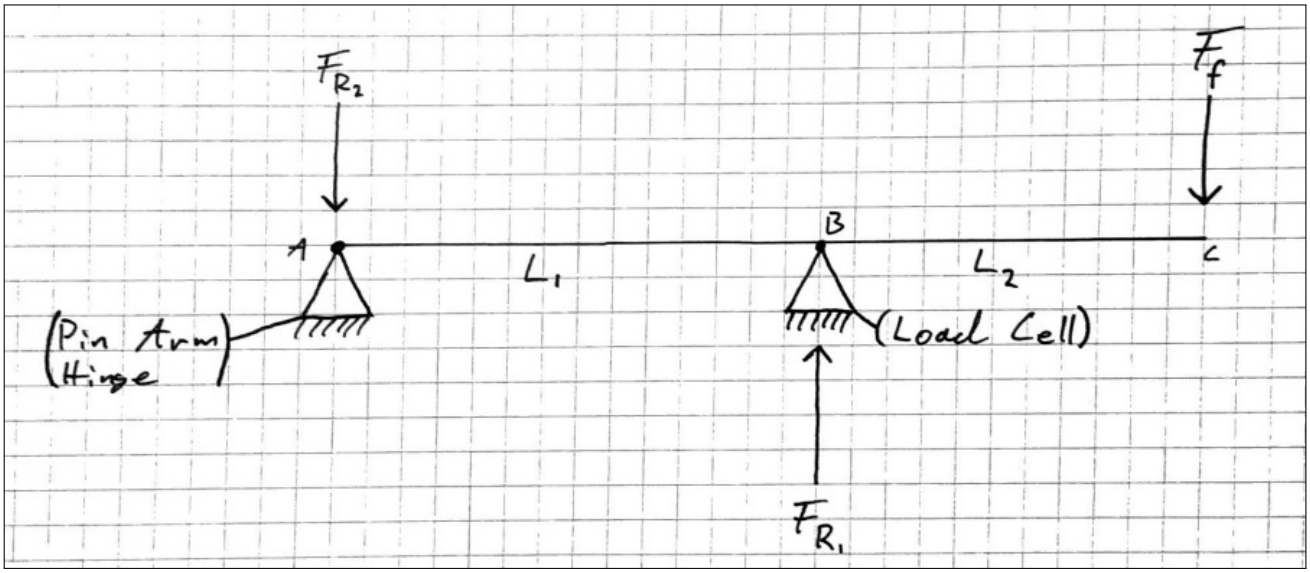

Figure 5.3.1: Influence on reaction force caused by the distance between pin and load cell linkage.

$$\begin{aligned} &\sum M_A = 0 : \\ &\rightarrow F_f \cdot (L_1 + L_2) + F_{R_1} \cdot L_1 = 0 \\ &\rightarrow F_{R_1} = -\frac{F_f \cdot (L_1 + L_2)}{L_1} \end{aligned} \tag{5.2}$$

If $L_2 = 0$:

$$\begin{aligned} F_{R_1} &= -\frac{F_f \cdot (L_1 + L_2)}{L_1} \\ \rightarrow F_{R_1} &= -\frac{F_f \cdot (L_1 + 0)}{L_1} \\ \rightarrow F_{R_1} &= -F_f \end{aligned}$$

If $L_2 = L_1$:

$$F_{R_1} = -\frac{F_f \cdot (L_1 + L_2)}{L_1}$$
$$\rightarrow F_{R_1} = -\frac{F_f \cdot (L_1 + L_1)}{L_1}$$
$$\rightarrow F_{R_1} = -2 \cdot F_f$$

As illustrated in the equations above, the reaction force on the load cell will increase proportionally as the distance between the load cell linkage and the pin increase. This was also taken into consideration when deciding on what load cell to use. The dimensioning load for the load cell was used as a reference point and guidance when selecting load cells. It is also important to note that the load cell needs to be able to record very small forces, and high resolution on the measurements is significant. A more common value for the frictional force is $50\ N \cdot 0.5 = 25\ N$, based on commonly measured COFs in this kind of tribological testing.

As high modularity and ease of assembly are design criteria for the tribometers, the load cell is also required to be easy to install. The following four criteria for the load cell were established before contacting different companies and deciding on the final load cell for the rotational tribometer.

- Compatibility with Kistler 5018A charge amplifier.
- Load capacity for friction forces between 0 N to 50 N.
- Ease of assembly and installation.
- Reasonable cost.

Initially, it was decided that a load cell from Kistler would be selected to ensure that it would be compatible with the charge amplifier at the lab. There are several load cells from Kistler that could be suitable for the purpose of the rotational tribometer, and a table of suitable load cells from Kistler was established to make it easier to decide on what sensor to use. the project group also initiated contact with experts from Kistler, to make sure that the best possible load cell for the project was selected. The table below illustrates the most suitable load cells from Kistler, with selected key parameters.

	Kistler 9323A	**Kistler 9212**	**Kistler 9001C**	**Kistler 9712B5**	**Kistler 9301C**
Measuring Range	0 kN - 20 kN	0 kN - 22 kN	0 kN - 7.5 kN	0 kN - 0.022 kN	0 kN - 3 kN
Preloaded	Yes	Yes	No	Yes	Yes
Compatible With Amplifier	Yes	Yes	Yes	No	Yes
Ease of installation (0 to 10)	8	6	6	6	7
Price in NOK	23 733,-	16 077,-	31 443,-	–	33 989,-

Table 5.3.1: Kistler load cell comparison.

After consulting with Kistler and advisors, the Kistler 9301C was initially decided as the preferred load cell for the tribometer. The reason for this was the ease of installation, compatibility with the charge amplifier, and that the sensor was preloaded. The Kistler 9301C is both preloaded and calibrated and according to Kistler, is ready to use immediately. This decision was abandoned when the official offer letter and price were received from Kistler, as it was determined to be too expensive. After multiple emails and consultations with experts from Kistler, the Kistler 9323A load cell was suggested as another suitable load cell. As the Kistler 9301C, the 9323A is also preloaded and calibrated, making it ready to use immediately. Additionally, the 9323A is compact and easy to install. This was further proposed to the advisors and project owners, but again, it was determined to be too expensive. Therefore a different load cell had to

be selected, and it was decided to look for cheaper strain gauges instead of piezoelectric sensors from Kistler. Together with this decision, it was decided to reduce the maximum dimensioning frictional force from 50 N to 30 N in collaboration with the advisors. The reason for this is that a COF of above 1 is rare in normal tribological test conditions and that a load cell with a low force capacity usually has a greater resolution on its measurements. High-resolution measurements are important in tribological testing, where the forces are very small.

Strain gauges are usually cheaper than piezoelectric sensors, but on the downside, they are not compatible with the Kistler 5018A charge amplifier at the lab. This meant that the project group had to design and develop a suitable charge amplifier for the selected strain gauge, compatible with the software requirements of the tribometers. There are several different strain gauge manufacturers and producers, with several suitable strain gauges. The project group made the following criteria for selecting a suitable strain gauge for the tribometer:

- Load capacity of minimum 45 N, ($1.5 \cdot 30$ N).
- Ease of mounting.
- Short delivery time.
- Compatible with HX711 charge amplifier and Arduino UNO.

Initially, Tedea-Huntleigh Model 1006 with a rated capacity of 5 kg (49.05 N) was selected and suggested for the advisors and project owners. This sensor would be capable of recording forces up to 49.05 N if the load cell is placed directly beside the pin. It is also relatively easy to install with four M3 through threaded mounting holes. This sensor was determined as suitable for the rotational tribometer, but unfortunately, this model was "out of stock" and the delivery time was not satisfactory. Due to the limited time frame, and the urgency regarding the decision of a load cell, the project group together with the advisors decided to order the same model (Tedea-Huntleigh Model 1006) with a load capacity of 3 kg. The advantage of Model 1006 is that it is small, modular, and very easy to install. The 3 kg load cell was mainly ordered to facilitate prototyping and testing due to the limited time frame of the project. It is possible to use both the 3 kg and the 5 kg strain gauge, as the dimensions are the same. The dimensions for Tedea-Huntleigh Model 1006 strain gauge are illustrated in Figure 5.3.2.

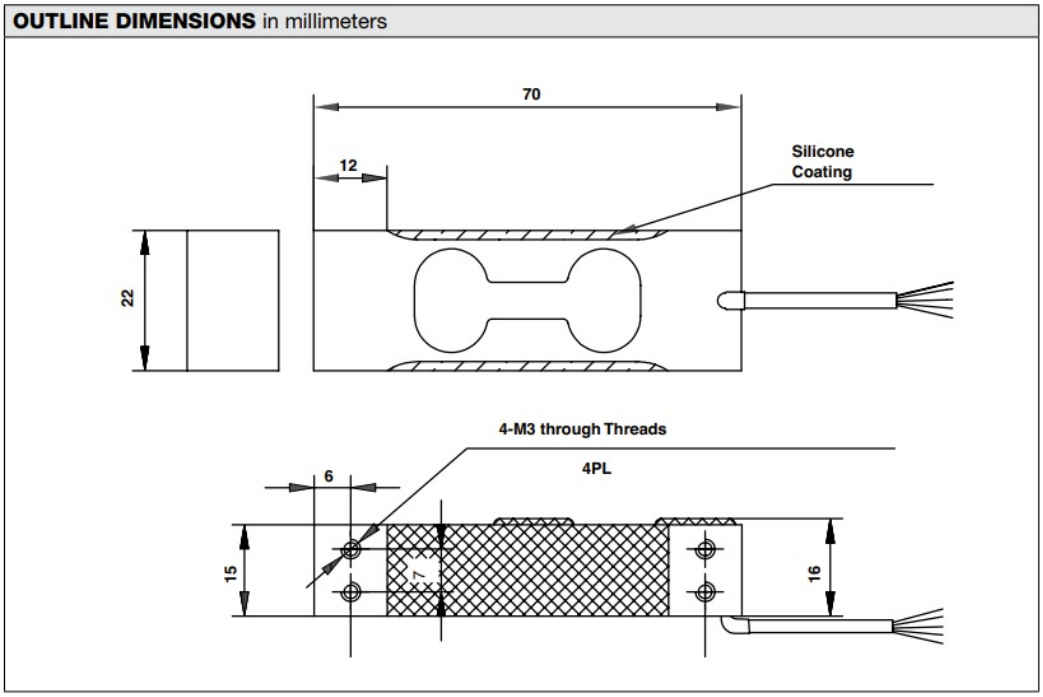

Figure 5.3.2: Tedea-Huntleigh Model 1006 (*Model 1006 Aluminum Single-Point Load Cell* 2014).

Since the strain gauge is not compatible with the Kistler 5018A charge amplifier at the lab, the project group had to develop a method of amplifying the signals from the strain gauge and transferring the data to the computer. This was done using an Arduino UNO Rev3 together with an SEN-13879 - HX711 Load Cell Amplifier ordered from Elfa Distrelec, illustrated below.

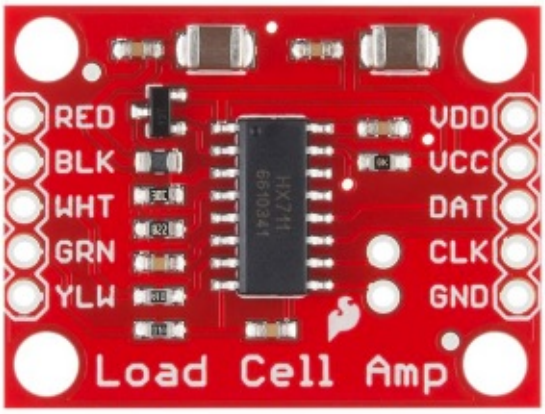

(a) SEN-13879 - HX711 Load Cell Amplifier (*SparkFun-HX711 Load Cell* 2019).

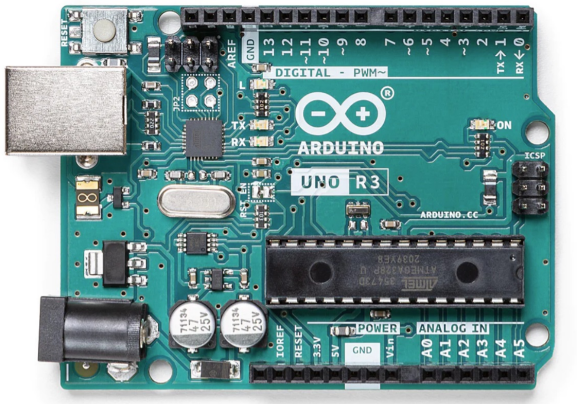

(b) Arduino Uno Rev3 (*Arduino Uno R3* 2022).

Figure 5.3.3: Illustration of Load Cell Amp and Arduino for the rotational tribometer.

The reason why Arduino UNO was selected as the preferable microcontroller is that some members of the project group were familiar with Arduino IDE. Additionally, Arduino is relatively easily programmable and is compatible with MatLab for providing graphs and data to a CSV file. Arduino is also compatible with the SEN-13879 - HX711 Load Cell Amplifier.

5.3.2 Motorized positioning stage

The motor for the rotational tribometer needed to have the ability to provide a rotational velocity of at least 300 rpm. In addition to this, it needed the ability to tackle a minimum of 50 N at a

radius of 15 mm away from the center, as this is the initial maximum dimensioning load for the tribometers. To calculate the minimum torque needed by the motor, a maximum load of 50 N and a COF of 1 were used as illustrated in the equation below.

$$\tau_{min} = F_{f\ max} \cdot r_{max} = F_{N\ max} \cdot \mu_{max} \cdot r_{max} = 50\ N \cdot 1 \cdot 0.015\ m = 0.75\ Nm \tag{5.3}$$

The minimum moment for the motorized positioning stage is calculated by multiplying the maximum wear track radius with the maximum dimensioning load, as illustrated in the equation below.

$$M_{min} = F_{N\ max} \cdot r_{max} = 50\ N \cdot 0.015\ m = 0.75\ Nm \tag{5.4}$$

As illustrated in Equation 5.3 and 5.4, the motor need the capability of handling at least 0.75 Nm of momentum and providing at least 0.75 Nm of torque.

As high precision, adjustable velocity, and position precision are important in tribological testing, a stepper motor was determined as the best choice of motor type for the rotational tribometer. Additionally, stepper motors are usually cheap and require minimal maintenance. During the development phase, a motor from Aerotech was initially selected, mainly because the reciprocal motor already present at the lab is produced by Aerotech. The motorized positioning stage from Aerotech could provide very high precision, as well as the required velocities and force capacities. After consulting with Aerotech and advisors, it was determined that the price of the Aerotech motor was too high (approximately 100.000,- NOK). A motor stage from MM-Engineering was selected instead, mainly due to the reduced price and integrated motor and motor controller.

The motor stage selected from MM-Engineering is the MDT360110-QN, as it provides high accuracy, a rotational output speed of up to 300 rpm, and is capable of handling the maximum forces and momentum expected. The technical data of the motor stage from MM-Engineering is illustrated in Figure 5.3.4 and Figure 5.3.5.

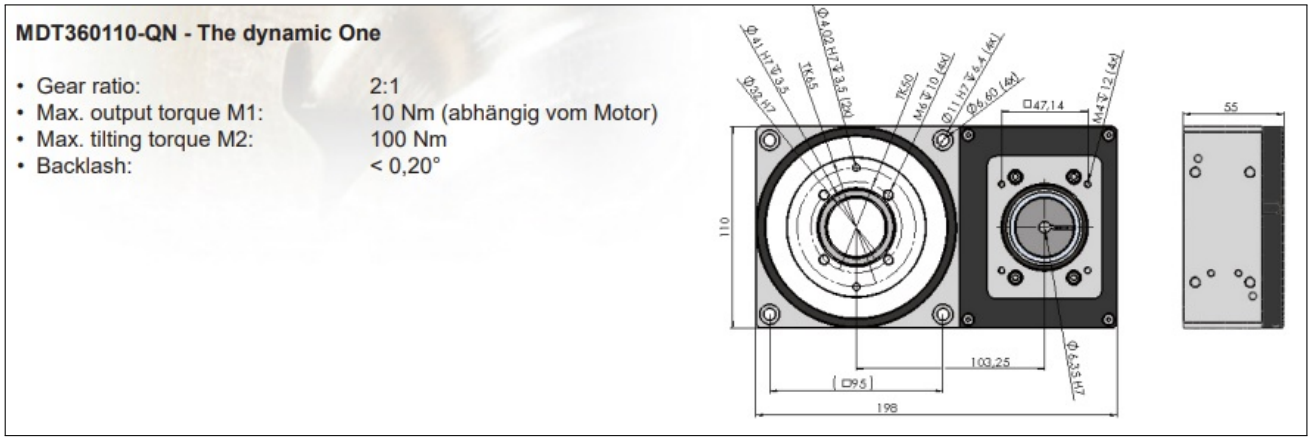

Figure 5.3.4: Technical data for MDT360110-QN from MM Engineering (*Motor rotary tables* 2021).

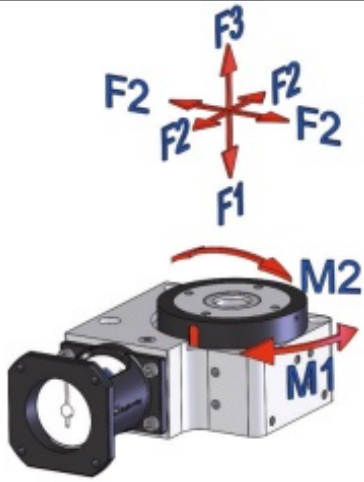

Belastungstabelle / *Load chart*

Bestellnummer *Order number*	F1 [N]	F2 [N]	F3 [N]	M1 [Nm]	M2 [Nm]
MDT360110-QN	5000	3000	5000	10	100

Figure 5.3.5: Load chart for MDT360110-QN from MM Engineering (*Motor rotary tables* 2021).

The motor included in the motor stage from MM-Engineering is a Design Colibri 23 Mini stepper motor. This motor has a holding torque of 1.75 Nm and is capable of providing a speed of 600 rpm. With the gear ratio of the motor stage of 2:1, the motor and the motor stage are capable of providing a rotational speed of 300 rpm. This is sufficient for the purpose of the tribometer. Additionally, with a holding torque of 1.75 Nm, it is capable of handling the maximum expected loads. Another advantage is that the motor stage includes an integrated motor controller, with an easy-to-use controller interface and software.

5.3.3 Linear translation stage

Another requirement for the rotational tribometer is the ability to adjust the radius of the wear track. This can be done by including a linear translation stage in the tribometer design. A translation stage usually consists of a translation screw, bearings, and two or more supports. Translation stages can either be manually adjusted or motorized.

During the development of the tribometer, it was initially decided that the project group would design and develop an integrated linear translation stage into the rotational tribometer. This would make the tribometer less modular, but more integrated and specialized. Additionally, if the linear translation would be integrated into the tribometer design, more parts and components are needed. A linear translation stage is also a high-precision device, requiring careful engineering and design. This was proposed to the advisors and project owners. Due to the limited time frame of the project, and the need for high modularity and ease of assembly, it was eventually decided that ordering a linear translation stage suitable for the rotational tribometer would be the best choice. This would also conform to the need for a modular and user-friendly design.

There are several suitable linear translation stages for the rotational tribometer. The requirement for the linear translation stage was the ability of a translation distance of at least 15 mm, a short spindle pitch, and high precision and rigidity. Additionally, it was determined that the linear translation stage needed to have locking features to ensure no translation during testing. As the motor selected was manufactured by MM-Engineering, it was decided that a linear translation stage from the same company would be the preferable option. The reason for this is that ordering parts from the same manufacturer would reduce the delivery time and costs. The most suitable linear translation stage from MM-Engineering is the "Short Positioning Table PT2512". The PT2512 has a translation distance of 25 mm and can be manually adjusted with an adjusting knob. It has a spindle pitch of 1 mm, which means great precision during the adjustment of the wear track radius. Additionally, integrating the tribometer into the translation stage, and

mounting the translation stage is relatively easy. This conforms with the design criteria of high modularity and ease of installation. The PT2512 is the largest positioning table from MM-Engineering with a "short translation distance". It is also relatively cheap compared to other linear translation stages on the market.

Support designed and developed by the project team is added on one side of the translation stage in order to limit the translation to 15 mm (maximum allowable wear track radius), as illustrated in 5.3.6. The dimensions and load capacity of the linear translation stage are illustrated in Figure 5.3.7, and is suitable for the rotational tribometer. As seen in Figure 5.3.7, the maximum vertical load for the linear translation stage is 100 N, which limits the final weight of the main frame of the rotational tribometer to a maximum of 10.8 kg ($\frac{100N}{9.81}$).

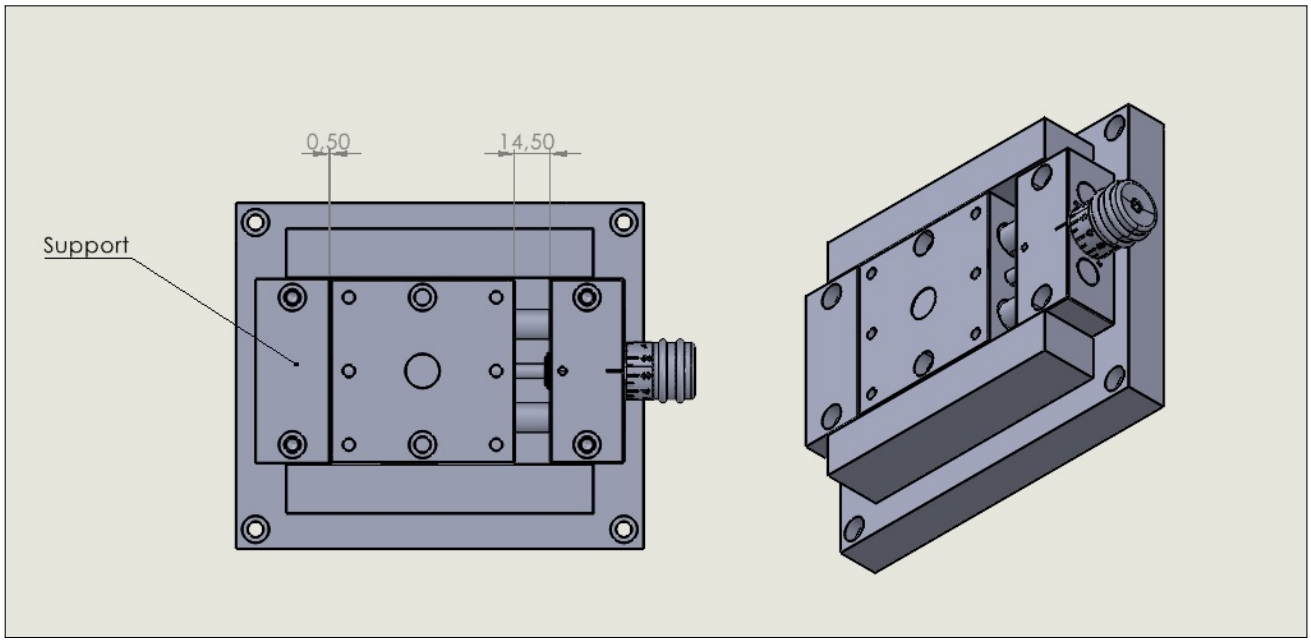

Figure 5.3.6: Linear translation stage and support.

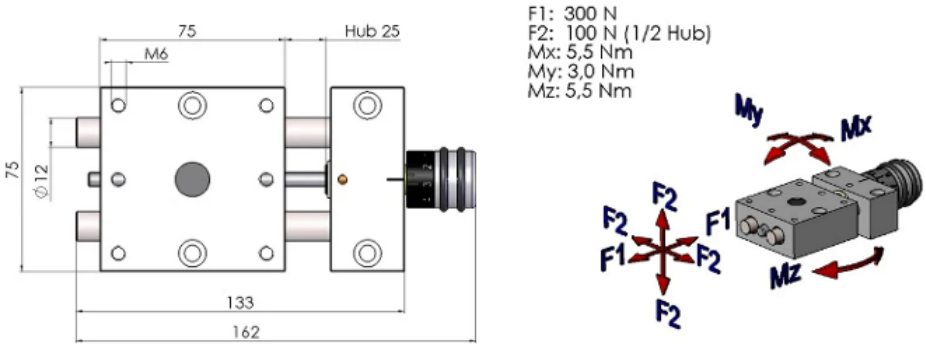

Figure 5.3.7: Dimensions and force diagram of PT2512 short positioning table from MM Engineering (*Positioning systems manually operated* 2019)

.

The project owner also requested an alternative solution to the PT2512 and suggested a "movable base plate" with traces for tightening screws. The challenge with this solution is that the weight/normal force of the tribometer will introduce friction between the base plate and the fastening block underneath. This will make it difficult to precisely adjust the wear track radius. Additionally, it will not be as user-friendly as a linear translation stage because of the added

need of tightening four screws each time the wear track needs to be adjusted. The alternative to a linear translation stage, as suggested by the advisors, is illustrated in Figure 5.3.8. The project group designed solutions so that the main frame of the tribometer will fit both with the PT2512 and the alternative suggestion proposed by the Adviser. This way, both of the solutions will work on the same main design.

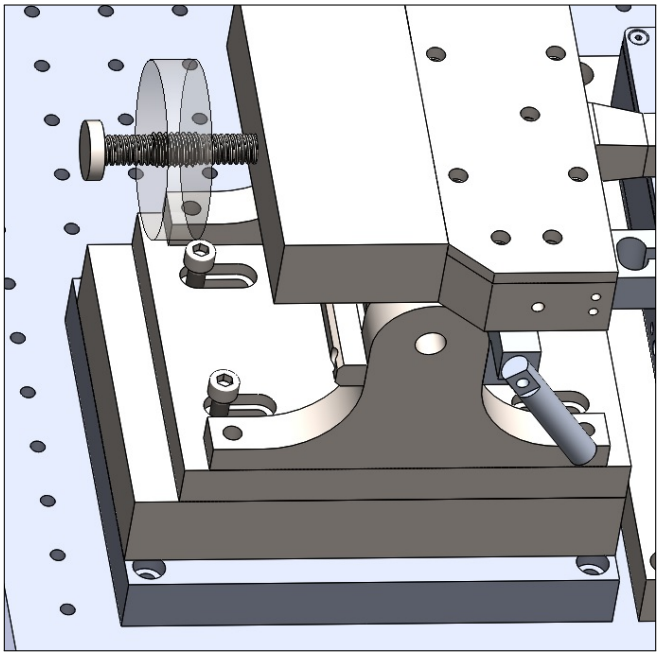

Figure 5.3.8: Alternative to linear translation stage, rotating tribometer.

The preferable option for adjusting the wear track is to order the PT2512 linear translation stage from MM-Engineering. This will reduce unwanted friction, and enable the possibility of precise adjustment of wear track radius with an adjustment knob. The spindle pitch is 1 mm, which is very suitable for the wear track radius adjustment. The PT2512 from MM-Engineering is also self-locking, which reduces the possibility of unwanted movement during testing. It is also possible to order a clamping screw to secure the stage from unwanted movement even more. The linear translation stage is highly modular and easy to assemble and integrate together with the tribometer. All of this conforms with the needs and design criteria for the tribometer, requested by the project owners and advisors.

5.3.4 Tribocorrosion

Tribocorrosion was also a feature for the tribometer requested by the project owners and advisors. The main challenge during the design and development of the tribocorrosion feature was transferring electrical signals from the stationary part to the rotating part. In addition, the tribocorrosion feature needed to be easily removable with a "plug in-plug out" feature. The tribocorrosion sample holder needed to be waterproof, and not leak out the electrolyte inside the sample holder. The following criteria were established for the tribocorrosion feature.

- Sealed and waterproof sample holder.
- Ease of assembly and mounting.
- The ability to transfer electricity from the potentiostat through the sample holder.
- Safe design.

The most difficult part during the design and development of the tribocorrosion feature was how to transfer electrical signals from the stationary part to the rotating sample. It was also

challenging to come up with a solution to keep the sample holder sealed combined with the capability of transferring electricity through the bore and sample holder. The small bore diameter of 32 mm meant that everything needed to fit together in a small space. Several possible solutions to these challenges were discussed and evaluated during the development of the tribocorrosion feature.

The first solution was to mount an electrical conducting carbon brush inside a PLA 3D printed housing in the bore of the motor, coupled with an electrical cable going through the base plate of the motor. Additionally, the sample holder would consist of a cobber plate on the bottom, so that the carbon brush could rub against the bottom of the copper plate and transfer electricity through the copper plate and sample. The downside with this solution is that friction would be introduced between the copper plate and the carbon brush. This means that eventually, the carbon brush would wear down and frequent replacements would be necessary. The added friction between the carbon brush and copper plate is not preferable, as it will increase the torque on the motor and consequently increase the energy consumption.

The second solution was to mount a slip ring inside the bore of the motor, placed in a housing of 3D-printed PLA plastic. The slip ring is capable of transferring electrical signals from a stationary part to a rotating part with minimal friction. Additionally, a slip ring would remove the need for frequent replacements, as the slip ring will not wear down as a carbon brush will.

A slip ring was decided as the best alternative for transferring electrical signals from the stationary part to the rotating part. A small size slip ring had to be selected, in order to fit in the bore of the motor. After extensive research and consulting with different companies, a slip ring from Penlink was selected as suitable. This was mainly because of its small dimensions, quick delivery time, and electrical qualifications.

A sample holder specialized for tribocorrosion testing is also needed. A tribocorrosion sample holder needs to be sealed so that no liquid can leak out during testing. Additionally, it must be easy to mount, and de-mount, onto the motorized positioning stage. The minimum volume of liquid required to perform a tribocorrosion test is 50 mL according to the advisors. The maximum angular velocity of the motorized positioning stage, and therefore also the sample holder, is 31.4 rad/s ($\omega = rpm \cdot \frac{2 \cdot \pi}{60\ s}$). With an angular velocity, the angular acceleration and the density (mass) of the liquid will cause a height difference from the original surface point (when no rotation is present) of the liquid, to the highest surface point of the liquid at full angular velocity. This is caused by pressure differences introduced by forces caused by the rotation. The pressure on the liquid surface has to be equal. This height difference can be described by the following equation.

$$h = \frac{R^2 \cdot \omega^2}{4 \cdot g} \tag{5.5}$$

The maximum height of the liquid (measured from the original surface point at zero angular velocity) at the maximum angular velocity of 31.4 rad/s is calculated below.

$$\begin{aligned} h &= \frac{R^2 \cdot \omega^2}{4 \cdot g} \\ h &= \frac{(30\ mm)^2 \cdot (31.4\ rad/s)^2}{4 \cdot 9810\ mm/s} \\ h &= 22.6\ mm \end{aligned}$$

The height from the bottom of the sample holder to the surface of the liquid, at zero angular velocity is calculated by Equation 5.6. The radius used is based on the design solution provided by the project group, and the maximum possible radius considering the diameter of the rotating stage.

$$\begin{aligned} V &= \pi \cdot r^2 \cdot H \\ \rightarrow H &= \frac{V}{\pi \cdot r^2} \end{aligned} \tag{5.6}$$

$$H = \frac{50\ 000\ (mm)^3}{\pi \cdot (30\ mm)^2} = 17.7\ mm$$

The maximum height from the bottom of the sample holder to the surface of the liquid, at maximum angular velocity can then be calculated as illustrated below. H is the original height at zero angular velocity, and h is the height difference at maximum angular velocity calculated above.

$$H + h = 17.7\ mm + \ 22.6\ mm = 40.3\ mm$$

This implies that the sample holder needs to have a height from the bottom to the top of at least 40.3 mm.

5.3.5 Possible solutions

Below are some of the initial design ideas for the rotational tribometer. These are only some of the most relevant examples of possible design solutions. Many more solutions and possibilities have been discussed during the project. The main difference in the following solutions is what kind of load cell is used, how the load cell is mounted, and how the load cell is connected to the pin arm. Each of these solutions has been discussed, and the final design solution has elements from all of these. The design and development process has been based on an iterative approach, where continuous improvements and new ideas have been evaluated and implemented in the final design. Additionally, several other solutions on where to place the load cell were discussed in the initiation phase of the project. Such as placing the load cell within the main frame, on the other side of a hinge. This would work like a lever, and introduce more force on the load cell than necessary. It was quickly decided that placing the load cell close to the pin was the preferred solution.

5.3.5.1 Solution 1

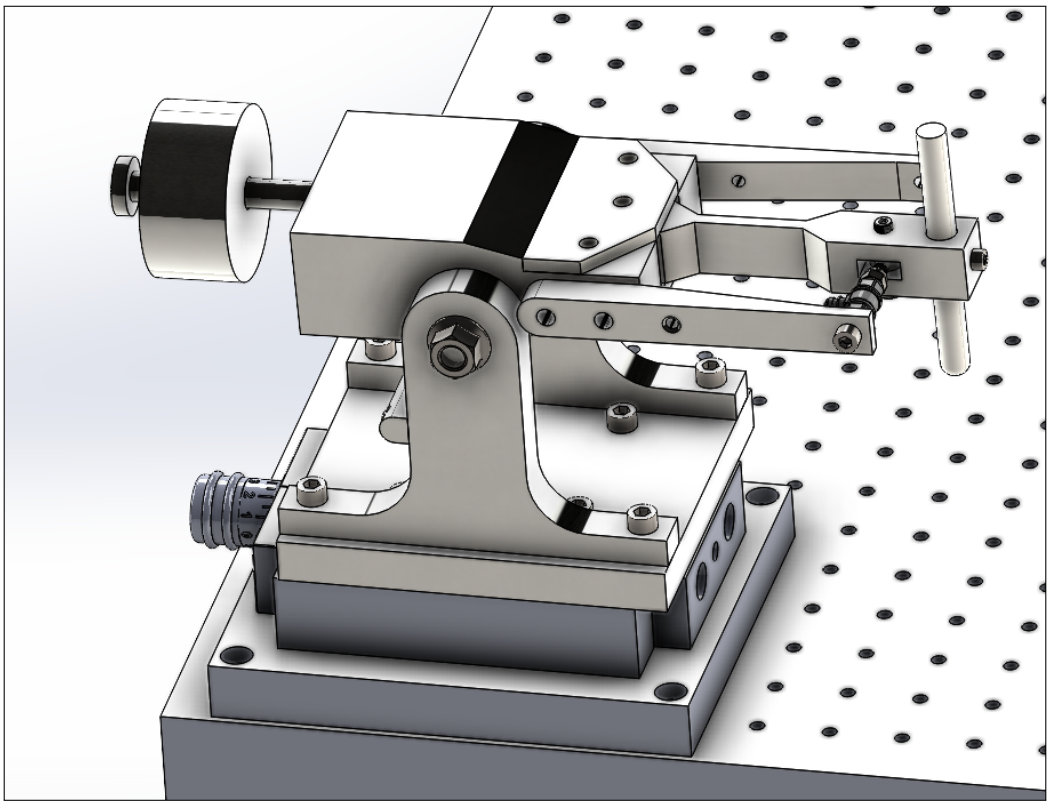

Figure 5.3.9: Solution of rotational tribometer design, with Kistler load cell.

The design illustrated above in Figure 5.3.9 shows one of the design solutions of the rotational tribometer. This design is based on using Kistler 9301C as the load cell. This design was developed during consultations with experts from Kistler. As seen in Figure 5.3.9, the inner support of the pin arm is a hinge support designed to support the pin arm both from sideways movement and moment caused by friction forces at the end of the pin. This way, the load cell will work as a support for linear forces perpendicular to the length of the pin arm. The load cell is connected to a male threaded ball joint in the pin arm through threaded holes in the load cell. The ball joint will only transfer linear forces and are not capable of transferring significant moments to the load cell. This will ensure that minimal unnecessary moments are transferred to the load cell, which could influence the quality of the measurements. One of the differences with this design is the "removable" sensor arms on the side of the main frame. The thought

behind this design was the need for a modular design and easy manufacturing. This design has a lot of similarities with the final design.

5.3.5.2 Solution 2

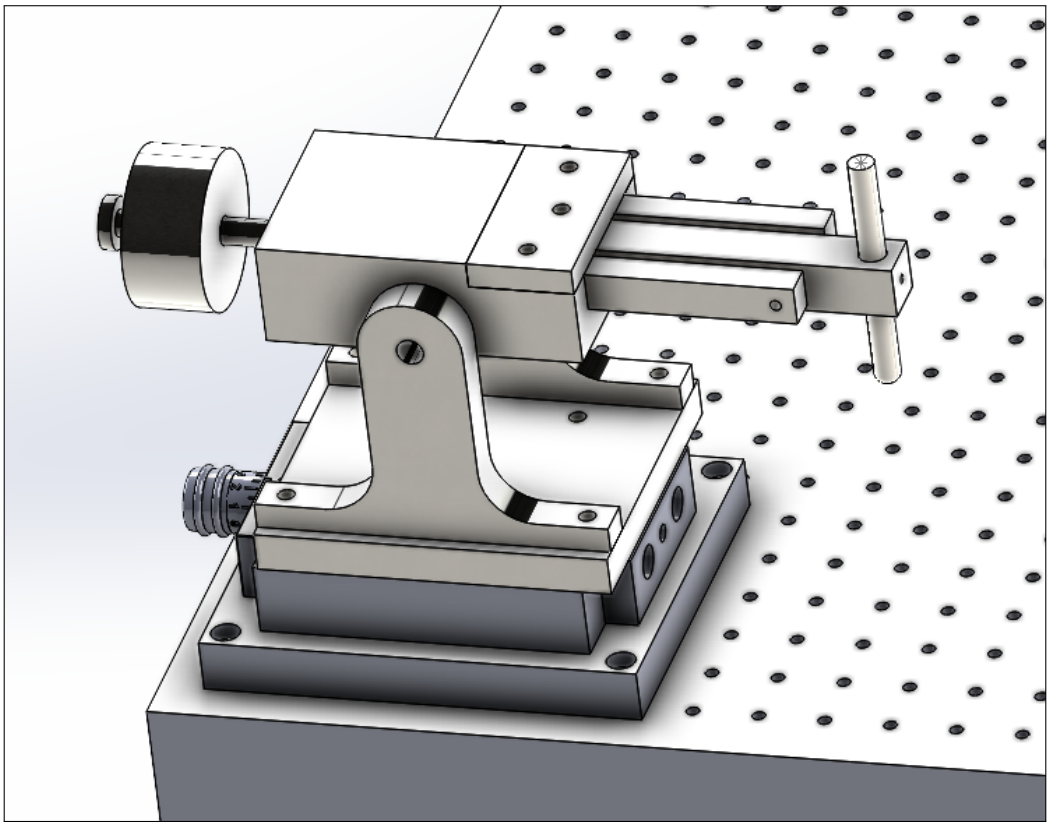

Figure 5.3.10: Solution of rotational tribometer design, with Kistler force cap load cell.

The design illustrated above in Figure 5.3.10 illustrates a different solution to the rotational tribometer. This design is also based on using a Kistler piezoelectric load cell, though small strain gauges could also be used in this design. The forces from the pin arm will in this case be transferred to the load cell through a force-introducing cap without a fixed connection to the pin arm. This way, only linear forces perpendicular to the pin arm will be transferred to the load cell. This will also ensure that no unnecessary moments are transferred to the load cell, as the force cap is not fixed to the pin arm. Like solution 1, the pin arm is connected to the main frame through a hinge support. This ensures that the pin arm can rotate "towards the load cell". The advantage of this design is that the load cell only will record forces in the preferred direction, as no moments or vertical forces are transferred to the load cell. The downside with this solution is that the pin arm is not fixed to the load cell, and may cause unnecessary vibrations. Additionally, it will be less stable, as the pin arm is free to rotate around the hinge support (to a certain degree). It will also be difficult to install and mount the load cell correctly, and this design is dependent on small tolerances and precise machining.

5.3.5.3 Solution 3

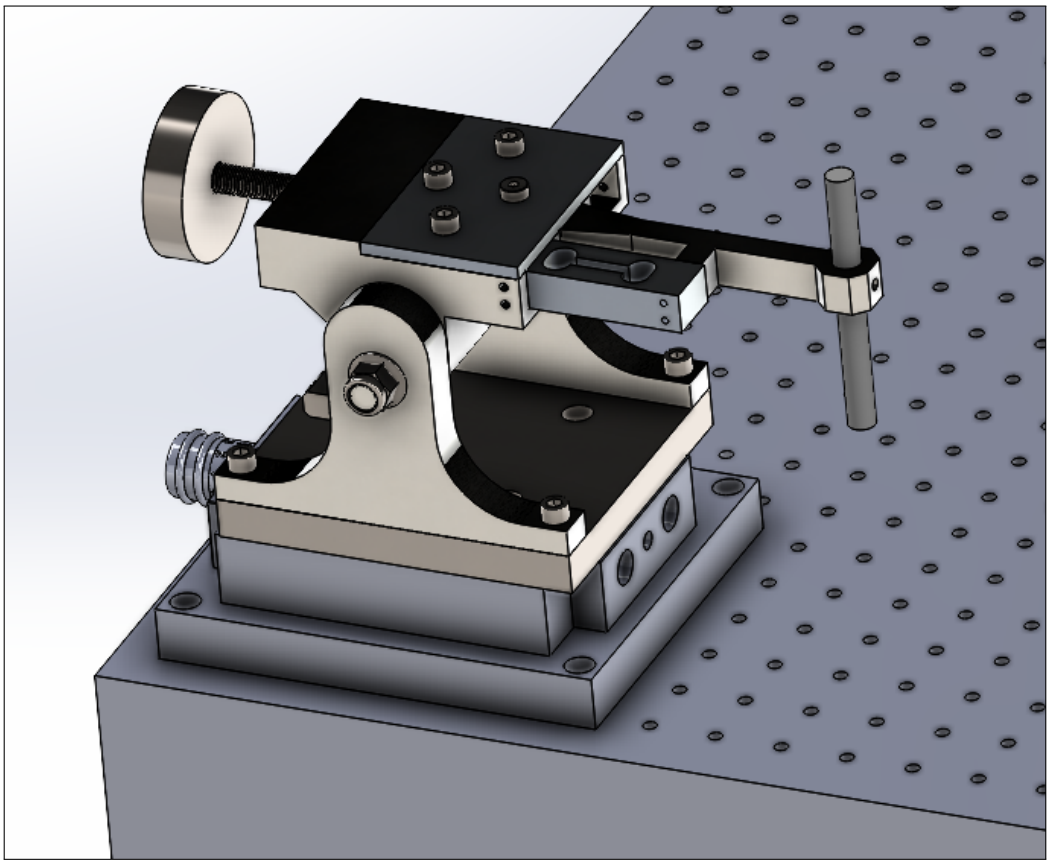

Figure 5.3.11: Solution of rotational tribometer design, with Tedea-Huntleigh strain gauge. Fixed connection.

As seen in Figure 5.3.11, this design is the "predecessor" of the final design. The difference here is that the load cell and pin arm have a fixed connection. This will introduce moments to the load cell, and the connections will not be statically determined in any direction. It is important that the construction is statically determined in the direction of the frictional forces. Together with solution 1, solution 3 also has a lot of similarities with the final design. As the design and development process is based on iterative improvements and continuous development, ideas from both solution 1 and solution 3 have been adopted in the final design. There have been several other ideas suggested and discussed during the design and development process, but the three solutions illustrated above are the main "predecessors" to the final design.

5.4 Electronics

The electrical motors for the tribometers need a power supply in order to transform the electrical energy into mechanical energy. Both of the motors have a working voltage of 24VDC and a maximum electricity consumption of 3A. This means that a current converter/external power supply is needed to power the motor.

The power requirement for the motor and control unit is 24VDC, secured with a safety circuit. The safety circuit consists of two fuses (0.5A and 3A) and a capacitor (3000µF). The safety circuit was not included in the package from MM-Engineering and had to be built by the project group. As there were no capacitors available with 3000µF, the project group decided to connect three 1000µF capacitors in parallel as a replacement for one capacitor of 3000µF. The safety circuit was then built and soldered by the project group before connecting the motor and motor controller to the power supply.

5.4.1 Safety circuit

Upon receiving the motor, the project group faced the challenge of unfamiliarity with its setup. To address this issue, they reached out to the producer, Gunda Automation, for assistance. Gunda Automation provided valuable support by sending a picture from the motor's manual illustrating the required safety circuit, shown in Figure 5.4.1. This information helped the group properly configure the safety circuit between the power supply and the motor system, ensuring the safe and correct operation of the motor.

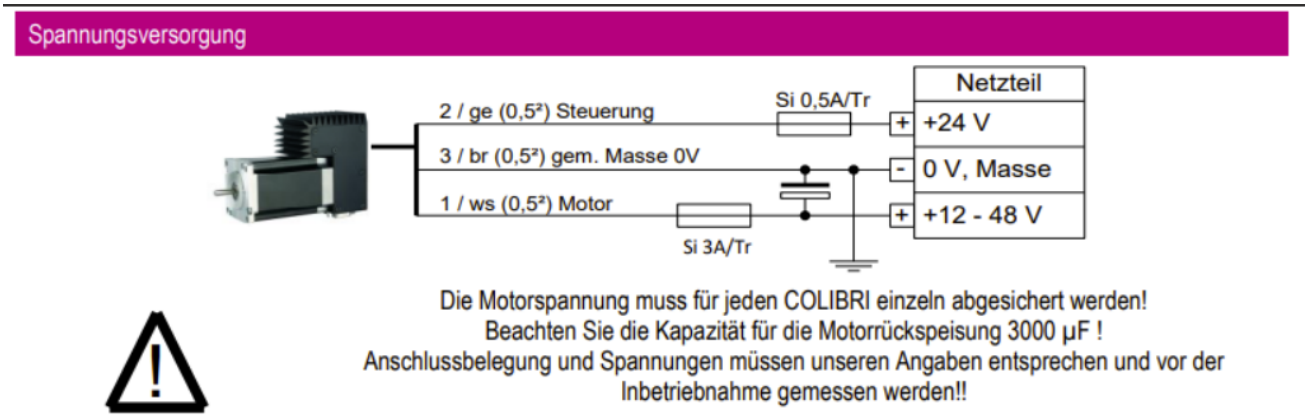

Figure 5.4.1: Safety circuit depicted in manual (*Colibri 23 Mini manual* 2022).

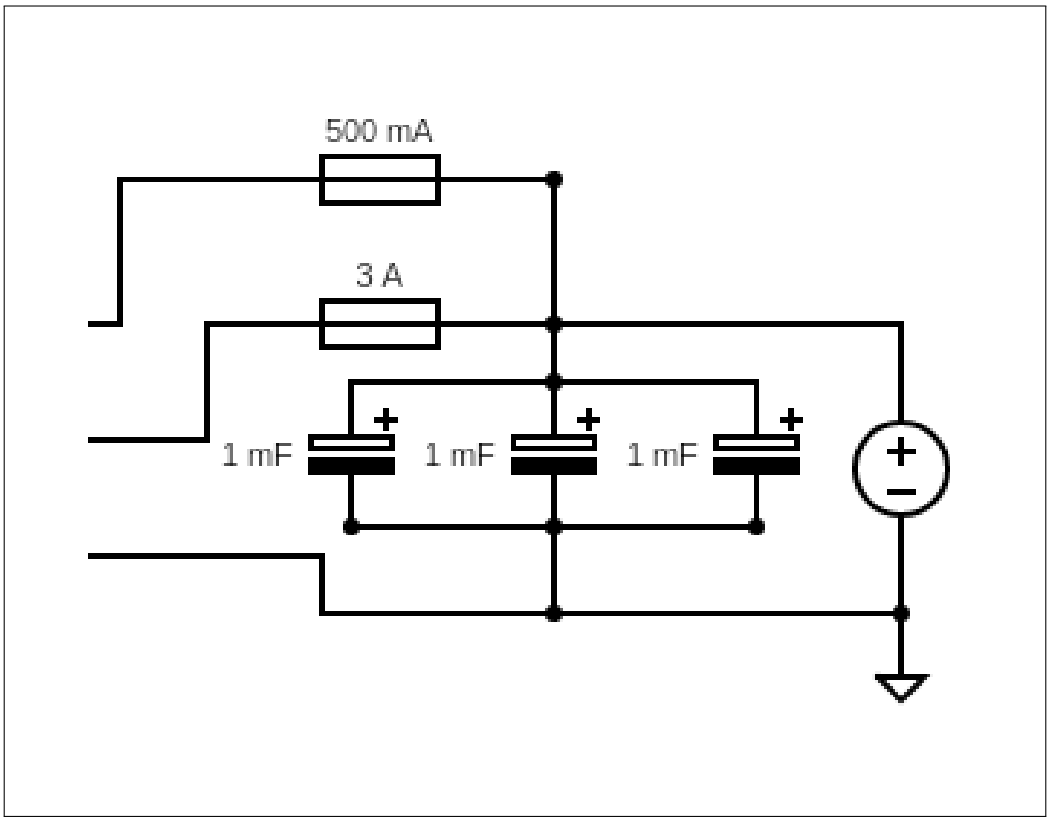

Figure 5.4.2: Safety circuit single line diagram.

After creating the schematic and planning the layout, the project group could grab a solderable prototyping board and create the circuit.

This was measured with a multimeter for both continuity and before connecting it to the motor tested with a power supply to measure the voltage across the lines on the endpoints to ensure

that there was an electrical potential difference, thus confirming no short between the live and neutral sides of the circuit due to excess solder or some mistake in wiring.

5.4.2 Power supply

To meet the power requirements of the motor system, the project group needed to find a suitable power supply that could deliver the correct type and amount of current and voltage. The motor system specifically required a 24VDC supply with a current rating of 3 amps. To calculate the power needed, the formula $P = U \cdot I = 24V \cdot 3A = 24W$ (power = voltage $\cdot$ current) was applied, resulting in a power requirement of 72 watts.

Several power supplies were considered by the project group, one of which was the LRS-150-24. This particular power supply was capable of delivering up to 6 amps, exceeding the required 3 amp rating.

The project advisors later put in an order for a power supply deemed fitting for the system.

5.5 Software

During the design and development phase, an important decision was to determine the programming language for the machine. Considering the time constraints and the requirement for ease of use, the options were narrowed down to two languages: Python and MATLAB. Both languages offer the necessary tools to develop the system as specified in the thesis.

Several factors influenced the choice of programming language. the project group considered their prior knowledge and the degree of customization each language could provide. However, the final decision was primarily based on the familiarity of the lab workers with the programming language. Selecting a language that the lab workers were already proposing, ensured that they could easily modify and further specialize the software in the future if necessary.

This decision aimed to facilitate future maintenance and development, allowing the project group to align their efforts with the expertise available within the lab. By leveraging the existing familiarity with the chosen programming language, the project group aimed to ensure a smooth transition for potential future modifications or enhancements to the software.

5.5.1 Design Criteria

The design of the software for the project was guided by several key criteria to ensure its effectiveness and usability. These criteria are as follows:

Descriptive software that can be understood and modified. It was essential to develop software that could be easily understood and modified in the future. To achieve this, a programming language familiar to both parties was chosen. MATLAB was deemed suitable for the task and met the software requirements effectively. Additionally, comprehensive comments were included throughout the code to describe the functionality of each function, calculation, and variable. Descriptive variable and function names were used to enhance the clarity and readability of the software.

Handling sensor data. The software needed to be capable of receiving, reading, and properly handling sensor data as per the project requirements. This involved identifying the corresponding COM port using the device manager and utilizing MATLAB-integrated functions to open the port and exchange data with the sensors.

Communicating with the motor. The motor used in the project was equipped with a Basic Automation Component module, requiring the establishment of a communication line using

the USB protocol. Similar to the sensor data handling, the motor communication would be achieved by connecting to the motor through the identified COM port. The process involved studying the functionality of the native software and replicating the motor control actions within the developed software.

Ease of use. The user interface of the software aimed to provide a simple and clean experience with minimal visual clutter. A top-down design approach was adopted, guiding the user from the top of the window to the start button. The interface facilitated the input and modification of values, ensuring a user-friendly interaction.

Calibration. The software requires a calibration procedure to establish a zero-value reference point for the sensor. To achieve this, the project group utilized a third-party MATLAB library developed specifically for the HX711 charge amplifier chip(Giacoboni, 2023). This library provided a set of predefined functions for data gathering, which were integrated into the software.

As part of the project requirements, the project group was tasked with developing a calibration procedure for the sensor. The calibration process involved calibrating the sensor for specific force values, namely 1N, 5N, 10N, and 20N.

Writing data to a file. The software was designed to record and store data in a results.csv file upon initialization. A WriteToFile function was defined within the code to calculate the distance traveled by the pin, structure the information in a row variable, and write it to the file using comma-separated values. The data logging process was initiated by pressing the "start logging" button in the interface and halted by pressing the "stop logging" button. The WriteToFile function is executed at an optimal interval to achieve a high-resolution data distribution with more than four data points per second, complying with the Nyquist theorem.

By adhering to these design criteria, the software development process aimed to create a descriptive, functional, user-friendly, and adaptable solution. These considerations ensured that the software met the specific needs of the project and provided a solid foundation for future modifications and enhancements.

5.5.2 Visual layout

A clean GUI was one of the main goals of this software, the project group requested examples of what types of GUI the advisors liked and thought clean, as a reference to the model after.

The project group was told to create an interface that resembled the interface of another tribometer at the lab developed in LabView Figure 5.5.1.

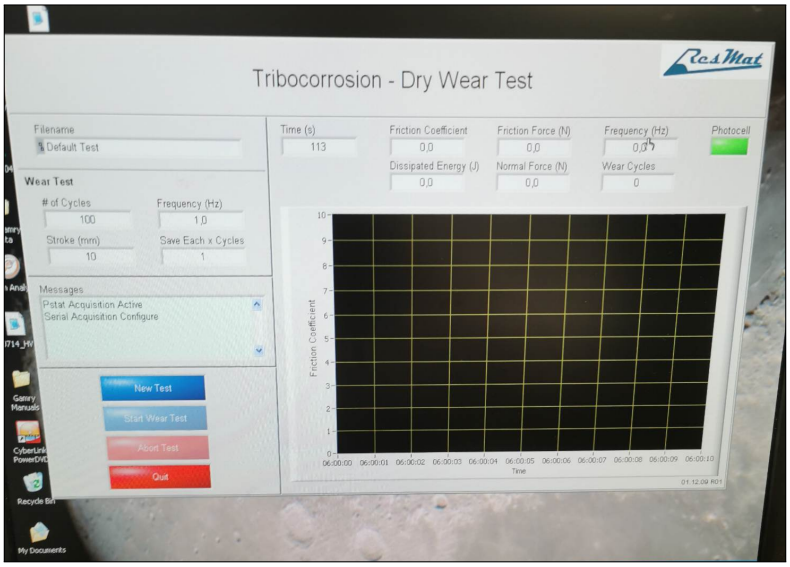

Figure 5.5.1: Example GUI.

With this inspiration, the project group worked towards the GUI shown in Figure 5.5.2.

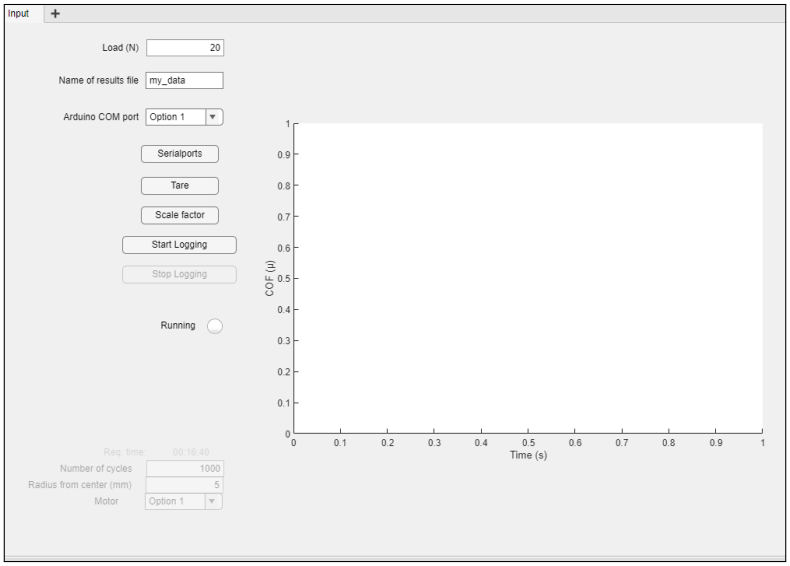

Figure 5.5.2: Developed GUI.

This initial design was approved by the advisors, and so the project group continued developing without having to worry about the layout.

5.5.3 Calibration

The software implementation included a 4-point calibration sequence, where known weights were used to adjust measured values to correspond accurately. This established a direct representation of force in the software. The calibration protocol involved progressing from 1N to 5N, 10N, and 20N in a specific order. To address the challenge of repetitive calibration, the project group developed a code that generated a calibration value stored in a text file, eliminating the need for repeated physical measurements.

5.5.4 Data gathering

To read accurate data from the strain gauge, the software first needs to set a zero value, and then have calibration values to have the correct spacing in measurements, in other words, the

proper distance between values to represent the correct measurement difference.

After consulting with the advisors, the project group recognized the importance of maximizing the data points collected per second. This objective was pursued with the aim of gathering as much information as possible. By increasing the data sampling rate, the project group and advisors ment the software to capture finer details and ensure a comprehensive analysis of the system's behavior. this comes with the drawback of being very system dependent, where a weaker system will suffer from a lack of computing power and cause the system to become slow and stutter.

5.5.5 Arduino

To capture and interpret the analog signals emitted by the strain sensor, a setup comprising a charge amplifier and an Arduino was utilized. The specific chip employed for the charge amplifier was the SEN-13879-HX711 load sensor chip. This chip plays a crucial role in amplifying the small changes in voltage from the sensor, converting the analog signal into digital signals. The amplified and digitized signals are then transmitted to the Arduino for further processing. Finally, the Arduino communicates with the MATLAB program, providing the processed data for analysis and manipulation. This system allows for accurate measurement and utilization of the sensor data within the project.

5.6 Additional notes

A while after the project group started dismounting the old tribometer and started mounting the prototypes the project group had made, there were observed places where corrosion had occurred on the optical table, where large metal plates had been mounted on the table for a long time. This has most likely resulted from moisture being trapped between the optical table and the plates when the part was assembled on the table. To prevent this from happening to our design the project group decided that all the large mounting bases were to stand on top of risers. In this case, the project group does not have to do many precautions considering extra measures for moisture control when assembling the tribometer. The risers will keep the surface of the bases and the surface of the optical table separated.

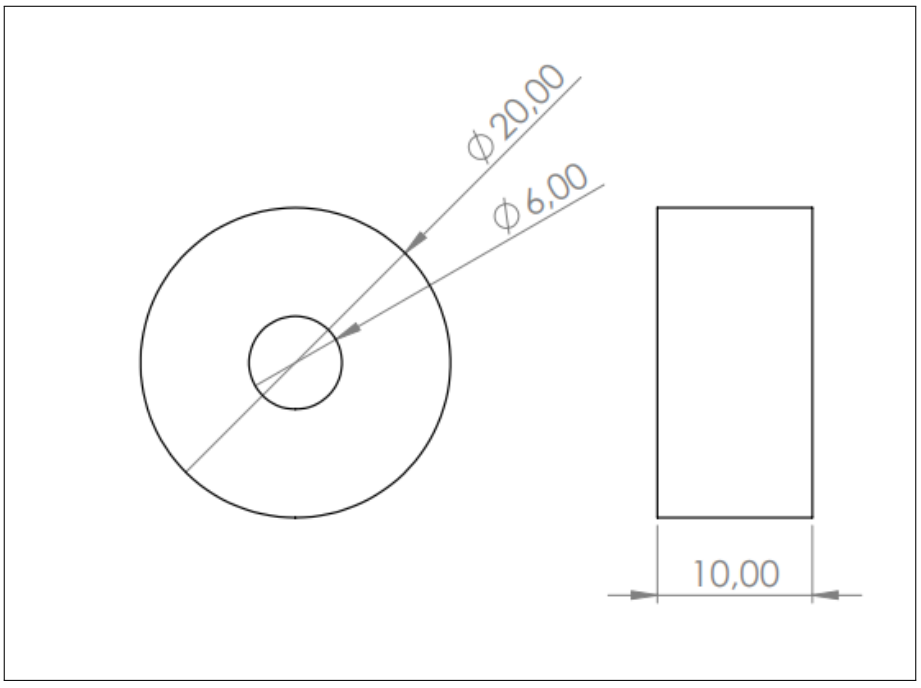

Figure 5.6.1: Drawing of risers.

Final Product

6.1 Reciprocal tribometer

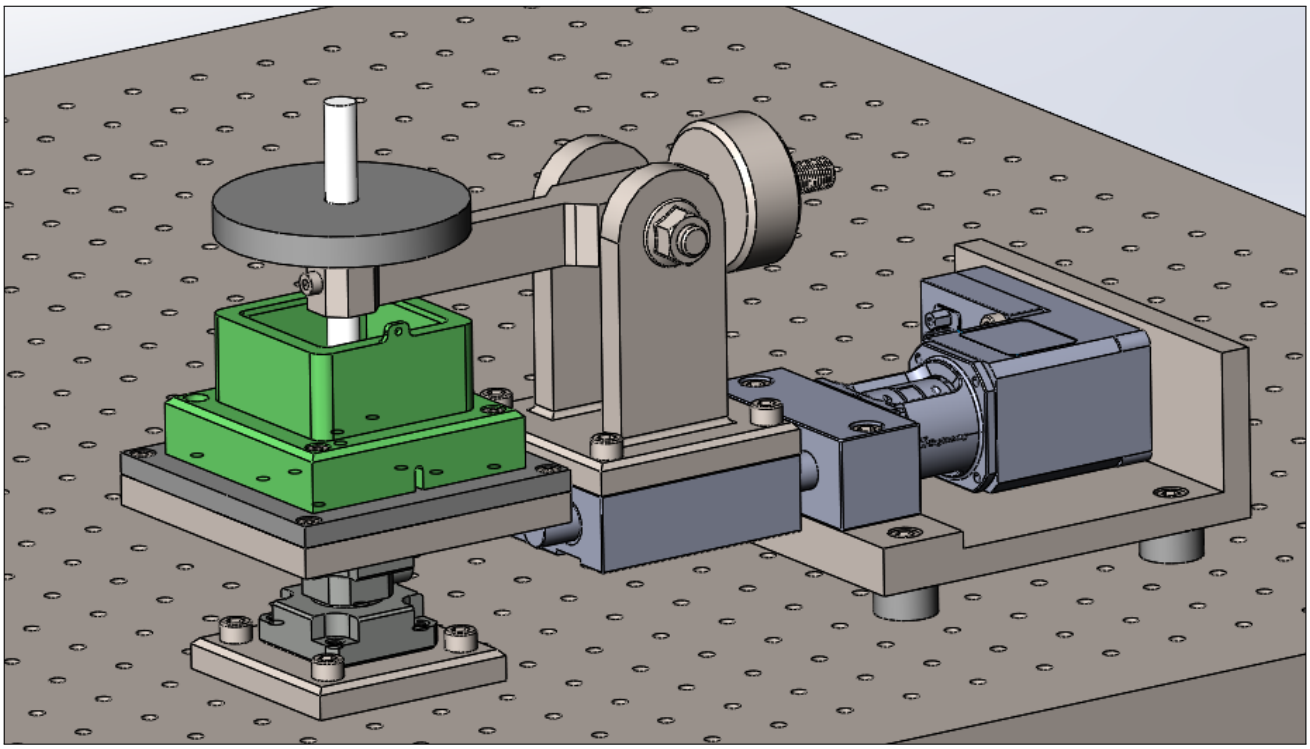

Figure 6.1.1: Final design of reciprocal tribometer with tribocorrosion sample holder.

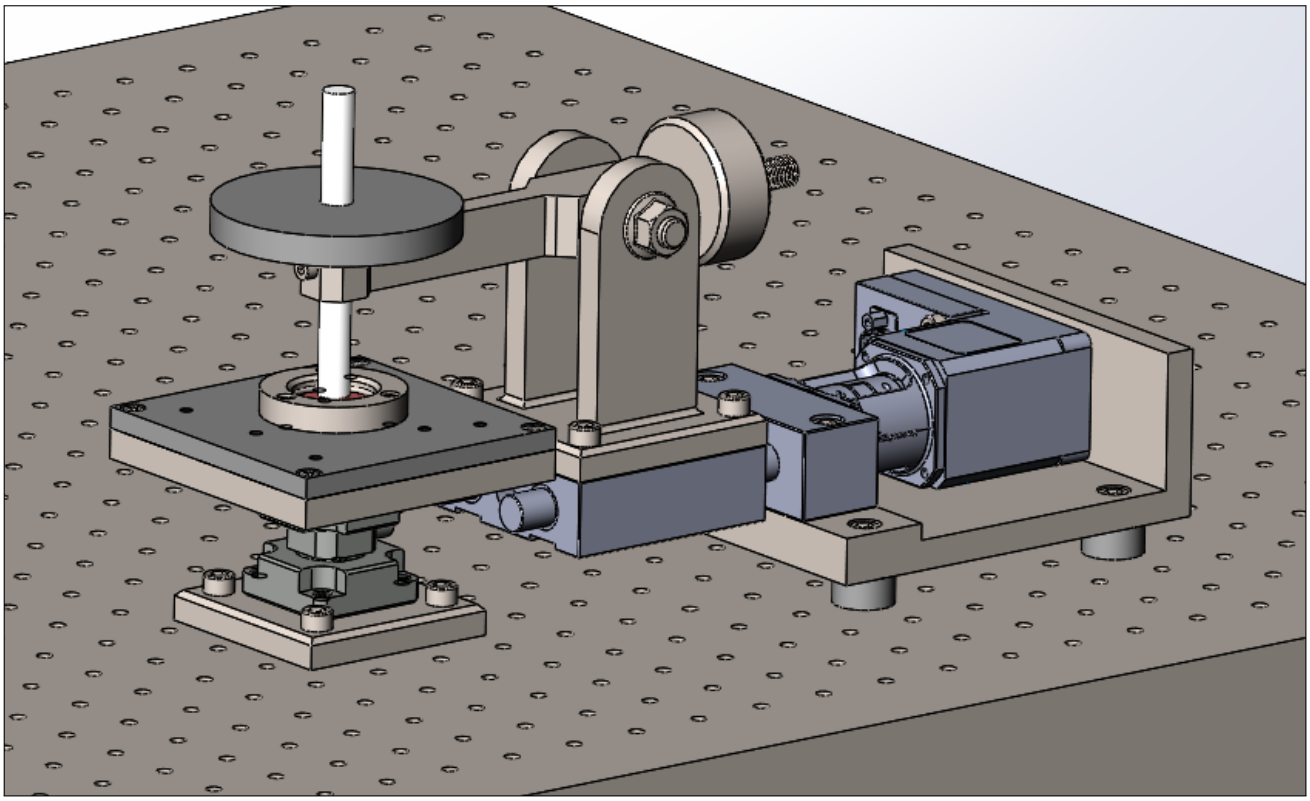

Figure 6.1.2: Final design of reciprocal tribometer with dry sample holder.

6.1.1 Arm

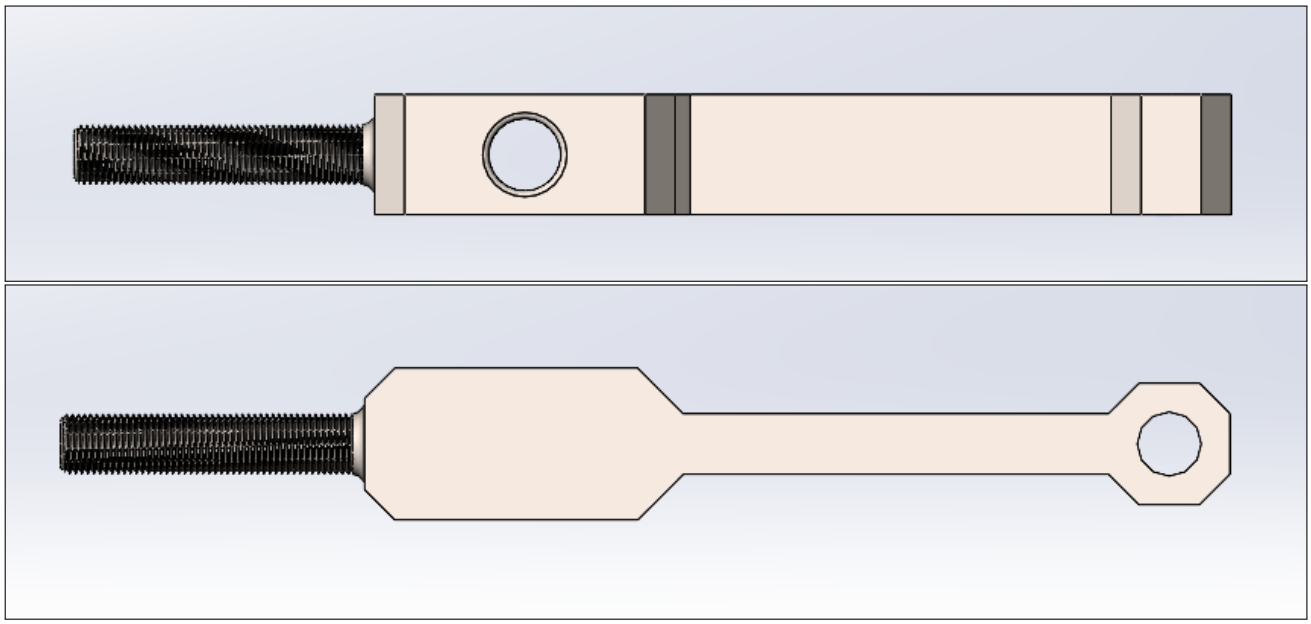

Figure 6.1.3: Final design of the arm.

In the final design, the arm shares similarities with solution 3 described in the design and development chapter. However, a key distinction is that the hole for the axle is precisely positioned along the x-axis, aligned with the center of balance of the arm. This placement reduces the momentum generated by the deadweights, resulting in a more precise tribometer. By aligning the counterweight with the center of balance, the force it creates is absorbed by the axle and does not interfere with the normal force in the experiment. Detailed calculations regarding this can be found further in the chapter. Additionally, balancing the arm becomes easier with this configuration.

Another factor influencing the decision to position the axle through the center of mass of the arm is that it achieves a more symmetrical shape around the x-axis. This symmetry facilitates machining the counterweight rod and threads using a lathe machine.

The distance between the axle and the arm is 107.5mm. Although it may seem like an unconventional value, it is determined by the assembly of the sensor and motor to the optical table.

6.1.2 Axle base

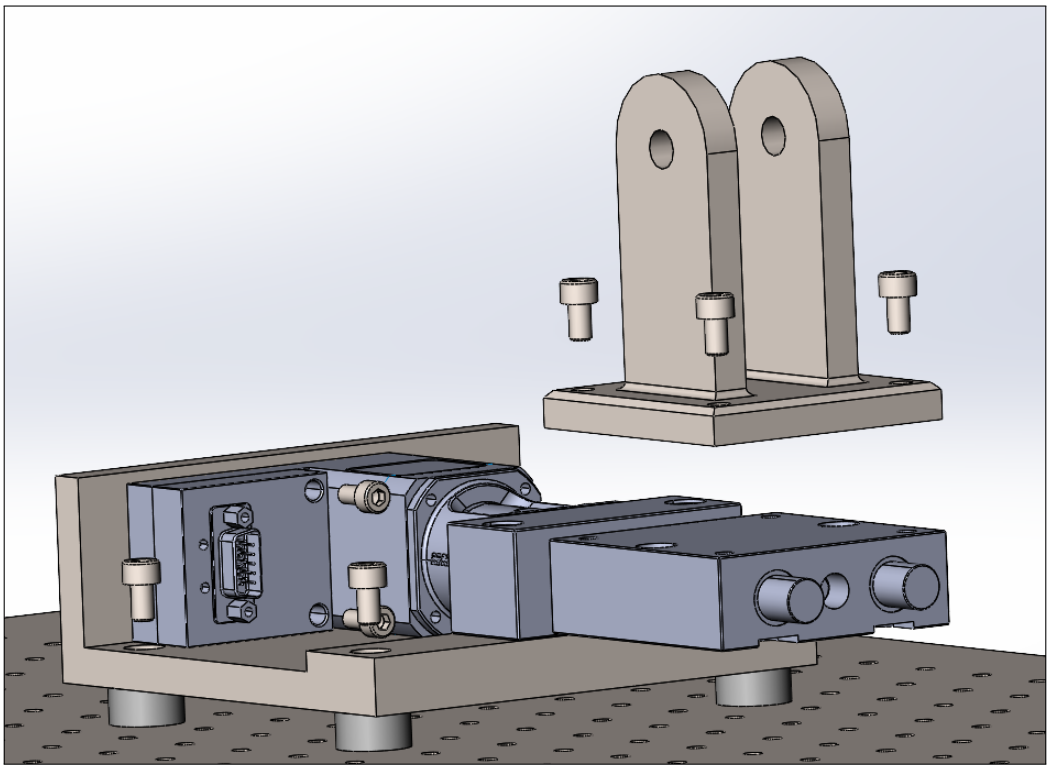

Figure 6.1.4: Assembly of the axle base, the motorized positioning stage and the motor stage.

Figure 6.1.4 depicts the axle base and its intended mounting on top of the motorized positioning stage, which is further installed on the motor stage and optical board. The axle base is designed with a simple geometric shape, taking into consideration the ease of machining using a milling machine, followed by drilling the holes to ensure proper fitting. The emphasis on simplicity in its design allows for efficient fabrication and assembly of the axle base.

Additionally, the design of the axle base incorporates features that make it easy to disassemble the arm. This design consideration enables other individuals using the laboratory to create their own arm designs while utilizing the same axle base. By ensuring easy disassembly, the interchangeability and flexibility of arm designs are promoted, allowing for experimentation and customization based on specific research needs or preferences.

6.1.3 Tribocorrosion cell

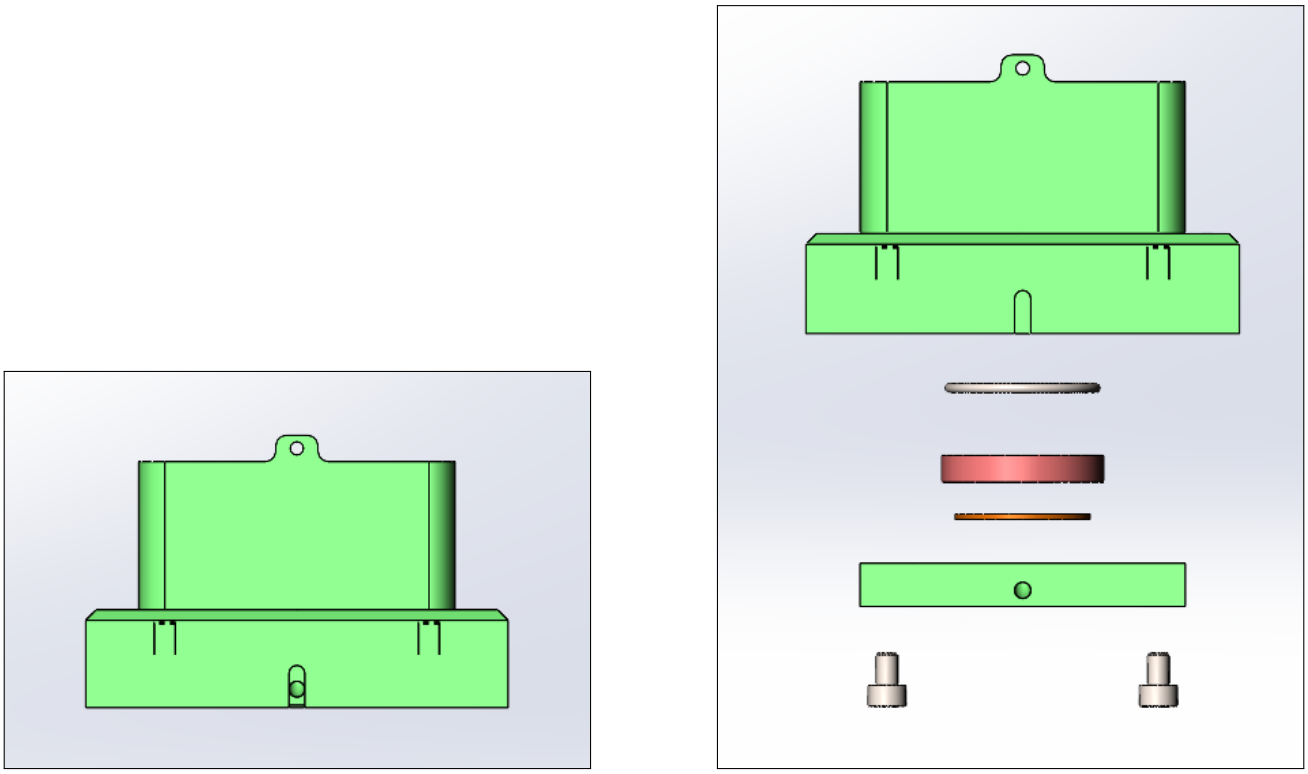

(a) Tribocorrosion sample holder.

(b) Exploded view, tribocorrosion sample holder.

Figure 6.1.5: Mounting of the tribocorrosion sample holder.

In Figure 6.1.5 it is possible to see how the tribocorrosion sample holder is supposed to be assembled. The sample is placed between the bottom part and into the holder with four screws with an o-ring in between to ensure that there is no leakage. Underneath the sample is a copper plate that will be soiled to a wire underneath the sample. This is where the connection between the sample and the potentiostat is. The wire will go from the bottom of the copper plate through a channel in the bottom part of the sample holder and into the potentiostat.

6.1.4 Mounting and connections

When examining the mounting and overall assembly of the reciprocal tribometer, it can be divided into two distinct subassemblies.

The first subassembly encompasses the sensor, the sample, and all the necessary components required to connect these to the optical table.

The second subassembly comprises the motorized positioning stage, the arm, the axle base, and the pin. These components work together to enable controlled movement and precise positioning of the arm and sample during testing. The axle base provides a stable foundation for the arm, while the motorized positioning stage facilitates the controlled motion required for the tribometer's reciprocating action.

By dividing the tribometer into these two subassemblies, it allows for easier understanding, maintenance, and potential modifications or upgrades to each individual component as needed.

Figure 6.1.6a presents the bottom view of the sensor base, which plays a critical role in mounting the sensor onto the optical board. The base features counterbore holes on one side to ensure that the screws used to connect the sensor do not obstruct the mounting process of the sensor

to the optical table. This design consideration allows for a clean and unobstructed attachment of the sensor, ensuring proper alignment and functionality during experimentation

Figure 6.1.6b depicts the top view of the sensor top. Similar to the sensor base, this component also features counterbore holes on one side. Due to the proximity of the screws that connect the sensor to the sensor top, an additional plate is included to cover these screws before mounting the sample. This design choice ensures that the screws are protected and do not interfere with the sample or the testing process. By adding the additional plate, the sample can be mounted securely on top of the sensor without any obstruction or potential damage caused by the exposed screws.

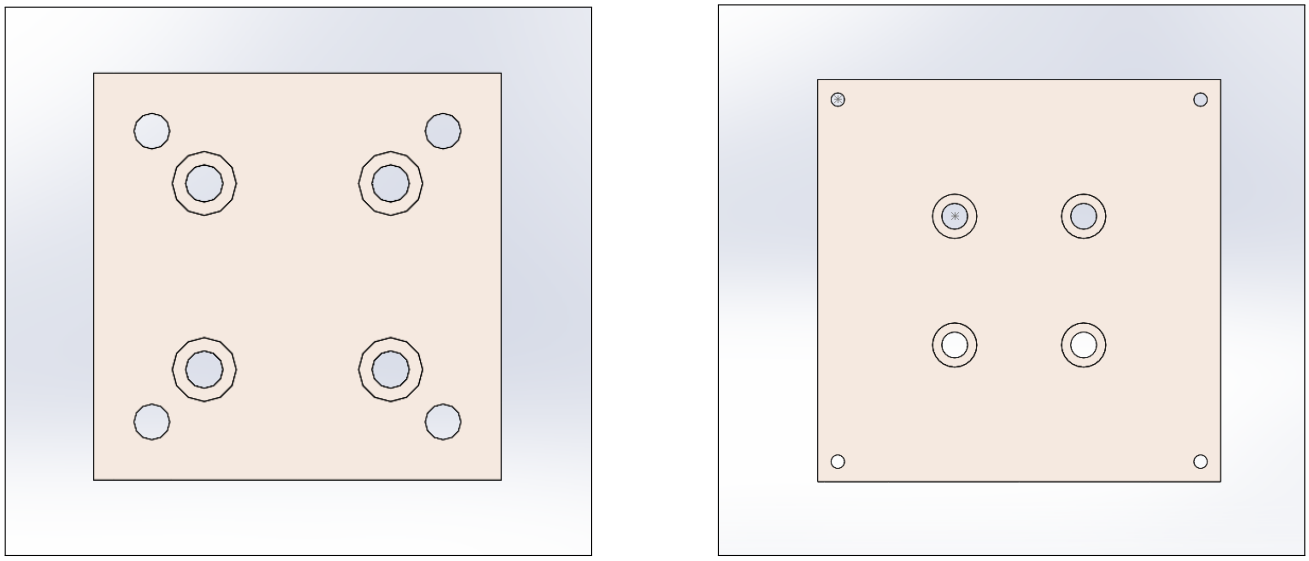

(a) Bottom view of the sensor base.

(b) Top view of the sensor top.

Figure 6.1.6: Mounting holes for the sensor base and the sensor top.

Figure 6.1.7 showcases the top view of the sample stage. It can be conveniently connected to the sensor top using four M4 screws. The design of the sample stage allows for its versatile use in both tribocorrosion and dry testing applications.

To accommodate different sample sizes, the sample stage incorporates three M3 threaded mounting holes for each of the dry sample holders designed for 30 mm and 40 mm diameter samples. This feature enables easy interchangeability and adaptability to various sample sizes used in dry testing.

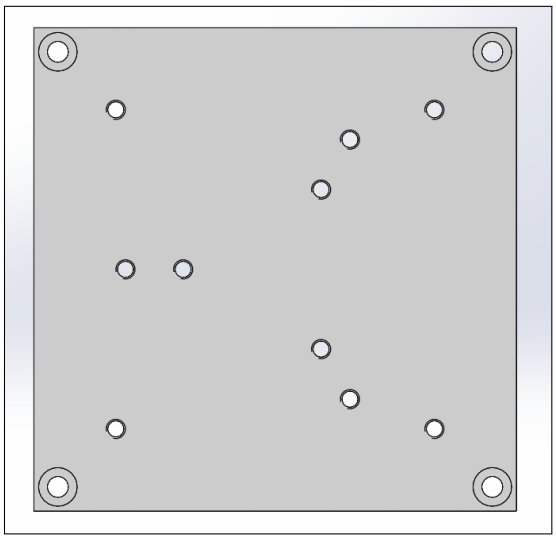

Figure 6.1.7: Top view of sample stage.

Furthermore, the sample stage also includes four M4 threaded mounting holes specifically designed for the tribocorrosion sample holder. These mounting holes are intended to securely attach the tribocorrosion sample holder, ensuring stability and reliability during tribocorrosion testing.

Figure 6.1.8 illustrates how the sensor base, the sensor, the sensor top, the sample stage, and the tribocorrosion sample holder are supposed to be mounted together. This is the completion of the first subassembly. When this part is connected it can easily be mounted wherever on

the optical board. Again this will give freedom to whoever wants to make modifications to the tribometer but want to use the same sensor and sample setup.

By enabling the independent mounting of these components on the optical board, researchers can customize and optimize the placement of the sensor and sample for their specific experimental requirements. For example, if a specialized arm is needed to be designed for a specific experiment. This adaptability enhances the versatility of the tribometer and facilitates further customization based on individual research needs.

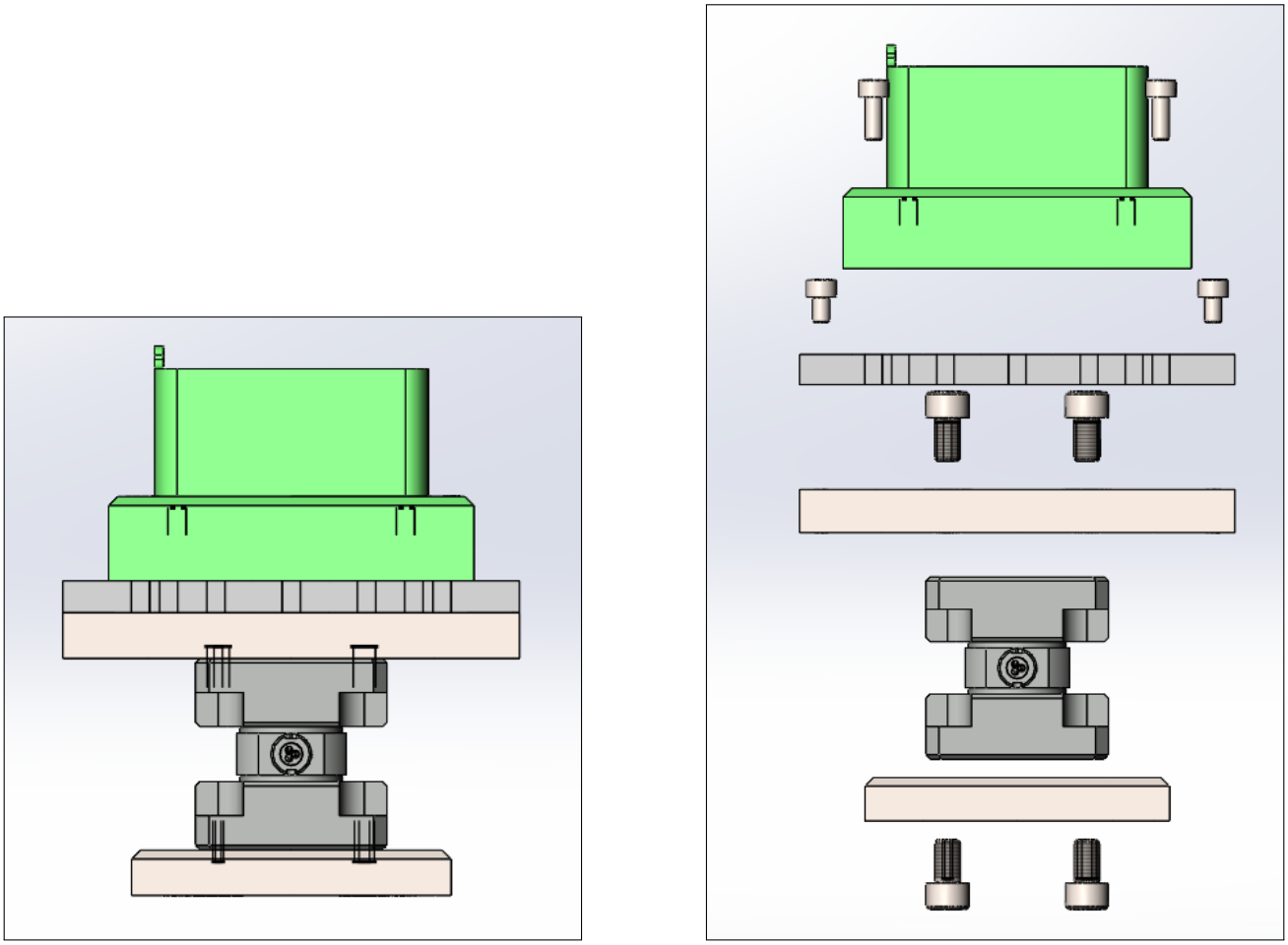

(a) Tribocorrosion cell and sensor subassembly.

(b) Exploded view tribocorrosion cell and sensor subassembly.

Figure 6.1.8: Mounting of the tribocorrosion sample cell to Kistler 9327A.

In Figure 6.1.9, the utilization of dry sample holders on the sample stage is depicted. In this setup, the sample is placed directly on the sample stage, with an O-ring positioned on top, and the dry sample holder is then placed and secured with three M3 screws. This arrangement allows for the use of samples with varying thicknesses, as long as the sample is thicker than the height of the inside of the sample holder.

It is worth noting that in Figure 6.1.9, a small gap can be observed between the sample stage and the sample holder, due to the thickness of the sample. However, this gap does not adversely affect the sample as long as the screws are properly tightened. The secure fastening of the sample holder ensures that the sample remains in place during testing, maintaining the desired experimental conditions.

The design of the dry sample holder and its attachment to the sample stage provides stability and reliable positioning of the sample, enabling precise and controlled testing. Researchers can

easily interchange samples and adjust the setup to accommodate different sample thicknesses, enhancing the versatility and usability of the tribometer for dry testing applications.

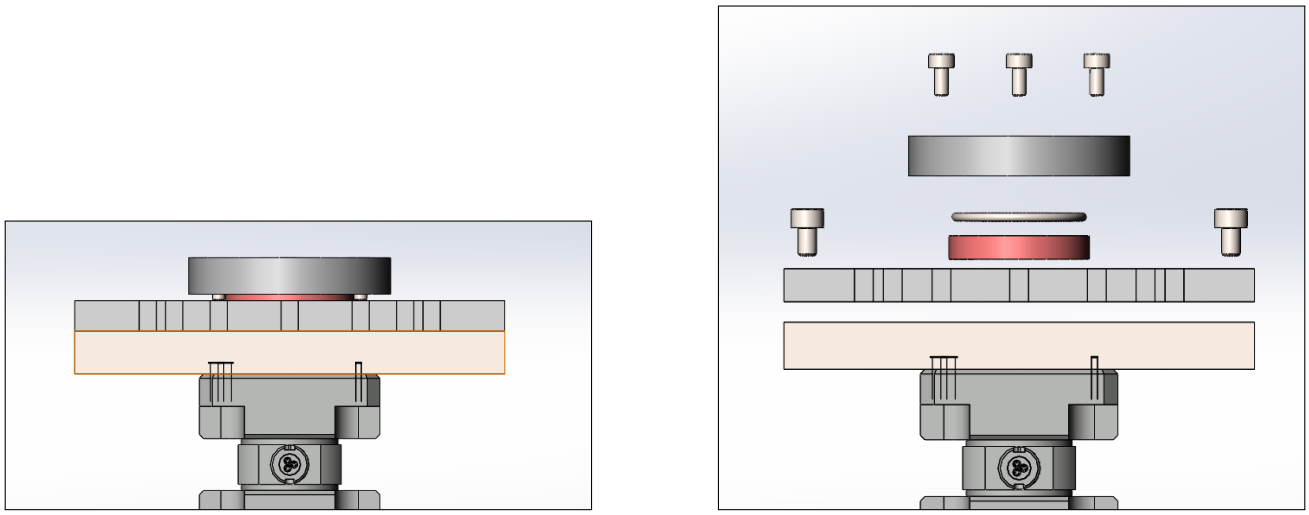

(a) Tribological dry sample holder.

(b) Tribological dry sample holder mounting.

Figure 6.1.9: Mounting of the tribocorrosion sample holder.

In Section 6.1.2, the assembly of the motorized positioning stage, motor stage, and axle base to the optical table is described. This forms part of the second subassembly of the tribometer. In Figure 6.1.10, the connection between the axle base, axle, and arm is illustrated. For this connection, a flange bushing from GGB is utilized, following the guidelines provided in the GGB DP4 manual.

The flange bushing serves as a bearing component, facilitating smooth rotation of the arm around the axle. It provides support and reduces friction between the moving parts, contributing to the overall functionality and performance of the tribometer. By following the guidelines outlined in the GGB DP4 manual, proper installation and fitting of the flange bushing can be ensured, promoting reliable and efficient operation of the tribometer.

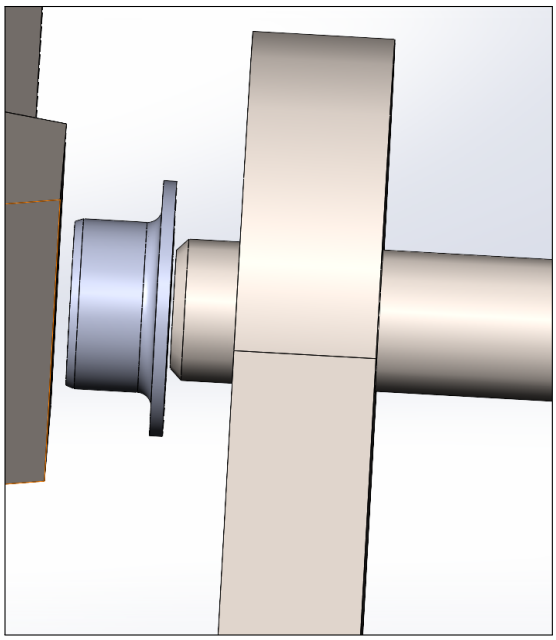

Figure 6.1.10: Connection between arm and axle base.

The chosen method of pin fastening, as shown in Figure 6.1.11, offers several advantages for the reciprocal tribometer. Firstly, it provides a simple and user-friendly construction. The pin is inserted through the hole in the arm and secured with an M4 screw. This straightforward design allows for quick and hassle-free assembly and disassembly of the pin, facilitating easy handling and manipulation for researchers. The use of a standard M4 screw for fastening further enhances accessibility, as it is readily available and easy to maintain or replace if needed.

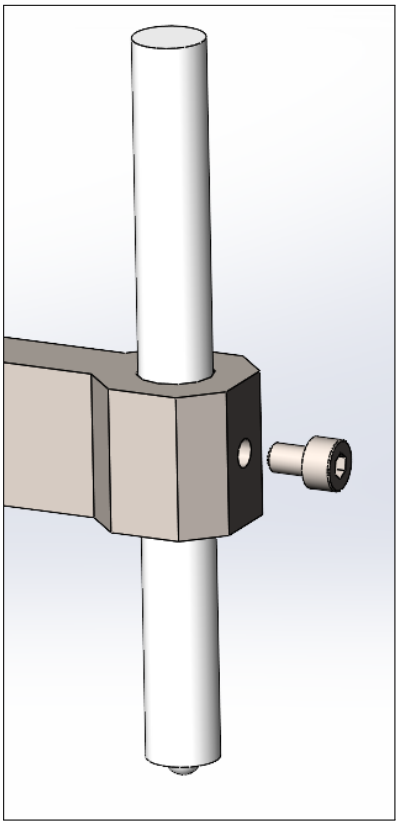

Figure 6.1.11: Connection between arm and axle base.

Furthermore, the chosen pin fastening method provides stability to the tribometer. The secure connection between the pin and the arm, achieved through the M4 screw, ensures a stable and reliable attachment. This stability is crucial during tribometer experiments to minimize unwanted vibrations or movements that could compromise the accuracy and reliability of the results.

The counterweight is attached to the arm by screwing it on, which provides a secure connection for most experiments, especially those conducted at slow speeds. The threaded design of the counterweight and the arm allows for easy assembly and ensures that it remains in place during the experiment.

To further enhance the stability and minimize any potential movement of the counterweight, additional fastening options are available. Figure 6.1.12 illustrates the use of two bolts on each side of the counterweight to provide extra reinforcement. These bolts can be tightened to further secure the counterweight to the arm, reducing the likelihood of any undesired movement or displacement during the experiment.

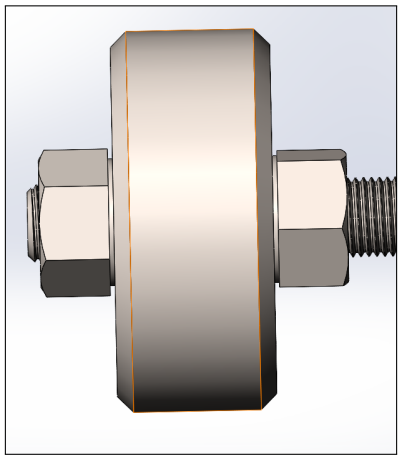

Figure 6.1.12: Additional fasteners for conterweight.

6.1.5 Materials

The selection of materials for the reciprocal tribometer involved considering both steel and aluminum. Aluminum offers the advantage of being lightweight, which can be beneficial for ease of handling and maneuverability. On the other hand, steel provides greater stiffness and rigidity to the construction, which can enhance the overall stability and performance of the tribometer.

After careful consideration and working on the design, it was ultimately decided to use stainless steel for the construction of the tribometer. This choice offers several advantages. Firstly, by

using steel, it becomes possible to create a slimmer and more user-friendly design. The increased rigidity provided by steel enhances the stability of the tribometer, which is crucial for accurate and reliable experimental results.

The total mass of the stainless steel construction is estimated to be around 1.55kg. While this will add some weight to the tribometer, it is not expected to have a significant impact on the motorized positioning stage, except for affecting acceleration during operation.

Overall, the decision to use stainless steel for the construction of the reciprocal tribometer was based on the desire for improved rigidity, user-friendliness, and the ability to achieve precise and reliable experimental outcomes.

6.1.6 Calculations

In the calculations regarding the deadweights and their impact on the tribometer, it is important to consider the forces created when accelerating and changing direction. As the arm moves, all components with mass contribute to the creation of these forces.

Envisioning the arm as a beam, with the centers of mass of all components aligned with the axle, the forces generated during acceleration will be absorbed by the axle and axle holder. However, since the deadweights are placed on top of the arm, there will be a height difference between the center of the axle and the center of mass of the deadweights.

Figure 6.1.13 illustrates this height difference, denoted as "h." The value of h will vary depending on the number of deadweights stacked on top of each other. The greater the number of deadweights, the higher the center of mass of the deadweights will be.

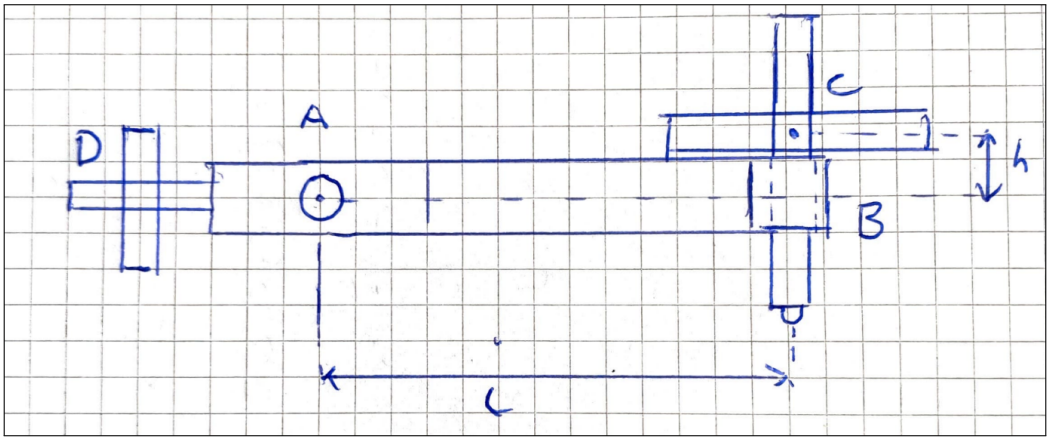

Figure 6.1.13: Illustration of arm marking the length l and h.

Now simplifying the figure even more by replacing the pin with a roller support in the x-direction and the axle with a pin support in the xz-directions. This is illustrated in Figure 6.1.14.

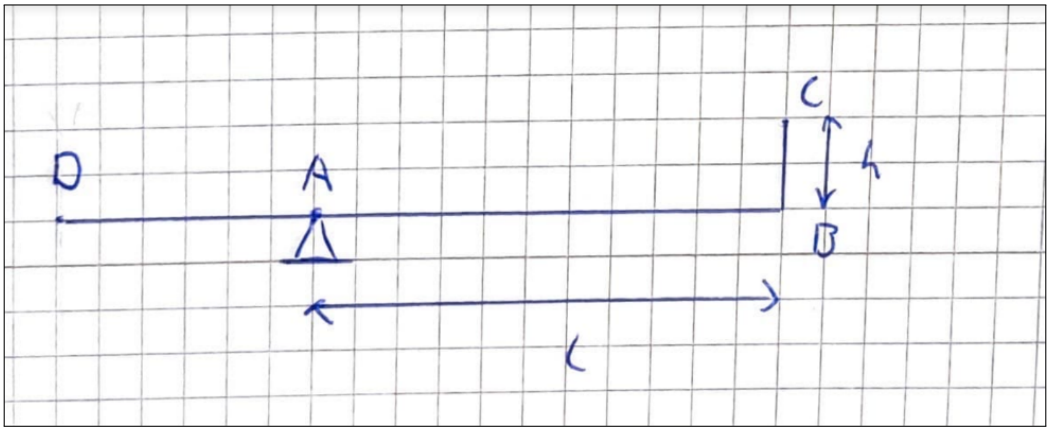

Figure 6.1.14: Simplified illustration of arm marking the length l and h.

When performing calculations for reciprocal motion, three different situations are considered, each represented by a separate free-body diagram. It is assumed that the acceleration remains constant at the endpoints. In these diagrams, forces Dz and Dx are depicted, but they are not essential for the calculations. Dz's momentum will be balanced by the mass of the arm on the right side, while Dx is aligned with the axle axis and does not create any arm momentum. Hence, these forces are disregarded in further calculations and set to zero. Consequently, the values of Az and Ax do not represent the actual reactive forces of the axle but rather indicate the difference in reaction forces generated when the deadweights are accelerated. Bz represents the normal force exerted by the deadweights.

Figure 6.1.15 illustrates the arm when the velocity remains constant. Since there is no acceleration in the x-axis, the only force resulting from the deadweights will be in the z-direction.

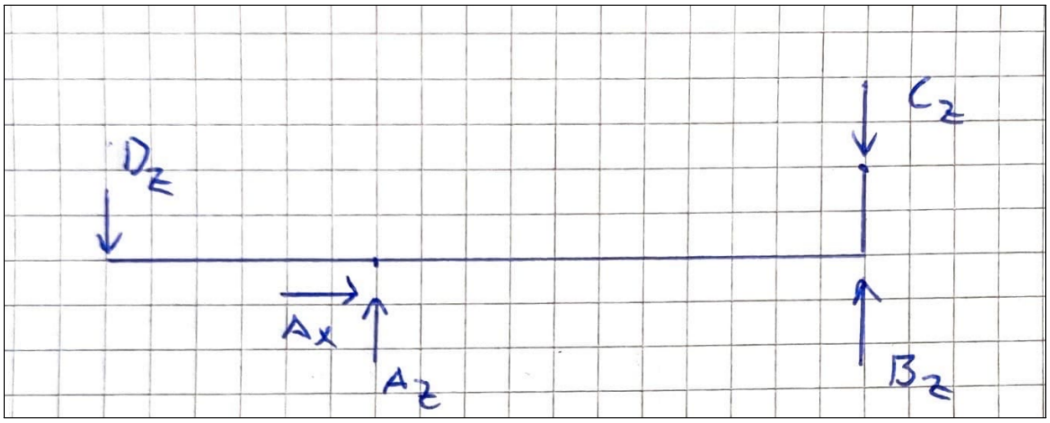

Figure 6.1.15: FBD of the arm when there is no acceleration.

$$C_z = m \cdot g$$

From this it is possible to find the normal force Bz with the static formula for momentum:

$$\begin{aligned} \sum M_a &= 0 \\ C_z \cdot l - B_z \cdot l &= 0 \\ C_z &= B_z \end{aligned}$$

The desired outcome is to establish an ideal scenario where the normal force is generated by the force exerted by the deadweights. In this scenario, the absolute values of the force exerted by the deadweight and the normal force are equal, ensuring that the input force represented in the software prior to the experiment is accurate. This particular scenario allows for the observation of a significant amount of reciprocal movement.

As illustrated in Figure 6.1.16, the free-body diagram where the arm is farthest away from the motor is accelerated backward towards the motor. In this situation, the force C_x can be determined using the following equation:

$$C_x = m \cdot A_x$$

Here, the mass of the deadweights generates a force that in turn creates momentum around the axle. This gives way to a new equation for the momentum around point A for the given situation:

$$\begin{aligned} \sum M_a &= 0 \\ C_z \cdot l - B_z \cdot l + C_x \cdot h &= 0 \\ (C_z \cdot l + C_x \cdot h)/l &= B_z \end{aligned}$$

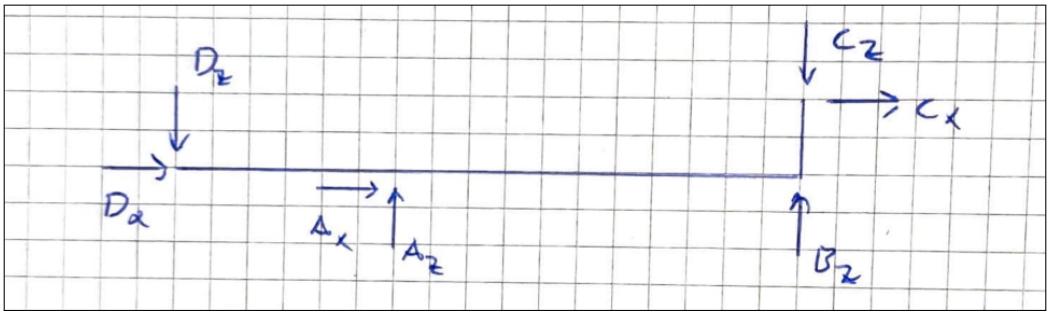

Figure 6.1.16: FBD of the arm when it is accelerated backwards.

In Figure 6.1.17 the free-body-diagram where the arm is nearest the motor and is accelerated forwards towards the motor. Here the force C_x will be equal to the scenario above but will be directed in the opposite direction.

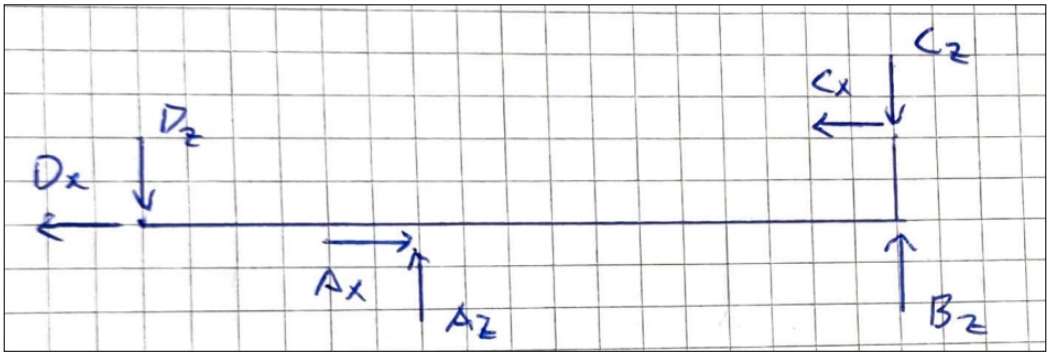

Figure 6.1.17: FBD of the arm when it is accelerated forwards.

In this scenario, the mass of the deadweights generates a force that results in additional momentum around the axle. Consequently, one can establish a new equation for the momentum around point A:

$$\sum M_a = 0$$
$$C_z \cdot l - B_z \cdot l - C_x \cdot h = 0$$
$$(C_z \cdot l - C_x \cdot h)/l = B_z$$

Based on the figures and formulas presented above, it is evident that the change in the direction of the arm has an impact on the magnitude of the normal force. In our tribometer setup, it is anticipated that two deadweights, each weighing 1kg and having a height of 10mm, will be predominantly used. While the acceleration for the MM-engineering Motorized Positioning Stage is not specified in the datasheet, the previous motor, the Aerotech ANT95L, had an acceleration of 4g (39.2 m/s^2) without any load. Considering the mass of the ANT95L stage as 0.63kg and the additional mass of the construction atop as approximately 1.56kg, one can estimate a maximum acceleration of approximately 11.29 m/s^2. It is important to note that in reality, the acceleration will be lower due to the frictional force of the experiment and the fact that the motor that is chosen has a completely different working mechanism than the Aerotech motor. However, for illustrative purposes in showcasing the relationship between acceleration and the normal force, this value will be utilized.

$$m = 2 \cdot 1kg = 2kg$$
$$h = \frac{10mm + (10mm + 10mm)}{2 = 20mm}$$
$$l = 107,5$$
$$a_x = 11.29 = 11290mm/s^2$$

For the scenario where the arm is accelerated backward, one can utilize the formulas to calculate the change in the normal force. This calculation yields the following value for the normal force:

$$B_z \cdot 1000 = \frac{(2kg \cdot 9810mm/s^2 \cdot 107.5mm + 2kg \cdot 11290 \cdot 20mm)}{107.5}$$
$$B_z = 23.82N$$

In the scenario where the arm is accelerated forward, one can utilize the previously presented formulas to calculate the change in the normal force at the endpoint. By applying the appropriate equations, one can determine how the normal force will be affected. However, without specific values and equations, I am unable to provide you with the calculated value for the normal force in this particular situation. If you can provide the necessary data, equations, and any additional information required, I'll be more than happy to assist you with the calculation.

$$B_z \cdot 1000 = \frac{(2kg \cdot 9810mm/s^2 \cdot 107.5mm - 2kg \cdot 11290 \cdot 20mm)}{107.5}$$
$$B_z = 15.419N$$

When the acceleration is extremely high, it can lead to a significant deviation in the normal force, which, in turn, affects the measured frictional force and the coefficient of friction. However, using the velocity formulas to calculate the distance (Equation 6.2) and time (Equation 6.1) associated with this acceleration (assuming a travel velocity of 20mm/s), one will find that the

arm will rotate over a distance of 0.0178mm and in a time of 3.562×10^{-3} seconds. These values represent very small distances and timescales. To put it into perspective, the rotational tribometer sensor records a data point every 0.1 seconds, indicating that the arm's motion occurs within an extremely short timeframe compared to the sensor's recording intervals.

$$v = v_0 + a \cdot t \tag{6.1}$$

$$v^2 = v_0^2 + 2 \cdot a \cdot s \tag{6.2}$$

Indeed, considering the differences in design and performance between the MM-engineering motorized positioning stage and the Aerotech one, it is reasonable to assume that the actual acceleration will be lower than the example provided. This would result in a longer distance and longer duration of the normal force deviation. As the acceleration decreases, the force Cx will also decrease, leading to a smaller overall deviation.

Furthermore, after consulting with advisors, it has been determined that this deviation will have a minimal effect on the measurements conducted in the tribometer. Therefore, while there may still be some impact on the normal force due to acceleration, it is not expected to significantly affect the accuracy and reliability of the measurements obtained in the tribometer setup.

6.1.7 Simulations

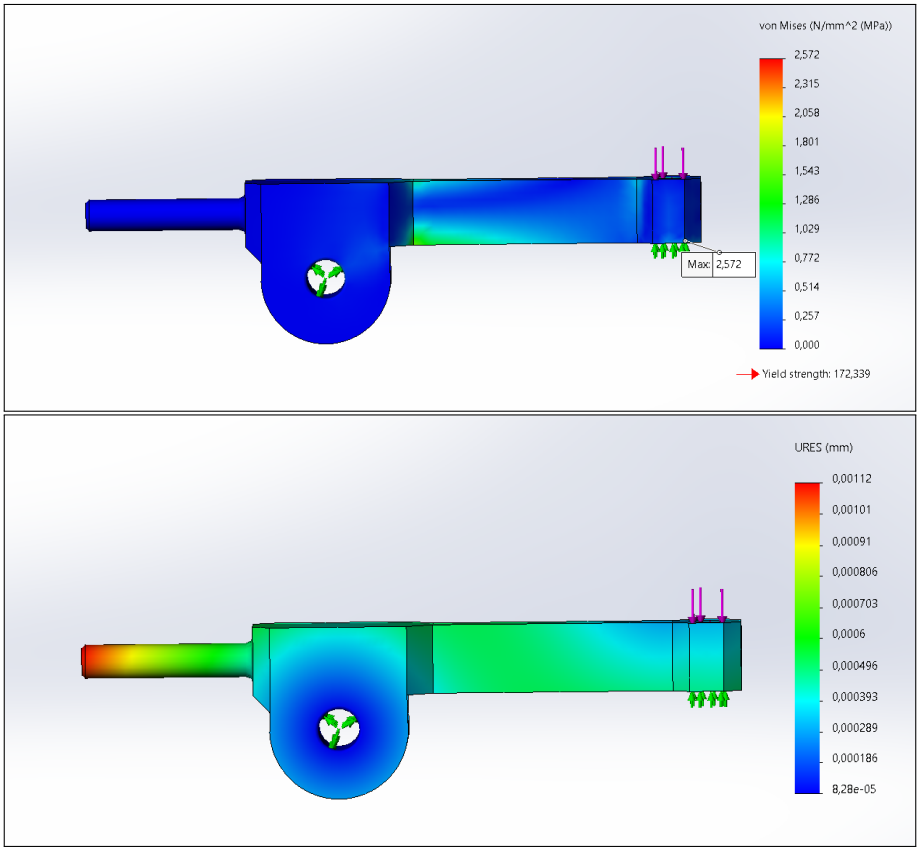

Figure 6.1.18: Static simulation of arm solution 3.

In Figure 6.1.18, a static analysis of the arm is presented, simulating the arm under a high load of 50N and a friction coefficient of $\mu = 1$.Although this load and coefficient of friction represent extreme conditions unlikely to be encountered in most experiments, they are used to assess the arm's performance under rigorous conditions.

The forces in the simulation are applied to represent the arm moving forwards, as this motion generates the maximum stress and displacement. The results of the simulation show that the maximum stress experienced by the arm is $2,572MPa$.which is significantly lower than the arm's yield strength of $172.338MPa$. This indicates that the arm can be manufactured with less material, potentially reducing its weight and cost. However, it is important to consider other factors such as user-friendliness, stability under load, and overall robustness, which may be compromised if the arm is excessively lightweight.

The simulation also reveals that the displacement of the arm is minimal, with a value of only about 0.0006mm. The maximum displacement occurs at the tip of the arm, where the counterweight is mounted. This small displacement further confirms the arm's stiffness and rigidity, ensuring accurate and precise experimental measurements.

In summary, the simulation results demonstrate that the arm design is structurally sound and capable of withstanding high loads and friction coefficients. While the arm could potentially be optimized by reducing material, other important considerations such as user-friendliness and stability must be taken into account. The small displacement observed in the simulation confirms the arm's stiffness, contributing to the tribometer's overall performance and accuracy during experiments.

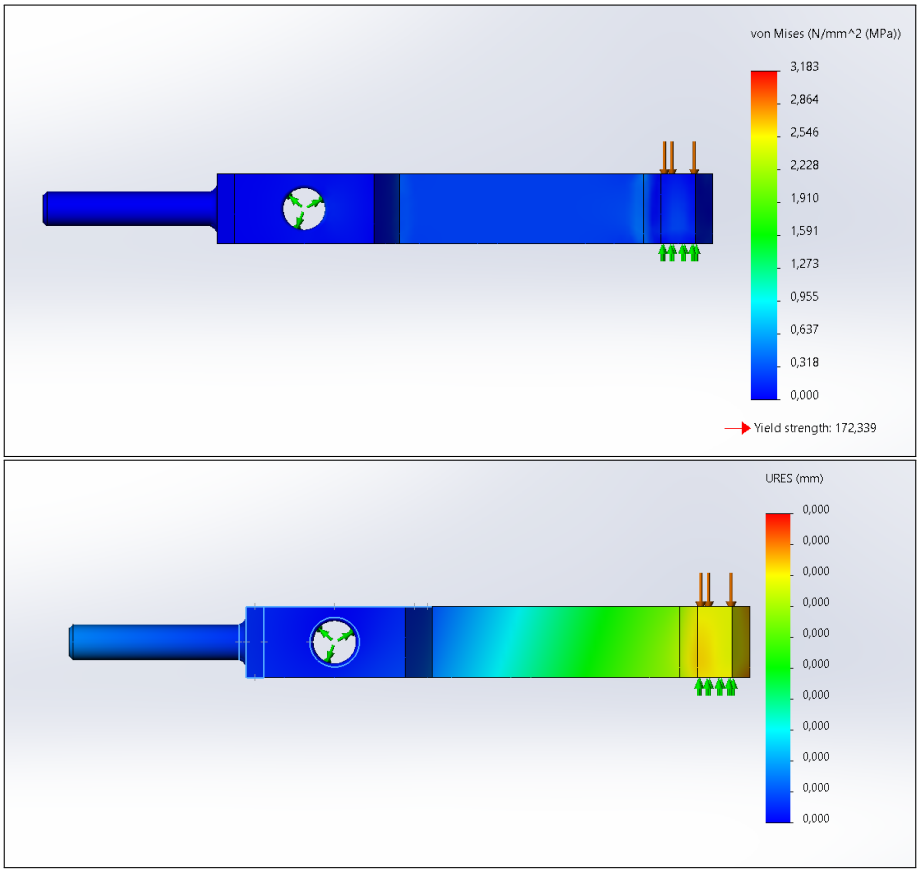

Figure 6.1.19: Static simulation of the arm.

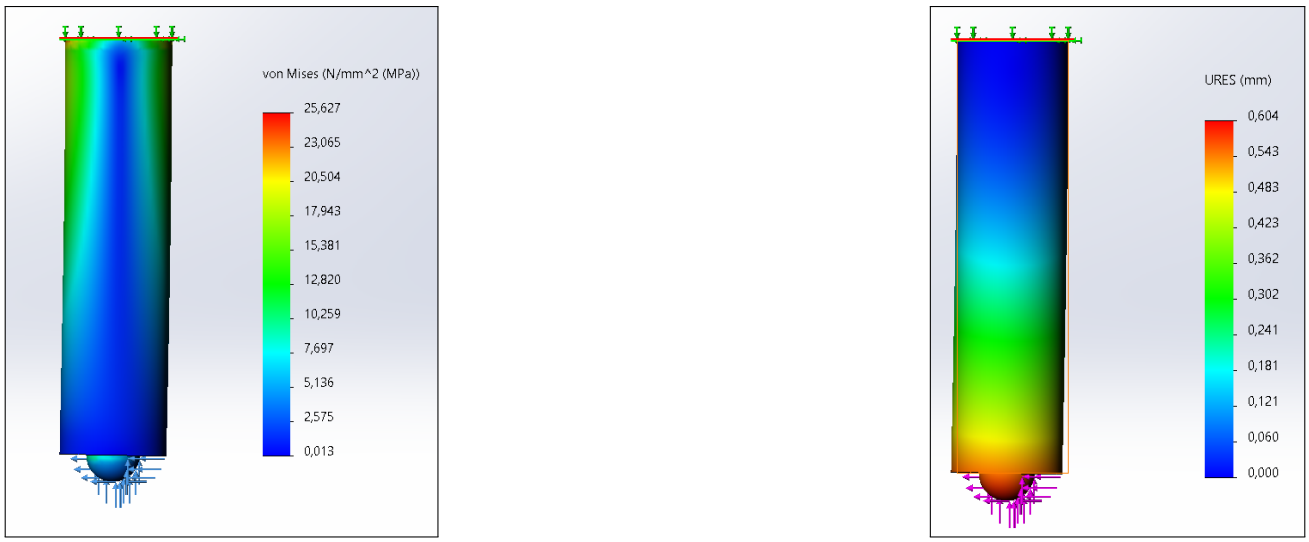

Figure 6.1.20: Static simulation of the pin.

In Figure 6.1.20, a static analysis of the pin is presented. The simulation focuses on the portion of the pin located underneath the arm, as the rest of the pin has a rigid connection to the arm. The results of the simulation show that the maximum stress experienced by the pin is approximately 25.7MPa. This value is higher than the maximum stress observed in the arm, which is expected due to the different cross-sectional areas of the arm and the pin.

PEEK, the material used for the pin, has a yield strength of around 60MPa. Therefore, it can withstand the applied loads without suffering permanent deformation or damage.

The simulation also reveals that the pin undergoes a displacement of approximately 0.604mm in the direction of the wear track. This displacement affects the length of the wear track, as the pin is somewhat dragged along with the arm during operation. For the given load and friction coefficient, the wear track length can be calculated as follows:

$$\text{Wear Track} = \text{Stroke Length} - 2 \cdot 0.604$$

Therefore, in this specific case, the load and friction coefficient will result in a reduction of the wear track length by 1.208mm. It is important to note that this load and friction coefficient represent extreme conditions, and in more realistic experiments with a load of 20N and a coefficient of friction of 0.2, the wear track will be significantly smaller.

6.2 Rotational tribometer

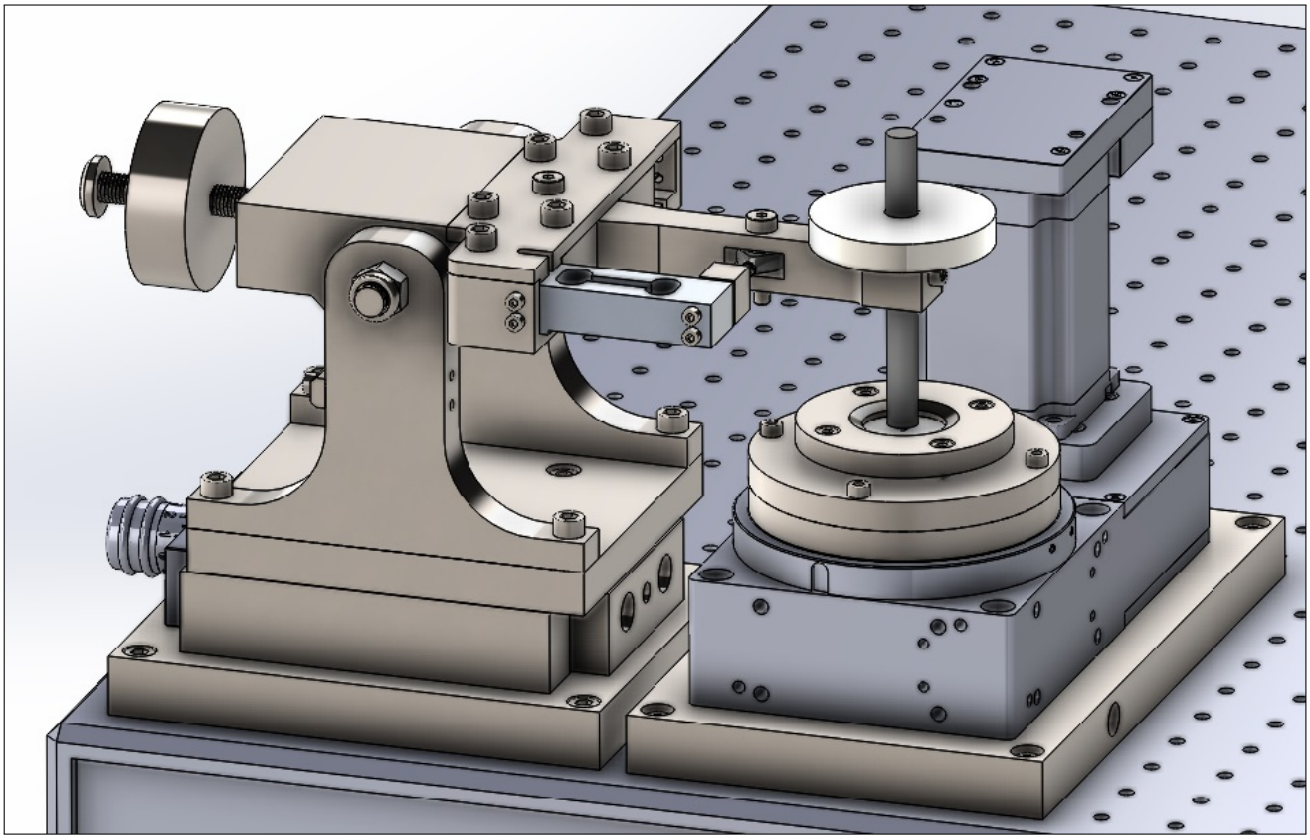

Figure 6.2.1: Final design of rotational tribometer, without tribocorrosion sample.

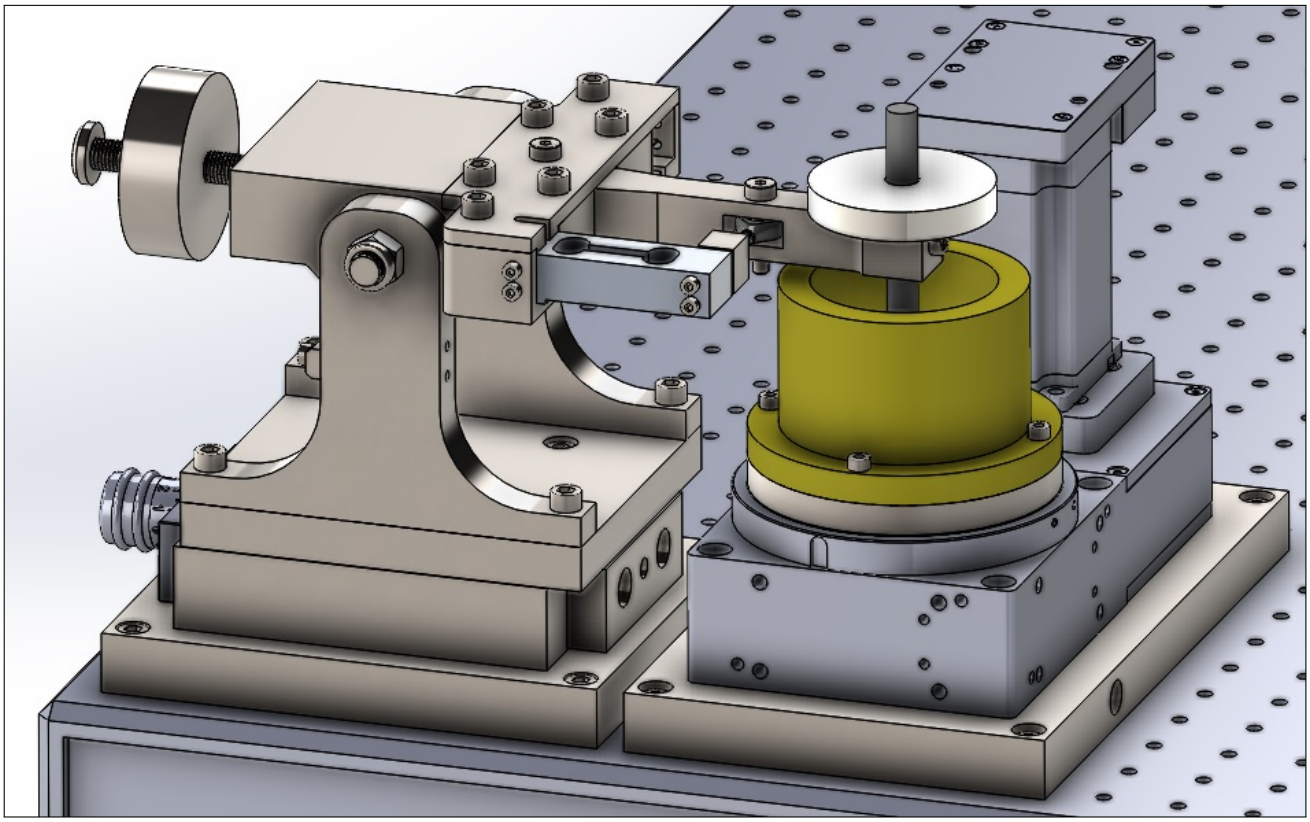

Figure 6.2.2: Final design of rotational tribometer, with tribocorrosion sample.

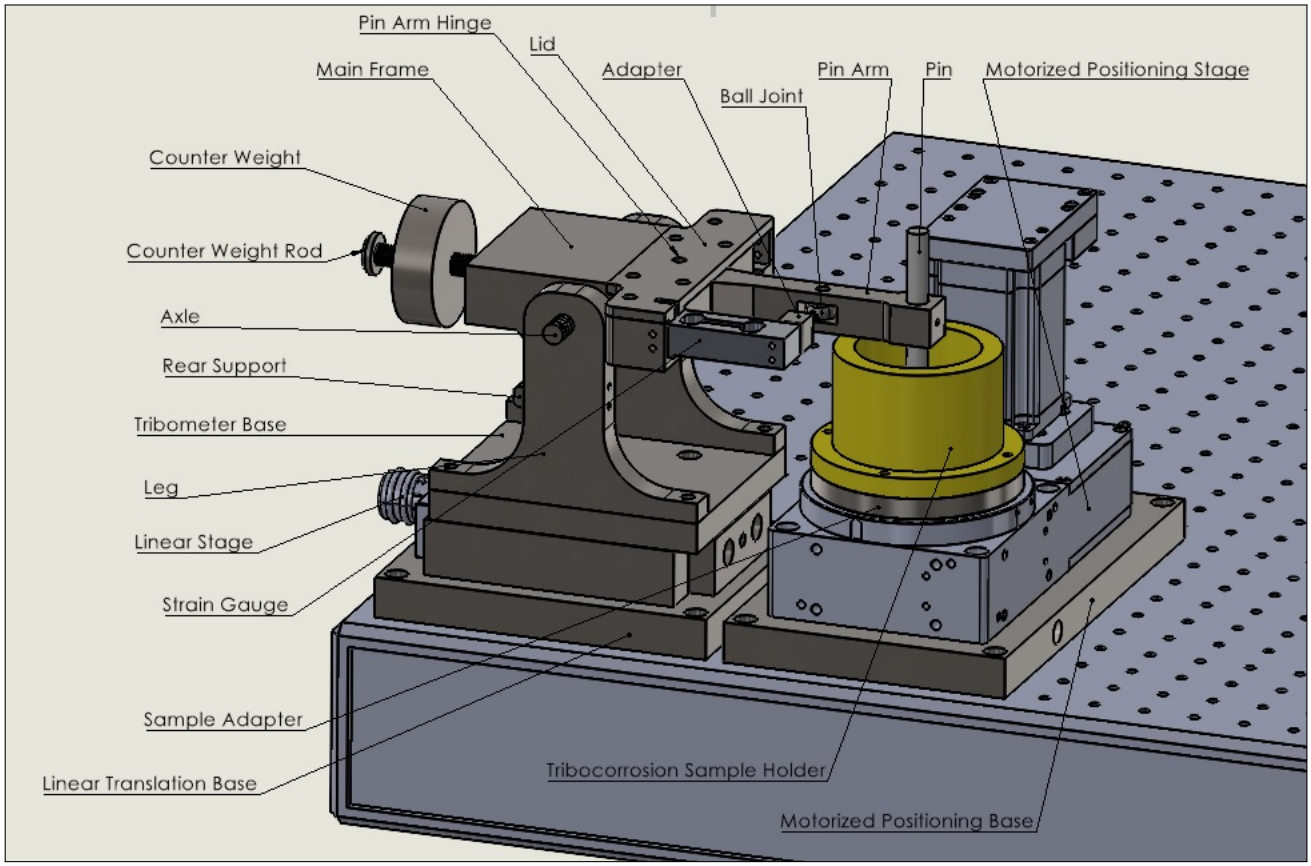

Figure 6.2.3: Name of main components, rotational tribometer.

6.2.1 Main Frame

The main frame of the tribometer is one of the most important elements of the construction. The main frame supports both the pin arm, counterweight, and load cell. The main frame is symmetrically designed, to allow for load cell mounting on both sides depending on what is more practical for the users. The symmetrical design will ensure that the COG is placed as close to the center of the tribometer base as possible, and avoid unessecary moments caused by an "off-center" COG. The added geometry at the underside facilitates for correct placement of the COG and includes two M6 threaded mounting holes for additional weight directly below the main joint, to facilitate added stability if needed.

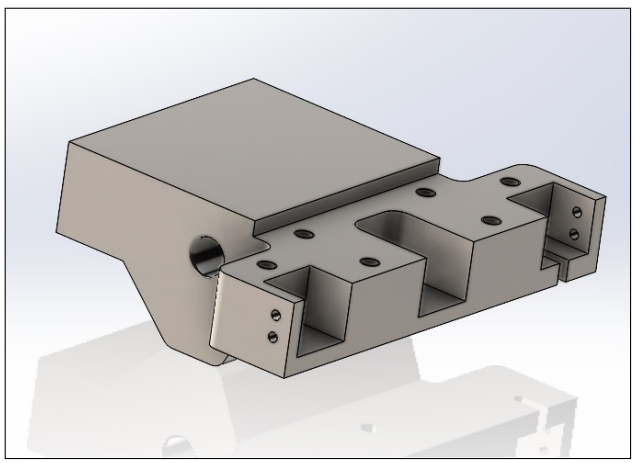

(a) Main frame, seen from above.

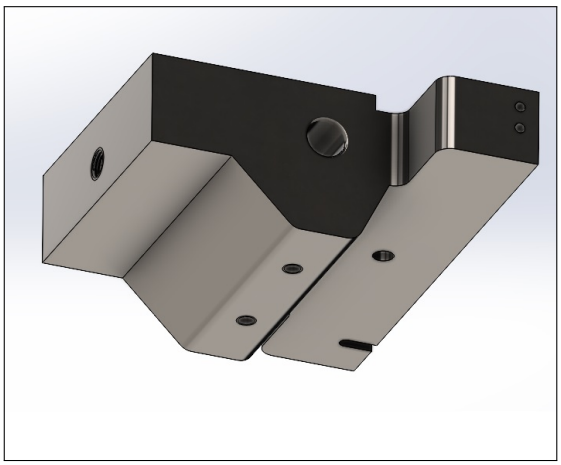

(b) Main frame, seen from below.

Figure 6.2.4: Main frame, rotational tribometer.

6.2.2 Pin arm design

The pin arm is an important element of the rotational tribometer, and the design is developed with great consideration for its function. The main function of the pin arm is to support the pin and transfer frictional forces to the load cell so that the COF can be calculated and evaluated continuously. Additionally, the pin arm will support the dead weights used for applying force to the sample.

The most important feature of the pin arm is its capability of transferring forces to the load cell, introduced by friction between the sample and pin. The pin arm is fastened to the main frame of the tribometer with a hinge support, as illustrated in Figure 6.2.5. The reason for this is that the hinge support will allow the pin arm to rotate so that the load cell can counteract the rotation caused by frictional forces on the pin. The hinge will also work as a support for torsional moments caused by frictional forces on the pin. Torsional moments will occur as there is a distance from the pin arm to the sample, perpendicular to the frictional forces. The pin arm will not rotate when connected to the load cell, as the load cell will work as a support for the pin arm. This way, only horizontal forces, and minimum momentum will be introduced to the load cell. The hinge consists of an M6 shoulder screw, secured by a locknut underneath.

It is important to notice and be aware that the pin arm is not statically determined in the x-direction, as there are two pinned connections connected to the arm. As there are no significant forces in the x-direction, this is not a significant problem. The pin arm is statically determined in the y-direction, which is the main concern in this design. Most of the forces will work in the yz-plane, and it is important that the construction is statically determined in that plane in order to be able to calculate the reaction forces on the load cell.

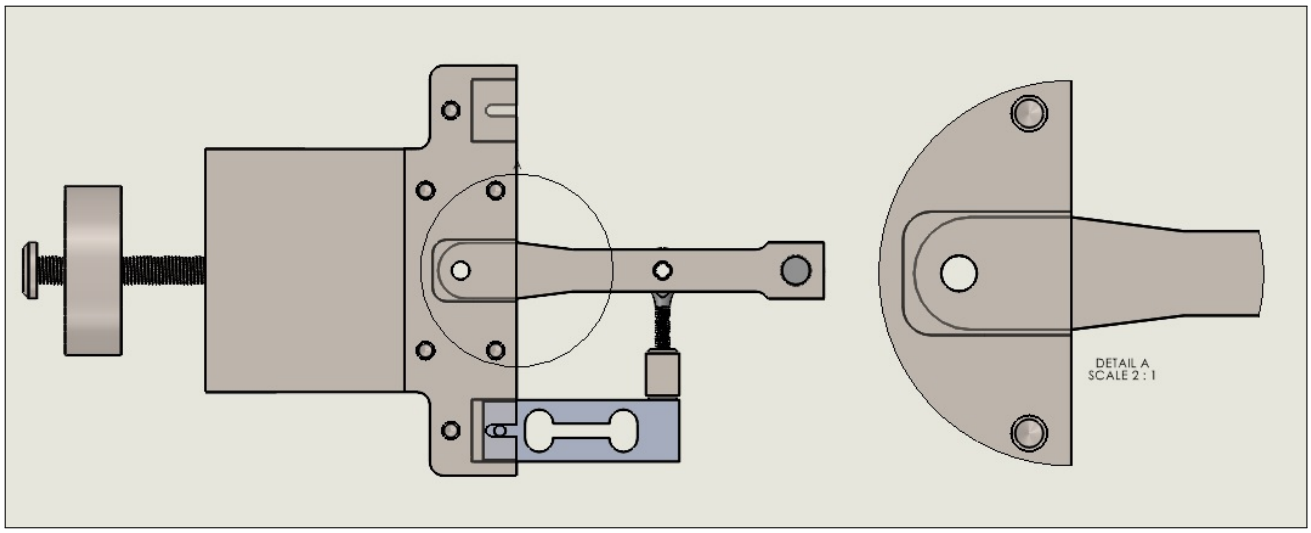

Figure 6.2.5: Pin arm hinge support, rotational tribometer.

6.2.3 Load cell

The load cell used in the final design of the rotational tribometer is the Tedea-Huntleigh Model 1006 strain gauge, as described in the "Design and Development" chapter. The load cell was selected mainly because of the short delivery time, but also because of its small dimensions and the mounting possibilities. Model 1006 has two versions, one with a rated capacity of 5 kg, and one with a rated capacity of 3 kg. Both of these can be installed in the rotational tribometer. The stress and displacement simulations are based on the version with 5 kg capacity, to ensure that both versions can be used. The reaction forces for both versions are calculated, and a load chart for both versions is included in the "Maximum loads and load charts" subchapter.

6.2.4 Load cell and pin arm linkage

To ensure that minimal moments are transferred to the load cell, a ball joint was selected as the preferred design choice for the linkage between the pin arm and the load cell. This way, the linkage will not be capable of transferring significant moments to the load cell. The ball joint selected is an M6x1 male threaded self-lubricated ball joint from Speedring with a swivel angle of 14°. The reason for this choice is that M6 is the standard screw dimensions used in the tribometer and optical board and the short delivery time from Speedring. The dimensions of the ball joint are illustrated in Figure 6.2.6 with article number NGCMLM6. The ball joint is fastened with an M6 shoulder screw, working as a hinge support for the pin arm from the load cell. The shoulder screw is secured from loosening with an M6 locknut underneath.

Artnr	G	J	D	T	V	B	H
NGCMLM6	M6x1	21	6	9	12	20	36
NGCMLM8	M8x1,25	25	8	12	13	24	42
NGCMLM10	M10x1,25	28	10	14	12	26	48
NGCMLM12	M12x1,25	32	12	16	12	32	54
NGCMLM14	M14x1,5	36	14	19	15	36	60
NGCMLM16	M16x1,5	37	16	21	14	38	66
NGCMLM18	M18x1,5	41	18	23	16	45	72
NGCMLM20	M20x1,5	45	20	25	13	45	75

Gäller även högergängat

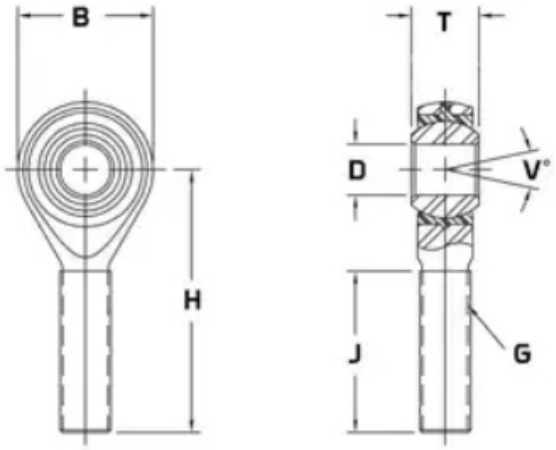

Figure 6.2.6: Speedring M6x1 ball joint used in the rotational tribometer.

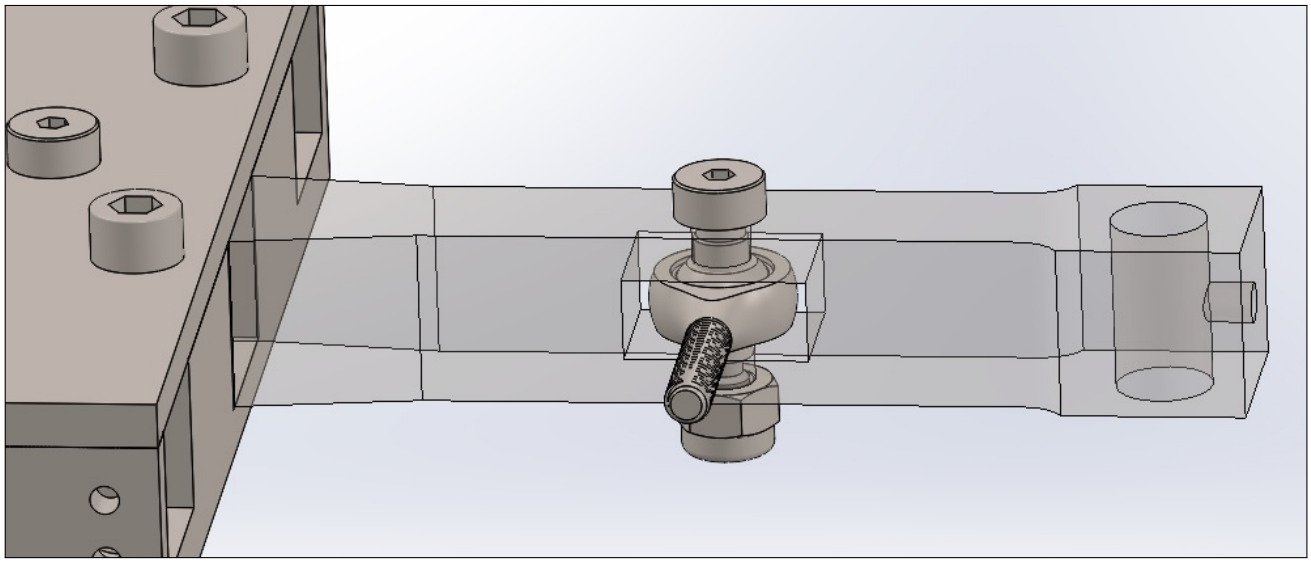

Figure 6.2.7: Ball joint connection, rotational tribometer.

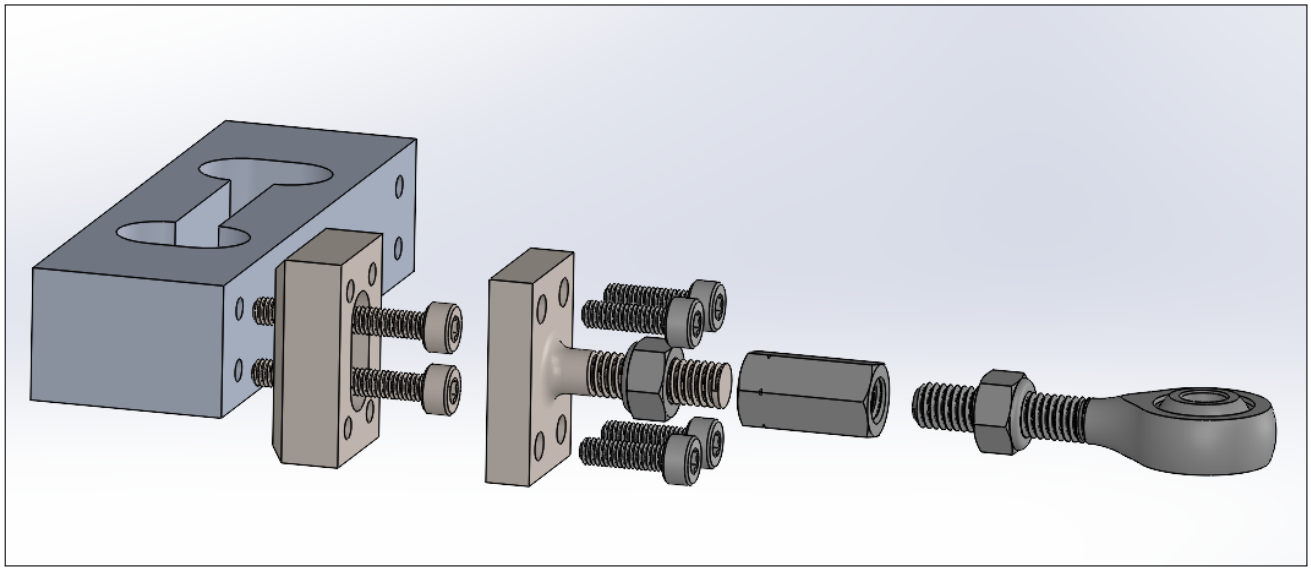

Figure 6.2.8: Initial adapter design for connection between load cell and pin arm.

The linkage between the load cell and the pin-arm was initially suggested as illustrated in Figure 6.2.8. This design makes sure that there are no threaded holes directly connected to the threaded holes in the load cell. The load cell has two M3 through threaded holes for mounting. To properly fasten the load cell, clearance holes should be used on one of the two mates (either in the load cell or in the other mate). Threaded holes on both mates are usually not a good idea if the two parts are tapped separately. The reason for this is that it will be difficult to mate the two parts properly, especially when there is more than one screw. There will always be a gap in the size of the thread pitch when mounting separately tapped parts together. The load cell and the ball joint are connected with an adapter. The adapter is connected to the ball joint with a coupling nut and two locknuts on each side. The coupling nut makes mounting and precise adjustment of the distance between the load cell and pin arm easy, as the distance will be adjusted by turning the coupling nut. The locknuts will secure the link from loosening after mounting or adjustment. The initial design as illustrated in Figure 6.2.8 was proposed to the advisors, but our concerns regarding the connection between the load cell and the ball joint were not considered a big deal. Therefore, a simpler design with fever parts was suggested by the advisor, as illustrated underneath in Figure 6.2.9.

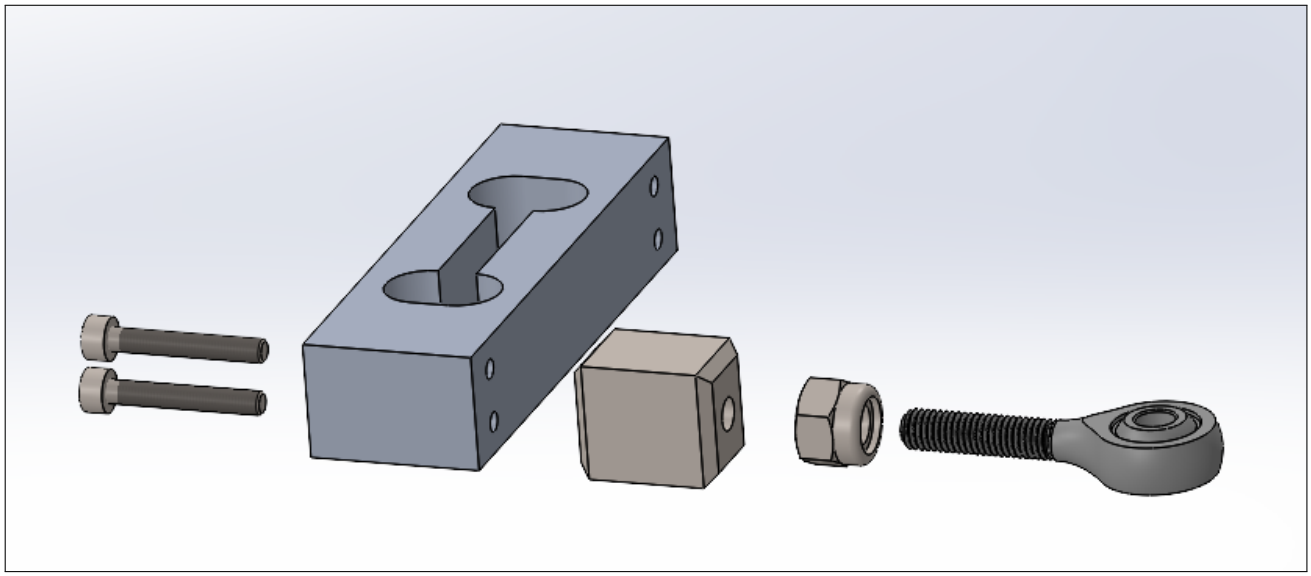

Figure 6.2.9: Alternative design for the adapter for connection between load cell and pin arm, as suggested by advicor.

Figure 6.2.9 illustrates the simpler design, as an alternative to the design initially suggested by the project group. This design includes an adapter to connect the ball joint to the load cell. The adapter has two M3 threaded holes for connection to the load cell, and one M6 threaded hole for connection to the ball joint. As mentioned above, the strain gauge also has two M3 threaded holes for mounting. The ideal case would be that one of the two parts had clearance holes. One way to do this is to remove the threads in the strain gauge so that it is easy to install and mount the two parts together. The strain gauge is relatively cheap, so removing the threads by drilling a hole slightly larger than Ø3 imposes no significant economical risk. Another option is to tap a new hole between the already existing M3 mounting holes on the load cell. This way, it is possible to eliminate the need for an adapter and use a threaded rod and a coupling nut to connect the load cell to the ball joint. The advantage of the alternative design is that it is fewer parts and a shorter distance between the load cell and the pin arm.

6.2.5 Center of gravity

In order to ensure proper testing conditions and to make sure that the weight of the tribometer does not influence the normal force between the pin and sample, an adjustable COG was established as a feature in the tribometer. This way, one can easily regulate the COG so that only the added dead weights will inflict the normal force between the pin and sample. The COG is placed slightly below the rotation point of the "hinge", to ensure the possibility of balancing the tribometer. This will also make the tribometer more stable. The tribometer is designed in such a way that the COG will be placed as close to the "hinge" as possible, and to reduce the need for a large counterweight. The added geometry below the hinge contributes to the correct placement of the COG. Two M6 threaded mounting holes are included directly below the COG to make room for added weight and increased stability if needed.

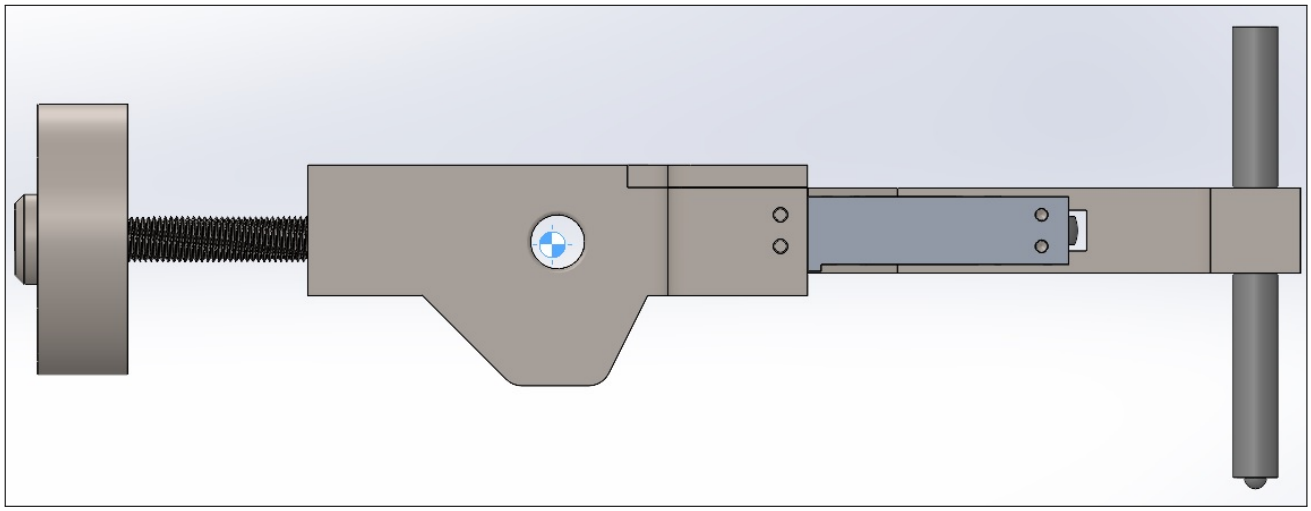

Figure 6.2.10: Rearmost center of gravity, single counterweight.

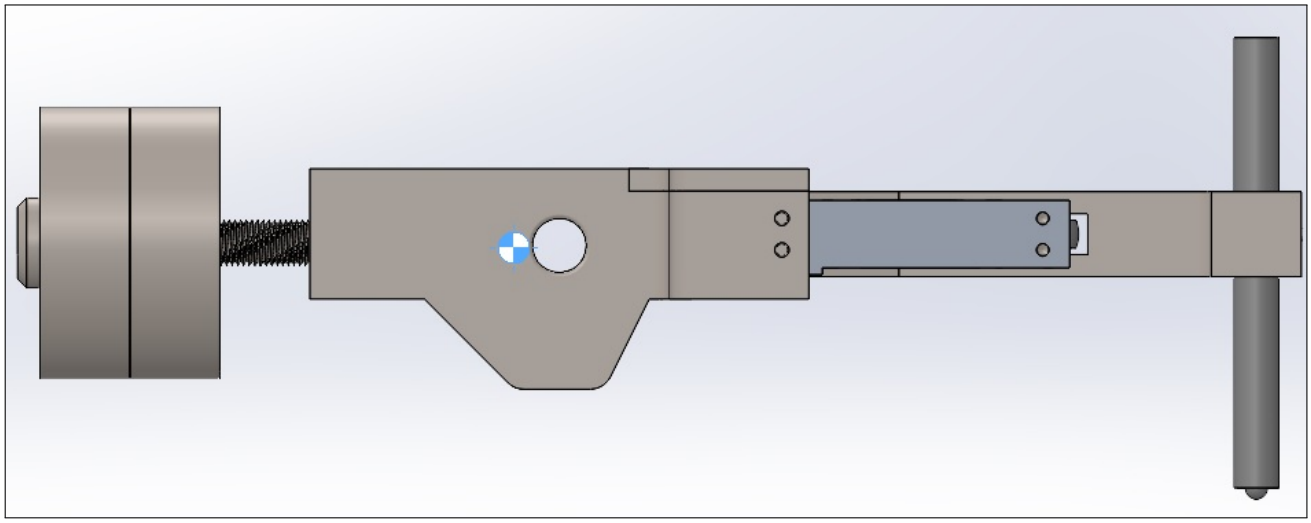

Figure 6.2.11: Rearmost center of gravity, double counterweight.

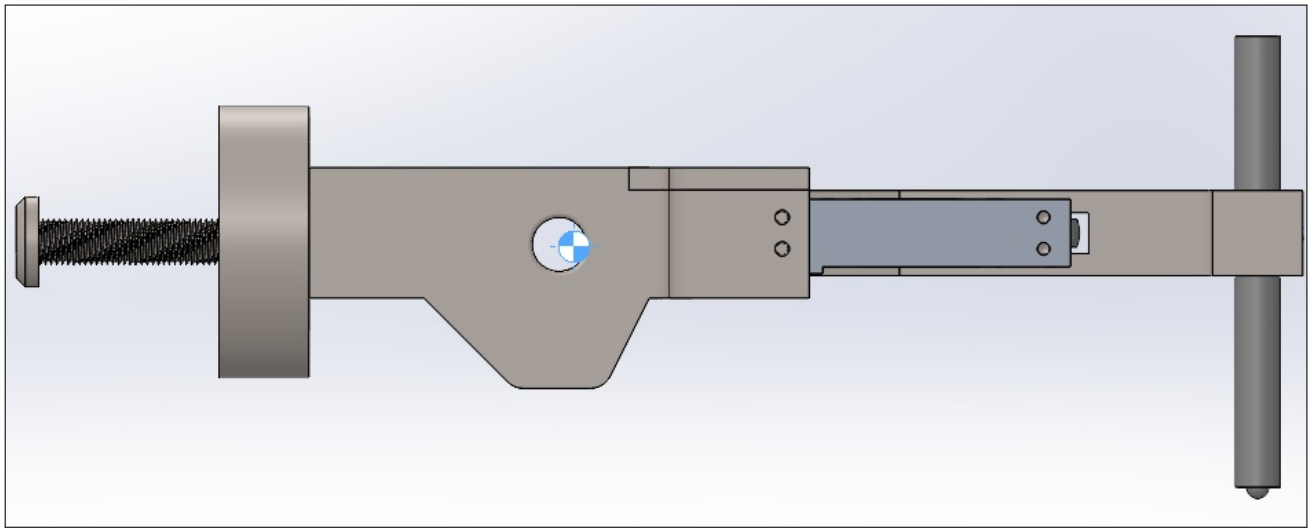

Figure 6.2.12: Foremost center of gravity, single counterweight.

As illustrated in Figure 6.2.10 and Figure 6.2.11, the COG is close to the main hinge even with the counterweight in the rearmost position. Therefore, it is possible to use more than one counterweight to increase the effect of moving the counterweight. With the counterweight in the foremost position, the COG is placed slightly in front of the main hinge as seen in Figure 6.2.12. The COG will almost always be close to the main hinge of the tribometer, to avoid large displacements when adjusting the COG. Only small adjustments are required to balance out the tribometer before testing.

The threads are fine threads to ensure the minimum possibility of loosening or displacement of the counterweight during testing. It is also possible to include two lock nuts on each side of the counterweight to further reduce the probability of counterweight displacement.

6.2.6 Main joint

The main joint of the tribometer supports the upper part of the tribometer. It is important that the main joint is rigid, smooth, and capable of withstanding the load of the upper part. The joint is designed with a focus on smoothness (low friction), high rigidity, and ease of assembly. The joint consists of two flange bushings to reduce friction. This will make the joint smoother, which in turn will make it easier to adjust the COG correctly. The flange bushings are produced

by GGB and have a dry friction coefficient between 0.04 to 0.25 depending on the contacting material, load, and operating conditions. The bushing consists of Polytetrafluoreten (PTFE), bronze sinter, and steel backing (GG Bearings, 2023). Figure 6.2.13 illustrates how the bushings are fitted in the main joint.

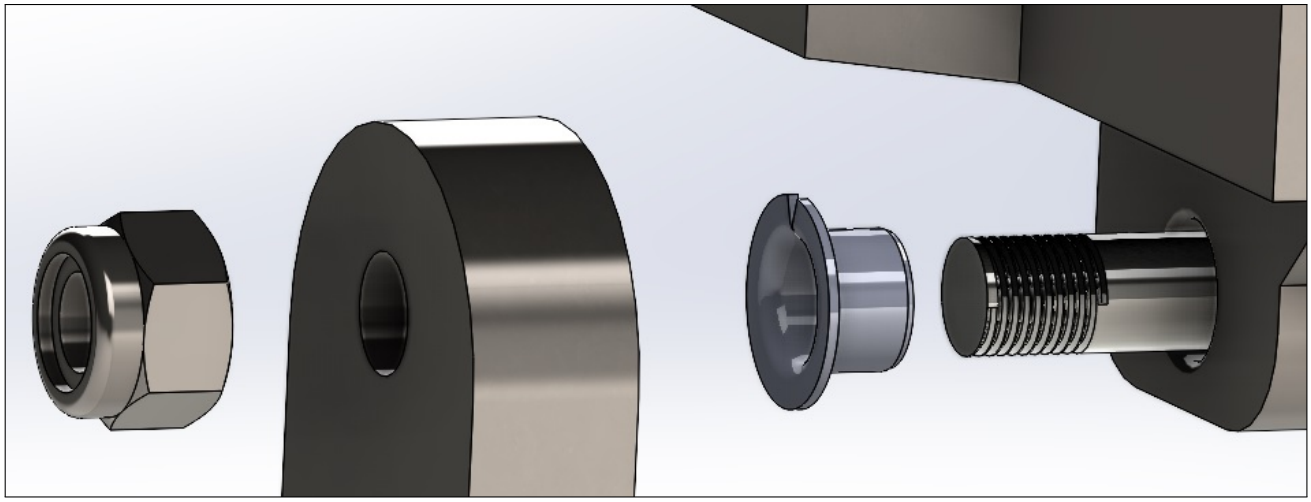

Figure 6.2.13: Exploded view of main joint, with DP4 flange bushing and locknut.

As seen in Figure 6.2.13, the flange bushing will be fitted in the bore of the main base of the tribometer. The bore is designed after guidelines provided by GGB in the DP4 manual. The diameter of the bore is 12 mm with H7 tolerance, and the shaft diameter is 10 mm with f7 tolerance. This means that the flange bushing will be stationary and fitted with an interference fit to the main frame. The axle will not rotate, but the main frame will rotate around the stationary axle. The axle is secured by two locknuts on the outer side of each leg, and an interference tolerance with the legs to secure the axle from rotating.

6.2.7 Tribocorrosion

As mentioned in Chapter 5, a slip ring solution was selected as the best choice for transferring electricity from the stationary part to the rotating sample. The PSC-X12 slip ring from Penlink, illustrated in figure 6.2.14, was selected as suitable as it would fit inside the bore of the motor. It is also capable of transferring the right amount of electricity and voltage needed for tribocorrosion testing. The housing of the slip ring was created of 3D printed PLA plastics, as it is a non-conductive material, and easy to manufacture and produce. The stationary part of the slip ring is mounted in the bore of the motor, in a housing of 3D-printed PLA plastics fastened to the motorized positioning base. The rotating part of the slip ring is mounted by adhesives, together with a 3D-printed housing. In the housing for the rotating part, a female copper plug is placed and soldered to the electrical cables of the slip ring, designed by the project group. The female copper plug will transfer electricity from the potentiostat to the rotating sample and work as a "plug in-plug out" feature when mounting the tribocorrosion sample holder.

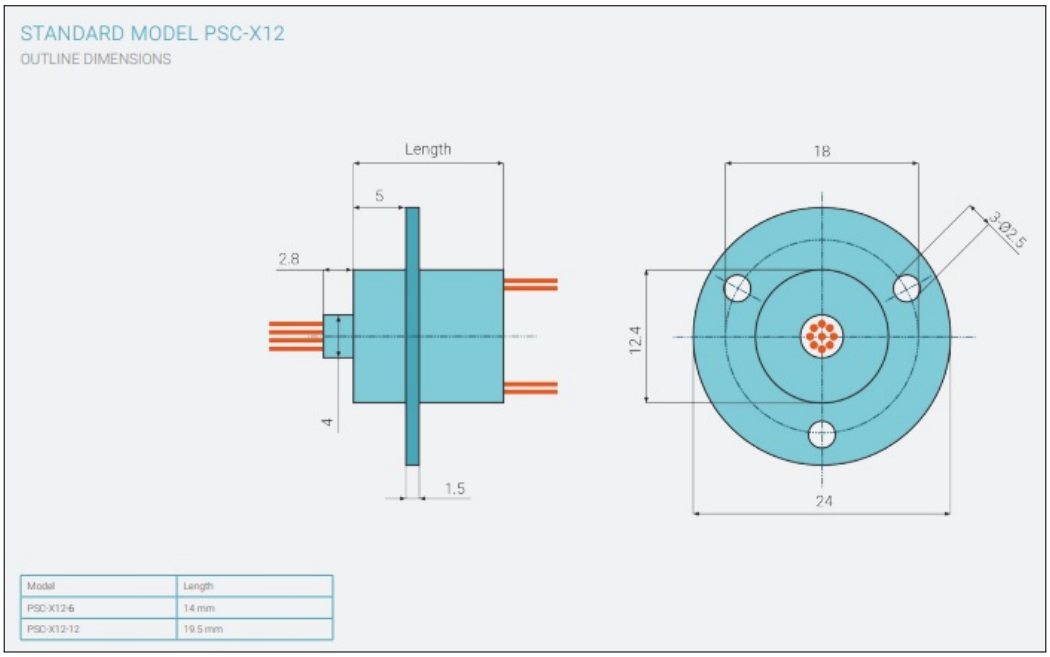

Figure 6.2.14: PSC-X12 SERIES slip ring dimensions (*PSC-X12-Technical-Information* 2019).

The tribocorrosion sample holder consists of a sealed container, capable of running electricity through the sample and electrolyte. The sample holder consists of two main parts, the upper part, and the lower part. These two are supposed to be mounted together before being mounted to the motorized positioning stage. The lower part of the sample holder consists of a male copper plug, to enable electrical transmission from the slip ring through the sample and electrolyte. The upper part of the sample holder is mounted to the lower part with four M4 screws, in counterbore holes underneath, before being mounted onto the motorized positioning stage. The sample is placed in between the upper and lower part together with an o-ring, to secure a sealed connection. This is important, to secure the electrolyte from leaking out during testing. The sample holder is designed with a height of 41.6 mm. As mentioned in Chapter 5, the maximum height of the liquid at full rotational velocity is estimated to be 40.3 mm. It is not recommended to run tribocorrosion testing with maximum velocity, as the liquid can spill over because of the tight clearance of 1.3 mm. The reason why the tribocorrosion sample holder is not designed taller is mainly because of the short length of the pin, and the diameter of the rotating stage. If tribocorrosion testing can be done with less than 50 mL at 300 rpm, it is recommended to do so to minimize the risk of spilling. It is worth noticing that because of the pin, the maximum height of the liquid from the bottom to the surface at 300 rpm will be slightly reduced from 40.3 mm. This is because of the added resistance in water flow caused by the pin. The amount of

height reduction depends on the viscosity of the liquid used.

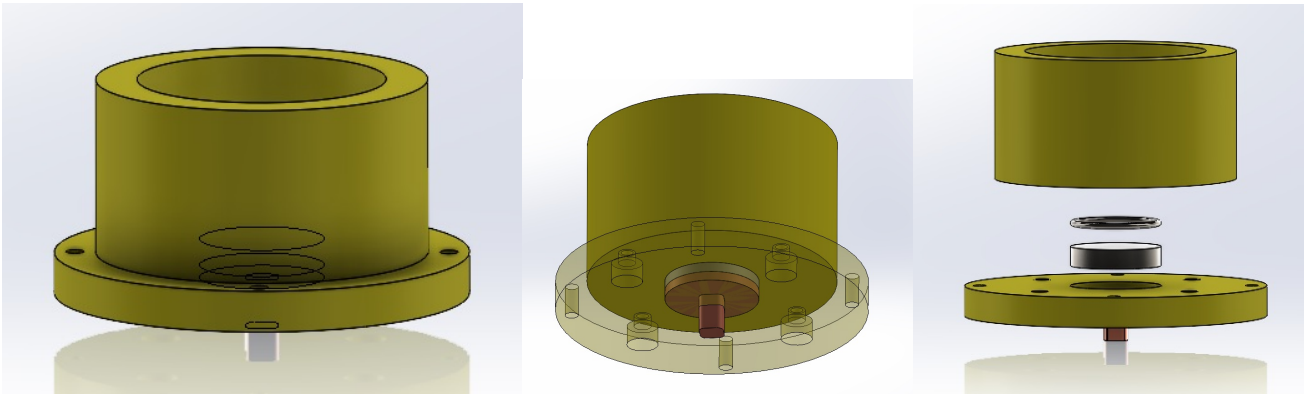

(a) Collapsed view. **(b)** Transparent, seen from underneath. **(c)** Exploded view.

Figure 6.2.15: Tribocorrosion sample holder, rotational tribometer.

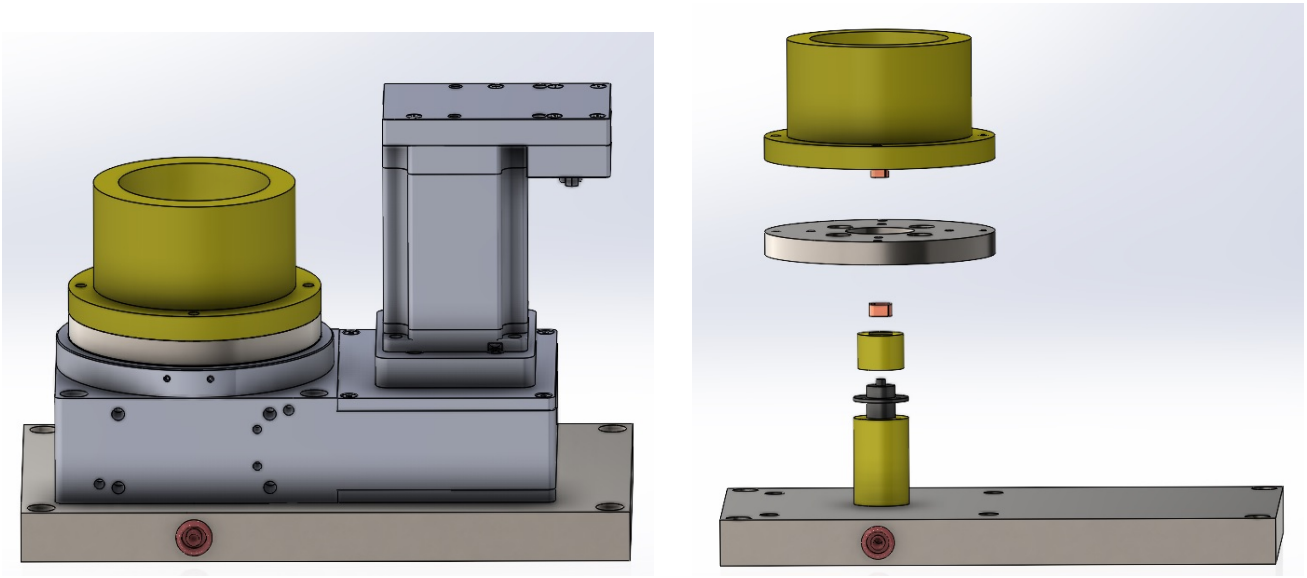

(a) Collapsed view. **(b)** Exploded view.

Figure 6.2.16: Motor assembly with slip ring feature, rotational tribometer.

Figure 6.2.16 shows how the 3D-printed housing for the slip ring is mounted and placed inside the bore of the motor. The yellow parts are 3D-printed PLA plastics and the black part is the slip ring. The copper-colored pieces are copper and work as a "plug in-plug out" feature. The red socket placed in the motorized positioning plate is a banana jack for transferring electricity from the potentiostat through the sample. As seen in Figure 6.2.16, the electrical cable will go through the hole at the side of the base plate and be connected to the stationary part of the slip ring inside the 3D-printed PLA housing. It is important to cover the electrical cables with additional insulation, such as a cable sock.

6.2.8 Materials

The most important criteria for the selection of materials during the design of the tribometer are the rigidity and stability of the construction. Machinability and cost are also significant parameters taken into account when deciding what materials to use. The tribometer will not

be introduced to heavy loads, as the maximum normal load on the tribometer is expected to be 50 N. As rigidity and stability of the construction are one of the most important factors, plastics are not a suitable material for the main frame of the tribometer. Aluminum and steel are solid and rigid materials, and their machinability is also considered to be satisfactory for this purpose.

The material of the primary machine elements in the rotational tribometer was decided to be stainless steel. Stainless steel has a yield strength of approximately 210 MPa and is highly rigid and corrosion-resistant. As one of the dimension criteria for the tribometers was high rigidity, stainless steel is a good option. Additionally, considering that the tribometer will have the ability of tribocorrosion, corrosion resistance is very important. There are several different types of stainless steel, and determining what kind of stainless steel is dependent on what is available from the preferred supplier. The strength calculations and simulations are based on stainless steel with a yield strength of 210 MPa, and it is not recommended to choose a material with a lower yield strength than this.

Material selection for the tribocorrosion holder, slip ring holder, and copper holders can not be stainless steel. It is important that these parts do not conduct electricity, as tribocorrosion and electricity transfer will be executed. Additionally, it is important that these parts are not permeable as the liquid will be stored in the tribocorrosion sample holder. Considering these factors, it is determined that PEEK is the material of choice for these components. 3D-printed PLA can also be considered if the prints are executed with 100 percent infill. A more detailed sheet with information on the materials for each component is included in the appendix.

6.2.9 Calculations

The forces on the pin, pin arm, and load cell are illustrated in Figure 6.2.17. When the sample is rotating counterclockwise, friction forces (F_f) will be introduced as seen in Figure 6.2.17. The size of the friction force depends on the applied load (F_L), and the opposite equal size normal force (F_N), given by Equation (2.1). The friction force will introduce a torque on the pin arm working clockwise, illustrated as T_f in Figure 6.2.17. The size of the torque is determined by the size of the friction force, and the distance from the friction force to the pin arm ($T_f = F_f \cdot L_3$). The linkage from the pin arm to the load cell consists of a ball joint. The ball joint has a maximum ball swivel of 14°, and is therefore not capable of transferring these torsional moments when the angle of twist is less than 14°. The ball joint will only counteract vertical and horizontal forces when the angle of twist is less than 14°. Therefore, the hinge support of the pin arm at the main frame will counteract the torque introduced by the friction force as seen in Figure 6.2.17 as T_R. The load cell will counteract, and record the reaction forces, F_R, introduced by the friction forces between the pin and sample.

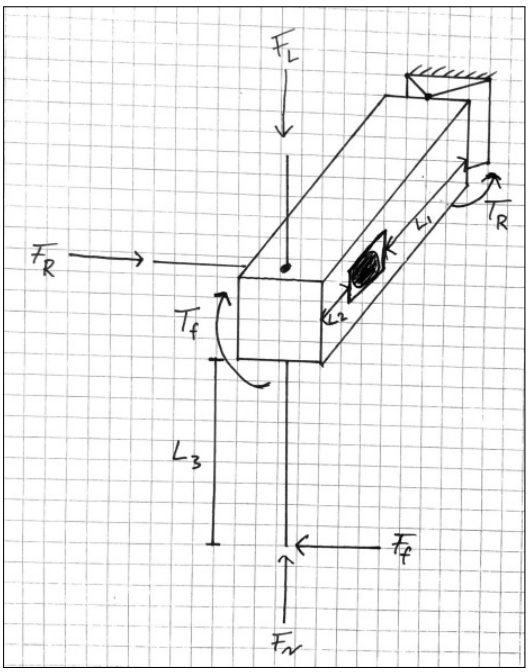

Figure 6.2.17: Three-dimensional FBD on pin, pin-arm, and load cell.

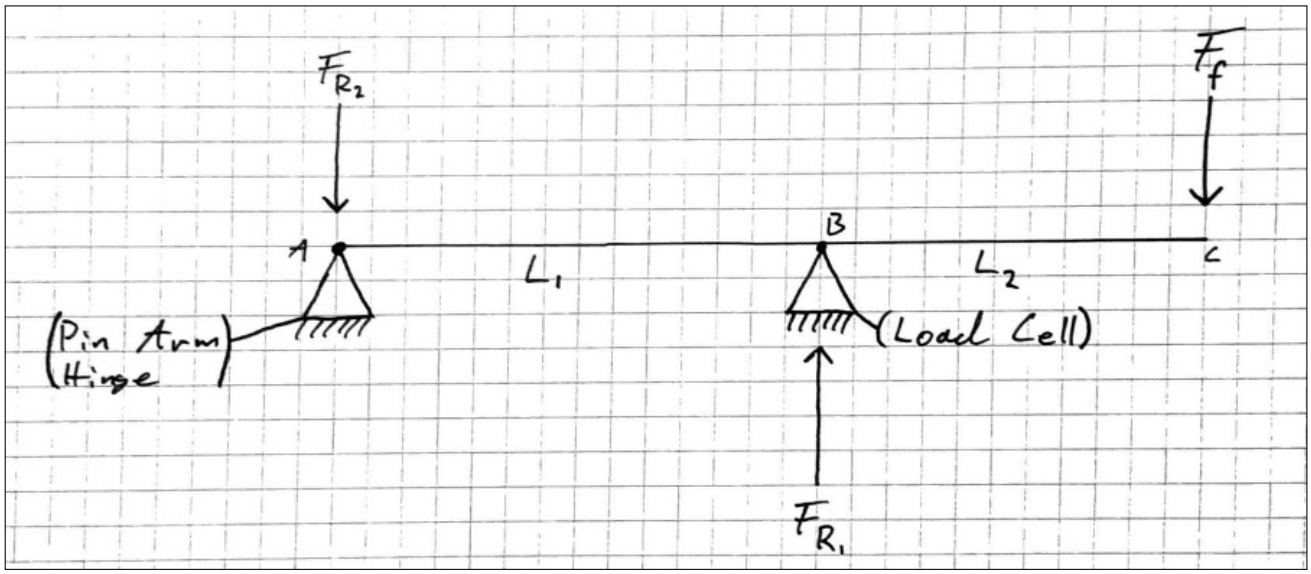

Figure 6.2.18: Influence on reaction force caused by the distance between pin and load cell linkage.

The friction force can be calculated using the horizontal distance from the pin arm hinge to the ball joint (L_1), and the ball joint to the pin (L_2) using Equation (5.2).

$$\sum M_A = 0 :$$
$$\rightarrow F_f \cdot (L_1 + L_2) + F_{R_1} \cdot L_1 = 0$$
$$\rightarrow F_f = -\frac{F_{R_1} \cdot L_1}{L_1 + L_2}$$

The maximum reaction forces on the load cell are given by the corresponding data sheet. The

maximum allowable friction force can then be determined using the known maximum possible F_{R_1}. L_1 in the final design is 72 mm, and L_2 is 47.5 mm. The maximum allowable friction force, and thereby the tribometer's maximum rated capacity are calculated below.

For the 3 kg load cell:

$$F_{f\ max} = \frac{29.43\ N \cdot 72\ mm}{72\ mm\ +\ 47.5\ mm} = 17.73\ N$$

For the 5 kg load cell:

$$F_{f\ max} = \frac{49.05\ N \cdot 72\ mm}{72\ mm\ +\ 47.5\ mm} = 29.55\ N$$

Based on the calculations, it is recommended to use the 5 kg load cell to facilitate a wider test range. It is worth noticing that the load cells have a safety factor included by the manufacturer. These values are included in the more detailed load charts for the tribometers in section 6.2.10.

There will also be a torque on the pin arm, introduced by the friction force. The maximum value of the torque can be calculated using Equation 6.3, shown below.

$$T_{f\ max} = F_{f\ max} \cdot L_3 \tag{6.3}$$

The length of L_3 is 45 mm, and maximum $F_{f\ max}$ is 29.55 N as shown above using Equation **??**. Using Equation 6.3, the following maximum torque are calculated.

$$\begin{aligned} T_{f\ max} &= F_{f\ max} \cdot L_3 \\ T_{f\ max} &= 29.55\ N \cdot 0.045\ m \\ T_{f\ max} &= 1.33\ Nm \end{aligned}$$

The torque introduced by the friction forces and L_3 will be counteracted by the pin arm hinge (T_R). This will introduce torsional moments in the pin arm. The torque and torsional moments are included in the FEA in section 6.2.9.

6.2.10 Simulations

6.2.10.1 Stress and displacement simulations

The results of FEA illustrated in Figure 6.2.19 desribes the maximum von Mises resultant stress and the maximum resultant displacement at a normal force of 30 N and a COF of 1. The distance from the contact point between the sample and pin to the pin-arm is 45 mm. This is established in the FEA as a torque working at the end of the pin-arm. The hinge support connected to the main frame is established as a "fixed hinge", and the linkage from the strain gauge to the load cell is connected with a "pin-connector" to the pin-arm. The same constraints are used in the FEA illustrated in Figure 6.2.20, but the normal force are increased to 50 N.

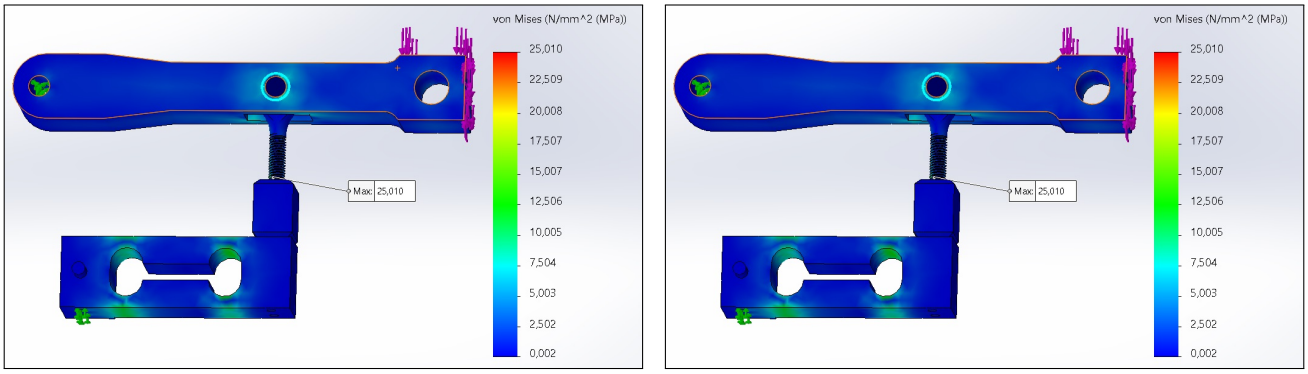

(a) Von Mises stress simulation of pin-arm, linkage and strain gauge. Max von Mises: 25.010 MPa.

(b) Displacement simulation of pin-arm, linkage and strain gauge. Max displacement: 0.055 mm.

Figure 6.2.19: Von Mises and displacement simulation of pin-arm, linkage and strain gauge. $F_f = 30\ N$, $COF = 1$, and $T_f = 1.35\ Nm$.

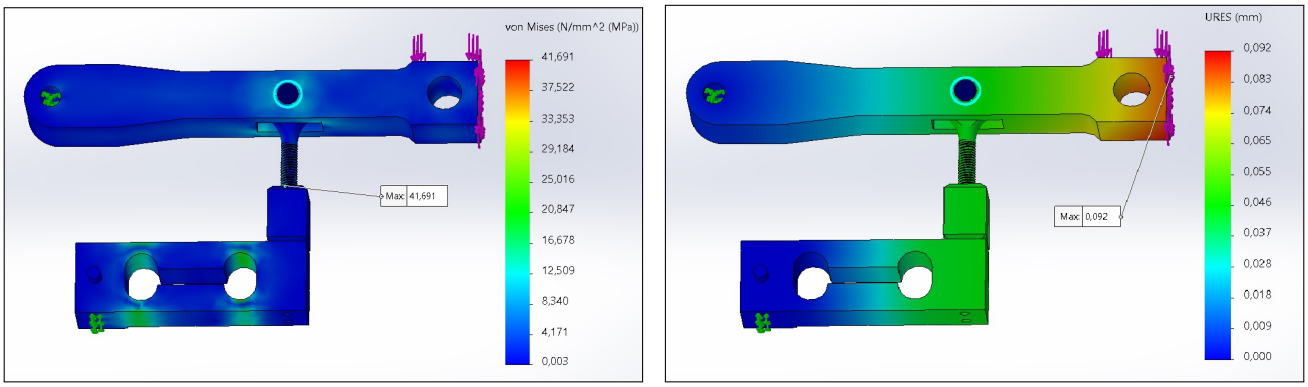

(a) Von Mises stress simulation of pin-arm, linkage and strain gauge. Max von Mises: 41.691 MPa.

(b) Displacement simulation of pin-arm, linkage and strain gauge. Max displacement: 0.092 mm.

Figure 6.2.20: Von Mises and displacement simulation of pin-arm, linkage and strain gauge. $F_f = 50\ N$, $COF = 1$, and $T_f = 2.25\ Nm$.

As illustrated in Figure 6.2.19 and Figure 6.2.20, the stresses and displacements of the pin-arm are very small. The pin-arm, linkage, and strain gauge are capable of withstanding the forces expected.

6.2.10.2 Reaction force simulation

The FEA of the reaction forces on the pin-arm are executed in Abaqus and are executed to illustrate and double-check the calculations done by hand.

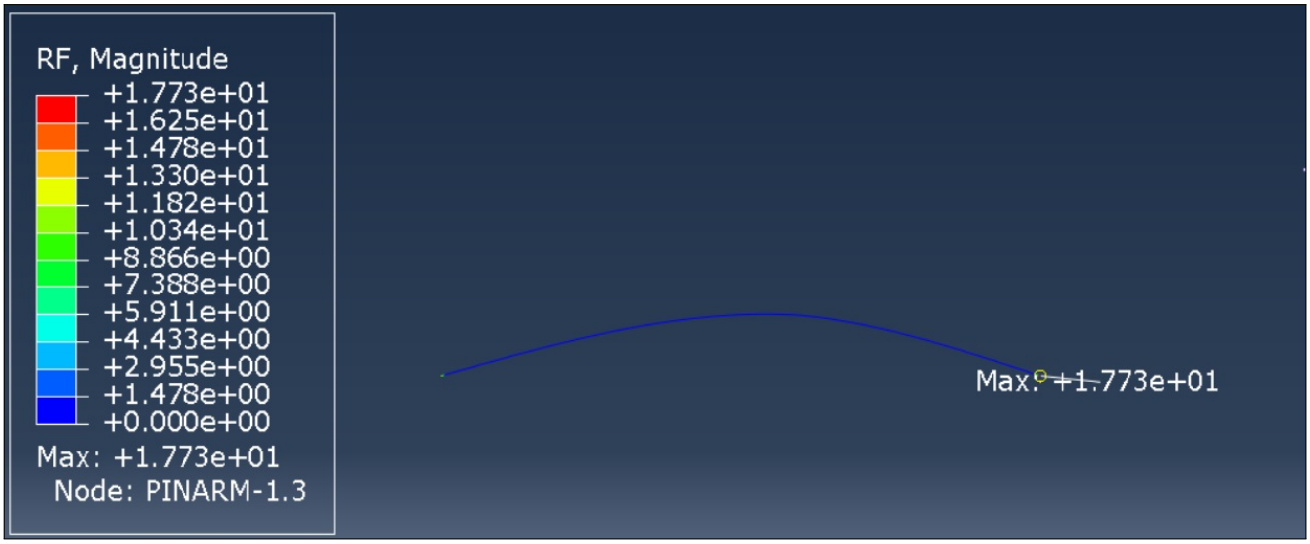

Figure 6.2.21: Max allowable friction force with Tedea-Huntleigh Model 1006, 3 kg. Values are in Newton [N].

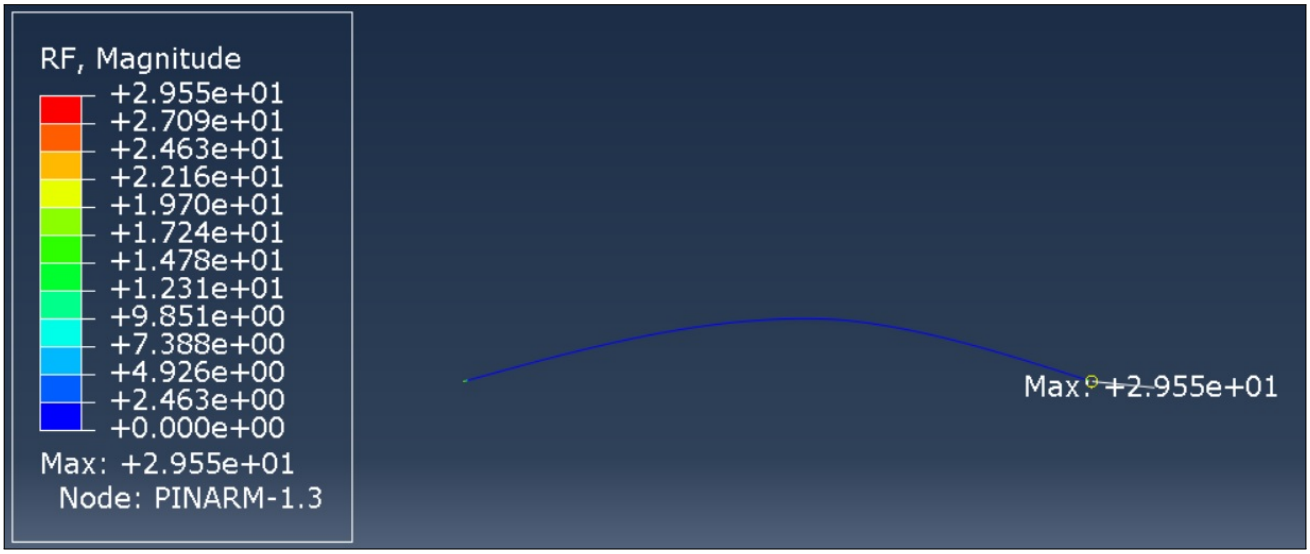

Figure 6.2.22: Max allowable friction force with Tedea-Huntleigh Model 1006, 5 kg. Values are in Newton [N].

As illustrated in Figure 6.2.21, the maximum allowable friction force with the 3 kg load cell is evaluated to be 17.77 N. With the 5 kg load cell, the maximum allowable friction force is evaluated to be 29.55 N. These values are similar to the values given using hand calculations. As mentioned earlier, both load cells can be used in the tribometer depending on the size of the expected frictional forces. The strain gauges also have a "safe overload" area, illustrated in Figure 6.2.23 and Figure 6.2.24.

6.2.11 Maximum loads and load charts

The weakest component of the rotational tribometer is the load cell. This is a conscious design choice made by the project group, in order to limit the damages if the tribometer would fail. The

tribometer is designed so that if the load cell breaks down, it is easy to dismount and replace. The load cell is relatively cheap compared to the other components included in the tribometer. The load chart for the rotational tribometer is illustrated in Figure 6.2.23 and in Figure **??**, and gives information about what load and COF combinations are allowed during testing. The load chart are meant to be a guideline to the users, so that the load cell are not overloaded.

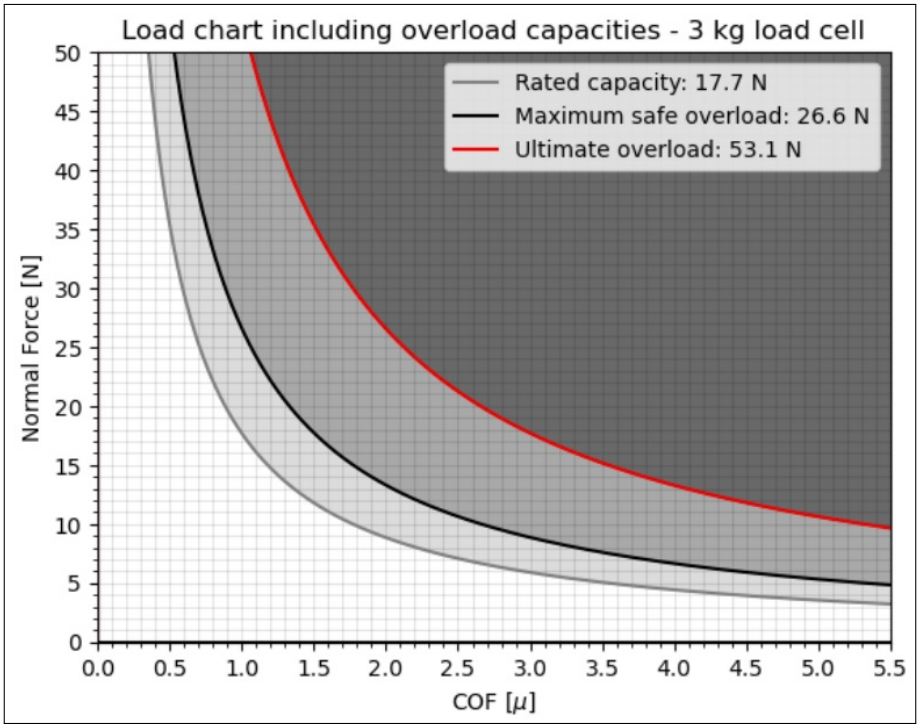

Figure 6.2.23: Load chart for rotational tribometer with 3 kg load cell.

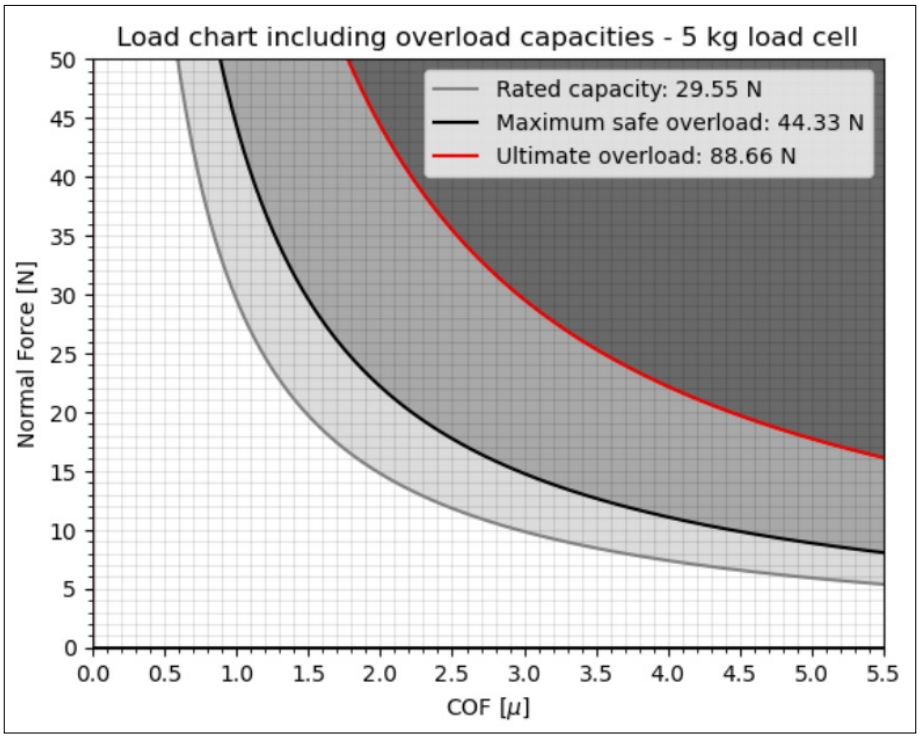

Figure 6.2.24: Load chart for rotational tribometer with 5 kg load cell.

The first grey line is equal to the maximum rated capacity of the load cell, taking into account the correction factor caused by the distance from the load cell to the pin. This means that the

tribometer has a rated capacity for the white area below the gray line. The black line describes the maximum value for safe overload, meaning that the light gray area below the black line is outside the rated capacity, but still not critical to the load cell. The red line describes the maximum overload of the tribometer, meaning that the load cell will most likely fail if this value is exceeded. The area between the black and red lines is also very uncertain, as this is outside the "safe overload" area. It is not recommended to exceed the rated capacity of the load cell.

The plot and maximum values are calculated using the equation below, with the help of Python and Matplotlib.

$$F_f = \frac{F_R \cdot L_1}{L_1 + L_2}$$

Maximum safe central overload	150	% of R.C.
Ultimate central overload	300	% of R.C.

Figure 6.2.25: Tedea-Huntleigh Model 1006 rated capacity and safety factors (*Model 1006 Aluminum Single-Point Load Cell* 2014).

The project group initially decided on the 5 kg load cell but discovered that it was out of stock from the manufacturer. After consulting with advisors, it was decided to order the 3 kg load cell to facilitate the testing of prototypes and the development of software. The software is also compatible with the 5 kg load cell, and it is recommended to use the 5 kg load cell to facilitate a wider test range.

6.3 Software

The final iteration of the software developed by the project group represents the least mature aspect of the overall project. While the design of the mechanical components was informed by the accumulated theoretical and practical knowledge acquired throughout the years of studying mechanical engineering, the group encountered greater challenges in the development of the software due to limited prior experience in terms of ensuring both quality and functionality.

- Record data from the sensor.
- Plot them in the GUI.
- Write them to a user-specified results file.
- Automatically connects to the Arduino.

The developed software includes a mechanism to address scenarios where the user's results file shares the same name as an existing file. In such instances, the software promptly presents the user with a dialog box, offering them the choice to either overwrite the preexisting file or cancel the creation of the new file. If the user selects the option to overwrite, the software proceeds to delete the old file and generates a new file with the identical name. Conversely, if the user opts not to overwrite, the corresponding function terminates, enabling the user to input a different name for the file, thus ensuring the integrity of the file management process.

Additionally, the software provides an automated process for listing all available serial connections. The user is presented with a dropdown menu to select the specific serial port to which the Arduino is connected. In cases where the user is uncertain about the correct connection, a "Serial Ports" button is provided. Clicking this button will open the device manager, allowing the user to inspect and select the appropriate connection. Once the user has chosen the desired

connection, the software establishes a connection and writes the necessary sensor library to the Arduino for further communication and data acquisition.

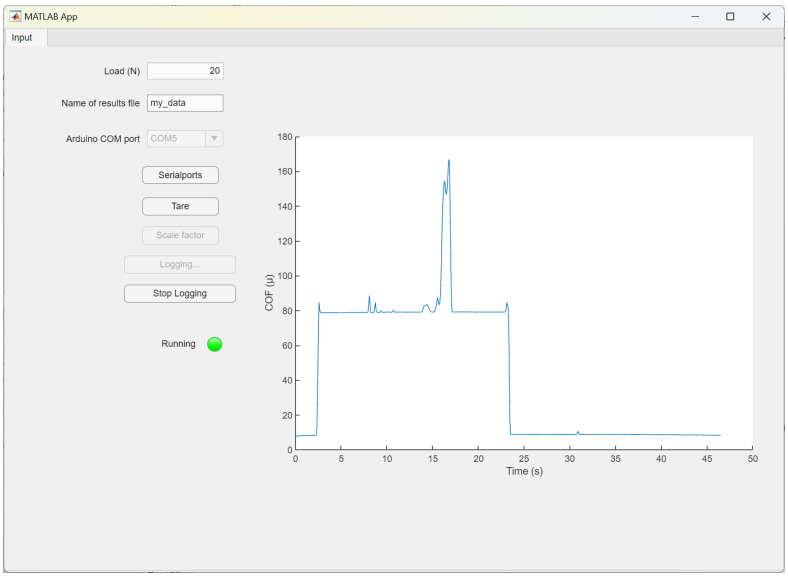

Figure 6.3.1: Program running, plotting data (Note: uncalibrated).

my_data.csv

	A	B	C	D
		mydata		
	Time	FrictionForce	LoadForce	COF
	Datetime	Number	Number	Number
1	Time	FrictionForce	LoadForce	coef. friction
2	2023-05-19 11:12:42.144	152.7457	20	7.6373
3	2023-05-19 11:12:42.271	153.8043	20	7.6902
4	2023-05-19 11:12:42.348	154.5297	20	7.7265
5	2023-05-19 11:12:42.408	156.0734	20	7.8037
6	2023-05-19 11:12:42.490	158.2455	20	7.9123
7	2023-05-19 11:12:42.587	158.8992	20	7.945
8	2023-05-19 11:12:42.686	159.2282	20	7.9614
9	2023-05-19 11:12:42.769	159.2113	20	7.9606
10	2023-05-19 11:12:42.865	159.5023	20	7.9751
11	2023-05-19 11:12:42.959	159.7301	20	7.9865
12	2023-05-19 11:12:43.063	159.7765	20	7.9888
13	2023-05-19 11:12:43.156	159.6373	20	7.9819
14	2023-05-19 11:12:43.250	160.2067	20	8.0103
15	2023-05-19 11:12:43.340	160.6073	20	8.0304
16	2023-05-19 11:12:43.427	160.7507	20	8.0375
17	2023-05-19 11:12:43.525	160.9954	20	8.0498
18	2023-05-19 11:12:43.618	161.3454	20	8.0673
19	2023-05-19 11:12:43.710	161.8895	20	8.0945
20	2023-05-19 11:12:43.796	162.0709	20	8.1035
21	2023-05-19 11:12:43.897	162.3492	20	8.1175
22	2023-05-19 11:12:43.998	162.4125	20	8.1206
23	2023-05-19 11:12:44.096	162.4504	20	8.1225
24	2023-05-19 11:12:44.189	162.8342	20	8.1417
25	2023-05-19 11:12:44.282	163.2223	20	8.1611
26	2023-05-19 11:12:44.371	163.4669	20	8.1733
27	2023-05-19 11:12:44.461	163.817	20	8.1908
28	2023-05-19 11:12:44.561	164.0531	20	8.2027
29	2023-05-19 11:12:44.654	164.3821	20	8.2191
30	2023-05-19 11:12:44.744	164.4791	20	8.224
31	2023-05-19 11:12:44.855	164.652	20	8.2326
32	2023-05-19 11:12:44.931	164.7954	20	8.2398
33	2023-05-19 11:12:45.024	246.4361	20	12.3218
34	2023-05-19 11:12:45.133	724.3146	20	36.2157
35	2023-05-19 11:12:45.229	1356.3475	20	67.8174

Figure 6.3.2: Result file with recorded data from 6.3.1.

The Figure 6.3.1 displayed depicts a reference run with an arbitrary calibration value. It serves as a demonstration to showcase the functionality of the software. However, it is important to note that the scale of the coefficient in the picture is not representative of the actual measurements.

Instead, it emphasizes the importance of proper calibration to ensure accurate and reliable results.

6.4 Safety circuit

Planning, soldering, measuring, and testing, the safety circuit was determined to be fully functional. Considering the limited timeframe of the project, this version of the circuit was deemed as the final iteration. However, recommendations for future development are provided at the end of the document.

To ensure the safety circuit's longevity and prevent any potential electrical hazards, it is strongly recommended to house it within a nonconductive container or housing. Alternatively, placing it on a nonconductive mat can also provide insulation and protection against accidental electrical contact. These measures will help maintain the integrity and reliability of the safety circuit over time.

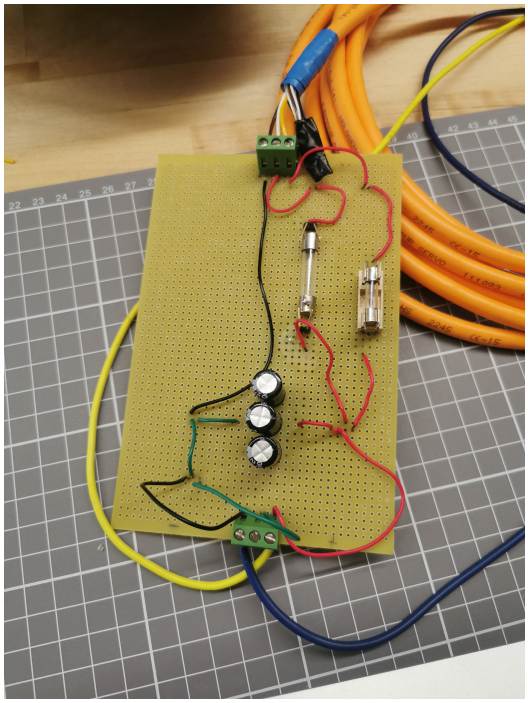

(a) Frontside of the circuit.

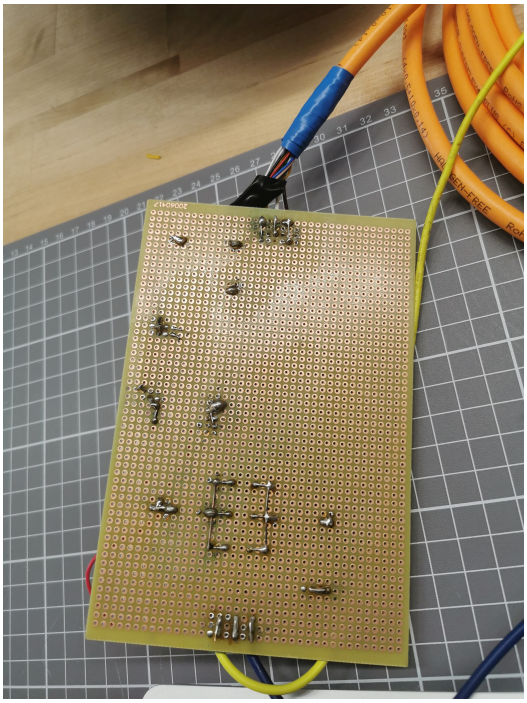

(b) Backside of the circuit.

Figure 6.4.1: Safety circuit for rotational table motor.

6.5 Additional notes

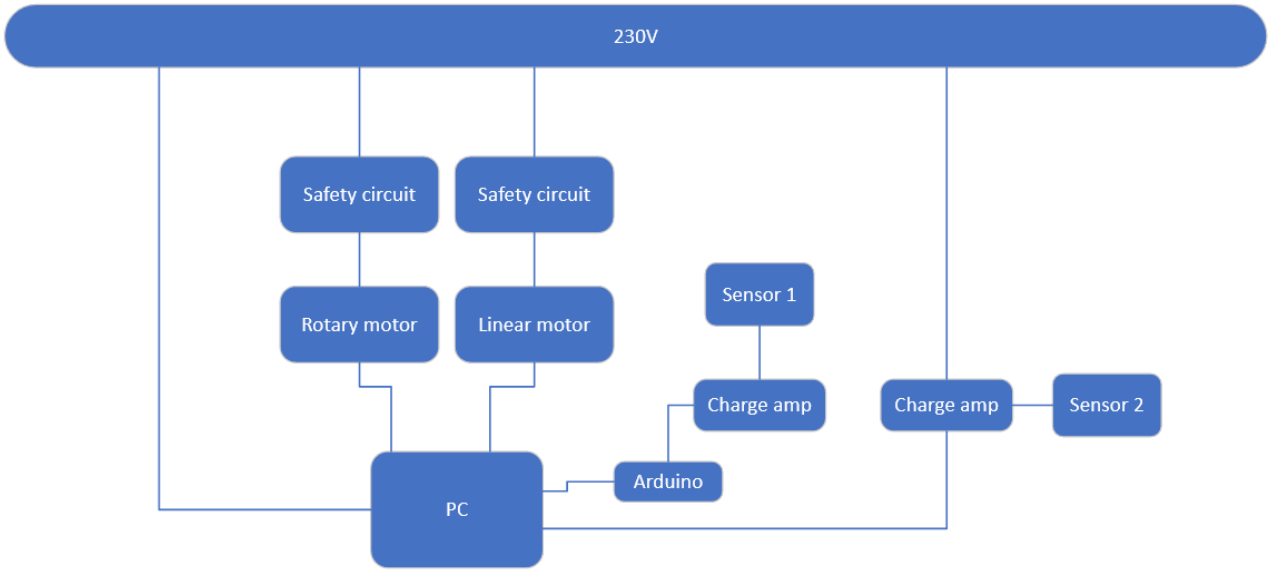

Figure 6.5.1: Block diagram of system.

While the various components have been developed and described separately in this report, it is crucial to recognize that they are all integral parts of a unified system situated on the same optical table. The components, including the motor, motor controller, positioning stage, and other relevant elements, work together synergistically to achieve the overall objectives and functionality of the system. Their interconnectivity and coordinated operation on the optical table contribute to the system's overall performance and effectiveness.

Challenges and Troubleshooting

7.1 Challenges

There were several challenges during the project and throughout the process, some more significant than others. One of the main challenges was poor communication between manufacturers and suppliers, limited time frame, and failure of components.

7.1.1 Communication

Communication with advisors and between group members was not a significant challenge during the project. There were weekly meetings within the project group and communication with advisors and project owners was easy and organized. The challenges related to communication revolve around different companies and manufacturers.

This was first encountered when deciding on what Kistler sensor would be suitable for the rotational tribometer. Multiple emails were sent to Kistler's representatives regarding different alternatives and requirements for the load cell. Initially, the response time was quick, but developed into late replies, no replies, and unorganized communication. This prolonged the decision-making on what sensor to decide on regarding the rotational tribometer. Another challenge related to Kistler and communication is that Kistler does not list the price of their load cells on the website. This meant that for each load cell suitable for the tribometer, the project group had to request an official offer letter from Kistler. Late replies and communication challenges made it difficult to easily evaluate the price of suitable load cells, which further prolonged the decision on what load cell to use. This also prolonged the design process of the rotational tribometer, as the load cell is a significant part and must be taken into consideration when designing the pin arm and load cell holder. Therefore, multiple designs with different suitable load cells were made in order to have several alternatives ready when the offer letters were received.

Another significant communication challenge was between MM-Engineering, Gunda Automation, and the project group. When the rotational motor arrived, the project group tried to understand the manuals provided by both MM-Engineering and Gunda Automation on how to connect and establish electrical power to the motor and motor controller. Additionally, the software for the motor controller was not included in the delivery from MM-Engineering. To fix this, the project group had to search for the software online. There was little to no information about the software on the MM-Engineering website, but the group finally found the right software on Gunda Automation's website. Gunda Automation's website is only in German, which was also a significant challenge. The manuals provided by both MM-Engineering and Gunda Automation is not easily understandable (as some paragraphs are in German), and multiple emails and consultations were needed in order to understand how to correctly wire the motor. Email communication with MM-Engineering was not good, with late replies, no replies, and vague answers and explanations. When all the wiring and connections to the motor were established correctly, the motor would still not run. Therefore, the project group initiated contact with both MM-Engineering and Gunda Automation through phone calls and Microsoft Teams meetings. After several phone calls and Teams meetings, engineers from Gunda Automation established a connection through TeamViewer to troubleshoot why the motor would not run. The engineers from Gunda Automation found out that the motor controller was not working as it should, and that it most likely was broken during manufacturing by MM-Engineering. The problems regarding communication with MM-Engineering, Gunda Automation, understanding of manuals,

and wiring of the motor were very time-consuming and had an impact on the project time frame. The project group used a lot of hours trying to establish the connection between the motor, motor controller, and software, just to find out that the motor controller was broken.

7.1.2 Lead times and deliveries

In this time-sensitive project, one of the major challenges faced was the extended delivery times associated with ordering components. To mitigate this issue, the group took a strategic approach and ordered as many components as possible from inland suppliers to minimize the time required for shipping and delivery. This allowed us to optimize our timeline and maximize our chances of completing the project within the allotted timeframe.

Components ordered from inland or neighboring countries:

- Arduino + USB A-B + 9V barrel jack power cable.
- HX711 charge amplifier chip.
- Strain Gauge.
- M6x1 Male ball joint.
- Penlink Slip Ring.

Even when bought in bulk the arrivals were sporadic and unpredictable, thus to optimize time, instead of waiting time was spent preparing for arrivals, such as not to waste precious time.

7.1.3 Failure of components

During the testing phase, the group faced difficulties in starting the motor component. Initially, they suspected that they might have made an error in their setup. To address this, the group initiated contact with both the motor supplier and the developer of the motor software. A collaborative Teams meeting was scheduled with the manufacturer to seek assistance in troubleshooting the issue. It was determined in the meeting that all the group's connections and configurations were correct. The software successfully communicated with the motor controller, accurately counting steps. However, when the controller was expected to initiate motor movement through the motor driver, no response was observed. The failure of the motor affected both the development of the software, but also the testing of the prototypes. As mentioned earlier, it was also very time-consuming, as a lot of time was used trying to solve this problem.

7.1.4 Time frame of the project

Considering the amount of research and work required to design, prototype, and produce a working software for the tribometers, the limited time frame of the project was a huge challenge. A lot of time went into researching existing literature on tribology and tribometers, to establish an understanding of the project. Additionally, getting familiar with all the existing relevant equipment and functionalities of previous tribometers in the lab was time-consuming. From the beginning, there was almost no room for error, considering the short time frame of the project. Consultations and requests to different manufacturers, and waiting for offer letters and replies were also time-consuming. The limited time frame of the project lead the project group to be organized and structured. The limited time frame also provided a great challenge with huge learning outcomes.

7.1.5 Software

Designing software for a product that is not yet available poses a significant question and challenge. This particular scenario presented a substantial concern during the waiting period for the arrival of the various components required for the project. Nevertheless, this circumstance provided an opportunity to dedicate additional time to familiarize oneself with the programming environment and language necessary for the software development process.

The originally planned software was designed to control motor behavior and ensure simultaneous measurements and motor movement. However, due to the motor never being in an operational state, testing the code and confirming its functionality became impossible. As a result, the scope of the software had to be scaled back.

The application is developed using app designer and implemented in MATLAB 2018A update. Unfortunately, the old Tribometer system operates on Windows XP, which is only compatible with MATLAB up to the 2015 version, when support for that system was discontinued. Consequently, the new software will not be compatible with the old Windows XP system.

The client has expressed their intention to upgrade the computer system in the near future if they require a better and more modern setup.

7.1.6 Electronics

In addition to the challenges mentioned above, the need for a safety circuit for the motor presented an additional exciting challenge for the project group. The challenge primarily arose from the group's limited knowledge and expertise in dealing with electrical components designed to operate at higher voltages, particularly exceeding 5 volts. This aspect became a significant concern due to the motor's power requirements, which drew a current of 3 Amps at 24 Volts. Overcoming this challenge required the acquisition of new knowledge and skills in working with higher voltage electrical systems to ensure the safe and reliable operation of the motor.

To overcome this obstacle, the group sought guidance from the main responsible for the mechatronics lab at Verkstedteknisk at NTNU. With his expertise and advice, the project group was able to devise a solution to ensure the safe operation of the motor. Provided valuable insights and recommendations regarding the selection and usage of appropriate electrical components capable of handling the required voltage and current specifications.

Through collaboration and guidance from main responsible for the mechatronics lab, the project group successfully tackled the challenge of constructing a safety circuit that could handle the motor's power requirements, thereby ensuring the safe and reliable operation of the system. This provided the group with invaluable learning outcomes and strengthened the group members' electrical knowledge significantly.

7.2 Troubleshooting

Throughout the project, the project group encountered several troubleshooting instances. Two significant issues that required considerable time and effort to resolve were related to the motor and the strain gauge.

The strain gauge posed challenges in obtaining accurate readings, often resulting in values that were either maxed out or unreadable. After thorough investigation, the root cause was identified as inconsistencies in the naming and color coding specified in the manuals of the charge amplifier and the strain gauge. It was necessary to make adjustments, specifically changing the data and clock pins, to rectify the issue. However, it is important to note that the solution was not immediately apparent, as there were no obvious indicators linking the problem to the pins.

Through analysis and experimentation(and luck), the group successfully resolved the strain gauge-related challenges.

Regarding the motor, the group initially encountered difficulties in starting the motor component. They suspected that they might have made an error in their setup and reached out to both the motor supplier and the producer of the motor software for assistance. A collaborative team meeting was scheduled with the producer to troubleshoot the issue. It was determined in the meeting that all the group's connections and configurations were correct. The software successfully communicated with the motor controller, accurately counting steps. However, when the controller was expected to initiate motor movement through the motor driver, no response was observed.

After the meeting with the producer, it was concluded that the likely cause of the problem was a defective motor controller. To rectify the issue, the group was advised to contact the supplier and request a component replacement, this was done by the advisors. By identifying the faulty component and taking appropriate steps to address it, the group was able to conclude that the issue would not be resolved before the end of the project and thus outside of our abitity to ensure functionality in the operation of the system.

In parallel, the software development process involved continuous troubleshooting. The Group followed a progressive approach, which involved writing code, testing it, and analyzing the outcomes to understand the reasons behind success or failure. This iterative process allowed for continuous learning and improvement throughout the development phase. The MATLAB environment proved to be helpful in identifying errors, as it provided specific line references where the compiler encountered difficulties. By leveraging this error feedback and acquiring additional knowledge through MATLAB online courses, the group gained a deeper understanding of the software. For example, they early on learned that a property in MATLAB is equivalent to a global variable, enabling access and manipulation inside and outside of functions.

By effectively troubleshooting and addressing these challenges, the group demonstrated their problem-solving skills and ability to overcome obstacles in both the hardware and software aspects of the project.

Further Development

There are several suggestions for further development of the tribometers designed by the project group. The reason why these ideas and suggestions were not implemented in the current designs, is mainly due to a limited time frame and unforeseen challenges during the project phase. The following elements are the main suggestions for further development and design.

- Implementing a single point load cell in the rotational tribometer, instead of the one implemented in the design by the project group.
- Implementing a load cell with higher load capacity in the rotational tribometer.
- Integrate a linear translation stage in the main frame of the rotational tribometer, as opposed to ordering from the manufacturer.
- Further development and improvement of the software. Points of importance to improve or correct are the Tare button with functionalities, the Calibration button with functionalities, and the implementation of a correctional factor on the read data.
- Investigate the possibility of developing one module capable of conducting both reciprocal and rotational testing with one motor.
- Design and development of a more user-friendly solution for adjusting the COG of the tribometers.
- Making the safety circuit into a PCB, as would be smaller and safer when put in a printed housing/container.
- Creating a housing for the Arduino and the load cell amplifier HX711 chip, to attach to the optical board

The project group had several meetings towards the end of the project and discussed and evaluated what could have been done differently. Some of the ideas proposed for further development are important elements from these meetings.

Conclusion

In conclusion, this project represents a significant undertaking in the field of mechanical engineering and tribology, offering valuable opportunities for the group members to learn and develop their skill sets. The study of friction, wear, and lubrication holds great relevance to the practical applications of mechanical systems, making this project challenging and fun. Throughout its duration, the project focused on designing a high-precision "pin-on-disk" tribometer capable of reciprocal and rotational testing. This accomplishment was achieved through dedication, problem-solving, and commitment to the project group and its goals throughout the project.

A primary objective of the project was the development of a modular testing platform capable of conducting a wide range of tribological experiments. By incorporating the capability for both reciprocal and rotational testing, the tribometer offers flexibility and adaptability to address the diverse requirements of various tribological studies. This achievement not only enhances the capabilities of the tribology laboratory but also contributes to the research and development of new tribological solutions.

The design and construction of the tribometer had four fundamental criteria: high rigidity and stability, modular and user-friendly design, stable load application to the sample, and simplicity of manufacturing. These criteria were established to ensure the tribometer's reliability, accuracy, and ease of use. Rigidity and stability were prioritized to minimize potential vibrations or disturbances that could influence the precision of test results. The use of a modular design approach allowed for simple assembly and disassembly, facilitating quick adjustments and modifications for diverse experimental setups. Ensuring stable load application was crucial in maintaining consistent and reliable test conditions. Finally, emphasis was placed on the simplicity of manufacturing to ensure that the tribometer design could be translated into prototypes with ease, considering factors such as machining feasibility and printability.

Throughout the project, various challenges were encountered that tested the group's problem-solving skills and collaboration. Delays in motor delivery, for instance, impacted the ability to thoroughly test the tribometer prototypes and verify their dimensions. In response, a cautious approach was adopted to avoid premature machining of parts, preventing potential rework or wastage. This experience highlighted the significance of careful planning, adaptability, and effective communication when engaging external suppliers and manufacturers.

Collaboration and teamwork were significant to the project's success. Recognizing the importance of effective teamwork in achieving common objectives, the project group maintained regular communication, shared knowledge and ideas, and leveraged each member's strengths to achieve progress. Collaborative decision-making, open dialogue, and a shared sense of purpose created a positive and productive group dynamic. This experience provided valuable insights into team-based engineering projects and confirmed the significance of effective communication, active listening, and respectful collaboration.

In addition to the project's technical aspects, a deeper appreciation was gained for the broader implications of tribology research. The relevance of friction, wear, and lubrication extends beyond the topic of engineering, encompassing global energy consumption. Tribological contact, for instance, is estimated to contribute to approximately 23% of worldwide energy consumption (Holmberg and Erdemir, 2017). By engaging in research and development of new tribological solutions, the project contributes to ongoing efforts aimed at reducing energy consumption and increasing sustainability.

Moreover, the project served as a conduit between academic knowledge and practical application, providing valuable hands-on experience in mechatronics, troubleshooting, mechanical design, and collaboration. The challenges encountered, such as motor delivery delays, highlighted the importance of careful planning, adaptability, and effective communication in engineering projects. This experience further emphasized the significance of attention to detail, thorough evaluation of design choices, and the ability to overcome obstacles in the pursuit of successful outcomes.

References

A-63X Datasheet (n.d.). Physik Instrumente. URL: https://www.physikinstrumente.com/fileadmin/user_upload/physik_instrumente/files/datasheets/A-63x-Datasheet.pdf.

Aerotech (2020a). *Aerotech ADRS Datasheet*. URL: https://www.aerotech.com/wp-content/uploads/2020/10/ADRS-Data-Sheet-D20220429.pdf.

– (2020b). *Aerotech ANT95L Datasheet*. URL: https://www.aerotech.com/wp-content/uploads/2020/10/ANT95L-Data-Sheet-D20230221-1.pdf.

Arduino (02/2018). *Introduction to Arduino*. accessed April 28, 2023. URL: https://www.arduino.cc/en/Guide/Introduction.

Arduino Uno R3 (11/2022). 1. URL: https://docs.arduino.cc/resources/datasheets/A000066-datasheet.pdf. Arduino.

Bartz, W.J. (1978). "Tribology, lubricants and lubrication engineering — a review". In: *Wear* 49.1, pp. 1–18. ISSN: 0043-1648. DOI: https://doi.org/10.1016/0043-1648(78)90019-4. URL: https://www.sciencedirect.com/science/article/pii/0043164878900194.

Beronque D., et al (2018). "MS-tribometer". In: *Final report*.

Birmingham, University of (no date). *What does the Young's Modulus tell us about a material?* URL: https://www.birmingham.ac.uk/teachers/study-resources/stem/physics/youngs-modulus.aspx. (Accessed: 10.03.2023).

Bowden, F. P. and D. Tabor (1974). *Friction*. Doubleday & Company Inc.

Cadence PCB Solutions (2020). *Force and Pressure Sensors with Piezoelectric Load Cell Transducers*. URL: https://resources.pcb.cadence.com/blog/2020-force-and-pressure-sensors-with-piezoelectric-load-cell-transducers. (accessed: 27.03.2023).

Colibri 23 Mini manual (2022). URL: https://gunda-automation.de/shop/amfile/file/download/file/85/product/1468/. Gunda Automation.

Corrosionpedia (2017). *Tribometer*. URL: https://www.corrosionpedia.com/definition/4634/tribometer. (Accessed: 14.03.2023).

GG Bearings (2023). *DP4 and DP4-B METAL-POLYMER SELF-LUBRICATING LEAD FREE BEARING SOLUTIONS*. URL: https://www.ggbearings.com/sites/default/files/2023-03/GGB-DP4-and-DP4-B-Metal-Polymer-Self-Lubricating-Lead-Free-Bearing-Solutions-2023.pdf?fbclid=IwAR364KCeoTAUgBn2eEax9I1H2ZvSwvjeCIcJZArKiIHJNcY031UYPDFLgp
(accessed: 01.05.2023).

Giacoboni, N. (2023). *Basic Custom Arduino Library for HX711*. Accessed May 20, 2023. URL: https://www.mathworks.com/matlabcentral/fileexchange/66641-basic-custom-arduino-library-for-hx711.

Greene, T. (2023). *PEEK vs PEK vs PTFE*. URL: https://www.gtweed.com/materials/peek-vs-pek-vs-ptfe/.

Groover, M. P. (2010). *Fundamentals of Modern Manufacturing*. John Wiley & Sons, Inc.

– (2019). *Fundamentals of Modern Manufacturing*. John Wiley & Sons Singapore Pte. Ltd., pp. 133–155.

Hioki (no date). *What is Voltage?* accessed March 18, 2023. URL: https://www.hioki.com/sg-en/learning/electricity/voltage.html.

Holmberg, K. and A. Erdemir (2017). "Influence of Tribology on Global Energy Consumption, Costs and Emissions". In: *Friction* 5, pp. 263–284. DOI: 10.1007/s40544-017-0183-5. URL: https://doi.org/10.1007/s40544-017-0183-5.

Holmberg, K., H. Ronkainen, et al. (12/2007). "Friction and wear of coated surfaces — scales, modelling and simulation of tribomechanisms". In: *Surface and Coatings Technology* 202, pp. 1034–1049. DOI: 10.1016/j.surfcoat.2007.07.105.

Johannessen, J. (2002). *Tekniske Tabeller*. J. W. Cappelens Forlag A/S.

Kistler 5018A Manual (2017). URL: https://kistler.cdn.celum.cloud/SAPCommerce_Download_original/000-719e.pdf. Kistler.

Kistler-9327A-datasheet (n.d.). URL: http://www.helmar.com.pl/helmar/plik/9327a_nn3878.pdf. Kistler.

Kovaříková, I. et al. (2009). "STUDY AND CHARACTERISTIC OF ABRASIVE WEAR MECHANISMS". In: URL: https://www.mtf.stuba.sk/buxus/docs/internetovy_casopis/2009/1/kovarikova.pdf.

Laurent, A. and Torres C. (2013). "Tribocorrosimeter (homemade)". In: *User Manual*.

Lennard, J. G. (2014a). *Primer on Flat Rolling (Second Edition)*. Elsevier Ltd., p. 193.

– (2014b). *Primer on Flat Rolling (Second Edition)*. Elsevier Ltd., p. 197.

M-403 Datasheet (06/2022). URL: https://www.physikinstrumente.com/fileadmin/user_upload/physik_instrumente/files/datasheets/M-403-Datasheet.pdf. Physik Instrumente.

Massola, C.P, Chaves A.P, and Albertin E. (2016). "A discussion on the measurement of grindingmedia wear". In: *J Mater Res Techno*. DOI: 10.1007/s40544-017-0183-5. URL: dx.doi.org/10.1016/j.jmrt.2015.12.003.

MathWorks (no date). *MATLAB*. https://se.mathworks.com/products/matlab.html. Accessed April 28, 2023.

Mazur, G. (2001). *Digital Multimeter Principles*. American Technical Publishers. ISBN: 9780826914989. URL: https://books.google.no/books?id=Id83PAAACAAJ.

Model 1006 Aluminum Single-Point Load Cell (15/2014). 63999. URL: https://docs.rs-online.com/e728/0900766b816ddff6.pdf. Tedea-Huntleigh.

Mohammed, O. A., Kamaruddin S. K., and Abu Osman M. N. (2014). "An overview of strain gauge applications and challenges". In: *Sensors* 14.11, pp. 20149–20181.

Motor positioning tables (10/2021). URL: https://www.mm-engineering.com/pub/media/productattach/0/4/04_mpt_inkl_zubeh_r_19-07-10_dt-eng_katalog-mme_1.pdf. MM Engineering.

Motor rotary tables (10/2021). URL: https://www.mm-engineering.com/pub/media/productattach/0/5/05_mdt_inkl_zubeh_r_22-04-20_dt-eng_katalog-mme_1.pdf. MM Engineering.

Omega (no date). *Stepper Motors, Introduction to Stepper Motors*. URL: https://sea.omega.com/th/prodinfo/stepper_motors.html. (Accessed: 15.03.2023).

Persson, B. N. J. (2000). *Sliding Friction, Physical Principles and Applications*. Springer Verlag, p. 5.

Positioning systems manually operated (08/2019). URL: https://www.mm-engineering.com/pub/media/productattach/0/2/02_pt-system_19-07-10_dt-eng_katalog-mme_1.pdf. MM Engineering.

PSC-X12-Technical-Information (01/2019). URL: https://www.penlink.se/fileadmin/user_upload/Penlink/content/Dokuments/PSC-X12-Technical-Information.pdf. Penlink.

Ramos, et al (04/2017). "Tribocorrosion and Electrochemical Behavior of DIN 1.4110 Martensitic Stainless Steels After Cryogenic Heat Treatment". In: *Materials Research* 20. DOI: 10.1590/1980-5373-mr-2016-0341.

Rouse, M. (05/2016). *Software library*. accessed may 16, 2023. Techopedia. URL: https://www.techopedia.com/definition/3828/software-library.

Sirohi, R. S. (2017). "Strain Gauges: Types, Working Principle, and Applications". In: *Measurement and Control of Engineering Systems* 6.2, pp. 71–80.

SparkFun-HX711 Load Cell (05/2019). 11. URL: https://www.elfadistrelec.no/en/hx711-load-cell-amplifier-sparkfun-electronics-sen-13879/p/30145509?ext_cid=shgooaqnono-Shopping-PerformanceMax-CSS&&cq_src=google_ads&cq_cmp=18221858120&cq_con=&cq_term=&cq_med=pla&cq_plac=&cq_net=x&cq_pos=&cq_plt=gp&gclsrc=aw.ds&gclid=CjwKCAjw8-OhBhB5EiwADyoY1Xnzs6UKfoBz5e3AKVENUsYx_vPtwFvbY7r1NreX_BskArmh0amZuBoCISMQAvD_BwE&gclsrc=aw.ds. SparkFun Electronics.

Stachowiak, G. W. and A. W. Batchelor (2014). *Engineering Tribology*. Elsevier Inc, p. 578.

STLE (no date). *Introduction to Tribology*. URL: https://www.stle.org/files/About_STLE/Tribology/files/What_is_tribology/Tribology.aspx. (Accessed: 13.03.2023).

– (No Date). *Introduction to Tribology*. URL: https://www.stle.org/files/What_is_tribology/Tribology_Wear.aspx. (Accessed: 17.03.2023).

Teach Engineering (No Date). *Engineering Design Process*. URL: https://www.teachengineering.org/populartopics/designprocess.

The Engineering Toolbox (n.d.). *Viscosity - Absolute (Dynamic) vs. Kinematic*. URL: https://www.engineeringtoolbox.com/dynamic-absolute-kinematic-viscosity-d_412.html. (accessed: 24.03.2023).

Tribonet (2016). *Friction*. URL: https://www.tribonet.org/wiki/friction/. (accessed: 17.03.2023).

TWI Global (no date). *WHAT IS PLA? (EVERYTHING YOU NEED TO KNOW)*. URL: https://www.twi-global.com/technical-knowledge/faqs/what-is-pla. (Accessed: 21.03.2023).

Wikipedia (2023a). *Load Cell*. URL: https://en.wikipedia.org/wiki/Load_cell. (accessed: 25.03.2023).

– (2023b). *Stress-strain curve*. URL: https://en.wikipedia.org/wiki/Stress%E2%80%93strain_curve. (Accessed: 14.03.2023).

– (2023c). *Viscosity*. URL: https://en.wikipedia.org/wiki/Viscosity. (accessed: 25.03.2023).

Yan, W., O'Dowd N. P., and Busso E. P. (2002). "Numerical study of sliding wear caused by a loaded pin on a rotating disc". In: *Journal of the Mechanics and Physics of Solids* 50.3, pp. 449–470. ISSN: 0022-5096. DOI: https://doi.org/10.1016/S0022-5096(01)00093-X. URL: https://www.sciencedirect.com/science/article/pii/S002250960100093X.

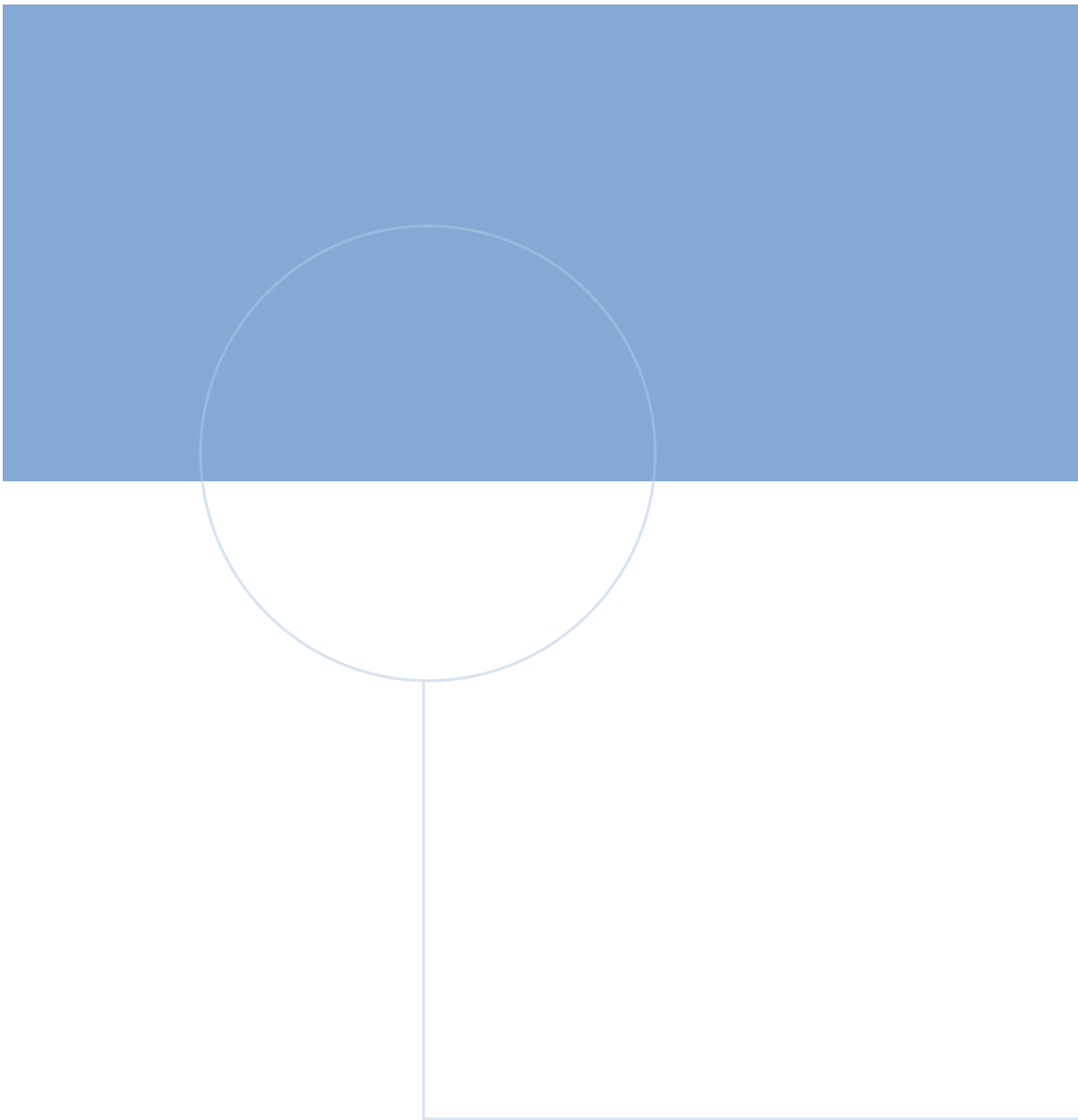

NTNU

Norwegian University of
Science and Technology